Doctoral Thesis

Hybrid Strategies for Sulfide Solid Electrolytes with Organic Materials: Toward Practical All-Solid-State Lithium-Ion Batteries

Dae Yang Oh

Department of Energy Engineering

(Battery Science and Technology)

Graduate School of UNIST

2019

Hybrid Strategies for Sulfide Solid Electrolytes with Organic Materials: Toward Practical All-Solid-State Lithium-Ion Batteries

Dae Yang Oh

Department of Energy Engineering
(Battery Science and Technology)

Graduate School of UNIST

Hybrid Strategies for Sulfide Solid Electrolytes with Organic Materials: Toward Practical All-Solid-State Lithium-Ion Batteries

A dissertation
submitted to the Graduate School of UNIST
in partial fulfillment of the
requirements for the degree of
Doctor of Philosophy

Dae Yang Oh

05/31/2019

Approved by

Advisor
Youngsik Kim

Hybrid Strategies for Sulfide Solid Electrolytes with Organic Materials: Toward Practical All-Solid-State Lithium-Ion Batteries

Dae Yang Oh

This certifies that the dissertation of Dae Yang Oh is approved.

05/31/2019

signature

Advisor: Youngsik Kim

signature

Advisor: Yoon Seok Jung

signature

Sang-Young Lee

signature

Sung You Hong

signature

Seok Ju Kang

Abstract

Hybrid Strategies for Sulfide Solid Electrolytes with Organic Materials: Toward Practical All-Solid-State Lithium-Ion Batteries

Dae Yang Oh
School of Energy and Chemical Engineering, UNIST, *2014 – 2017*
Department of Energy Engineering, Hanyang University, *2018 – 2019*
Supervised by prof. Yoon Seok Jung

Lithium-ion batteries (LIBs) should further deal with safety concerns as well as greater energy density so that they can become the core of future electrifications. In this regard, All-solid-state lithium-ion batteries (ASLBs) replacing flammable organic liquid electrolytes (LEs) with solid electrolytes (SEs) have been considered as the prospective system owing to following advantages: using solidified electrolytes (1) reinforces safety, (2) increases energy density of battery pack, (3) takes chance to adopt Li metal as an anode potentially, (4) realizes extremely high-loading density of electrodes. To guarantee impressive performance of ASLBs, tactical choice of SEs is important. Among various SEs, sulfide SEs generally exhibit high ionic conductivity in range from 0.1 to 21 mS cm^{-1} with unit transference number at room temperature (RT) and superb device integration due to their mechanical softness.

However, the ASLBs based on sulfide SEs should leap out two hurdles to realize commercialization. First, ionic percolations within electrodes should be optimized because the performance of ASLBs is strongly affected by interfaces where heterogeneous solids are in 2-dimensional contact with each other. Second, scalable techniques for tailoring sheet-type electrodes must be further developed. Notably, most of prior reports in this field have been demonstrated based on small-scale-composite electrodes prepared in dry condition, which is improper for scalable production.

To solve aforementioned issues and challenges, combining sulfide SEs and a small amount of soft organic materials (e.g., carbonate based liquid electrolytes, polymeric binders, N-Methyl-2-pyrrolidone (NMP) used in conventional LIBs) *via* wet-process, in terms of “hybrid configurations”, would be appropriate to improve ionic percolations within the electrodes and processability for practical sheet-type ASLBs. However, highly reactive nature of sulfide SEs against polar organic materials used in typical LIBs has restricted extensive researches for hybridization. Herein, I report on novel strategies for hybridization of sulfide SEs with diverse organic materials for high performance ASLBs.

The first part of my thesis is hybrid sulfide SEs employing solvate ionic liquids (SILs) to handle incomplete ionic percolations within all-solid-state electrodes. SIL is an equimolar mixture of Li salt and glyme, for instance, Li(G3)TFSI (referred as to "LiG3") comprised of G3 (triethylene glycol

dimethyl ether or triglyme) and LiTFSI (lithium bis(trifluoromethanesulfonyl)imide). The excellent stability of sulfide SEs (Li_3PS and $Li_{10}GeP_2S_{12}$) with LiG3 and their application were successfully demonstrated. The poor solid-solid contacts within the electrodes healed by addition of a small amount of LiG3, providing alternative Li^+-conductive pathways, resulting in drastically increased capacity of $LiFePO_4$ (LFP) electrode.

The second part of my thesis is sheet-type electrodes fabricated from wet-chemical route. In this work, scalable slurry-process for bendable sheet-type electrodes evolved from liquid-phase synthesis (LP) of sulfide SEs by adding active materials ($LiNi_{0.6}Co_{0.2}Mn_{0.2}O_2$ (NCM622) or graphite (Gr)) and polymeric binders (polyvinyl chloride (PVC) or nitrile-butadiene rubber (NBR)). These processes allowed to synthesize sulfide SEs and fabricate bendable sheet-type electrodes at the same time. A rocking-chair ASLBs employing sheet-type NCM622 and Gr electrodes exhibited a decent capacity of 110 mA h g^{-1} at extreme conditions (15C and 100 ^oC), emphasizing guaranteed performance of ASLBs at a wide range of temperatures.

Although some literatures have reported wet-slurry process for sheet-type ASLBs while using non-polar solvents with polymeric binders, the binders result in below par electrochemical performance because electric pathways in the electrodes are interrupted by binders. In the last study, slurry-fabricable Li^+-conductive polymeric binders enabled by SILs for sheet-type ASLBs were demonstrated to solve aforementioned obstacles. The less polar dibromomethane (DBM) allowed wet-slurry process to accommodate Li_6PS_5Cl (LPSCl) and SILs without undesirable dissolution problems. The NCM622 electrodes employing NBR-LiG3 showed higher capacity of 174 mA h g^{-1} at 30 °C, which was far superior than using only NBR (144 mA h g^{-1}). The facilitated Li^+-ionic contacts at interfaces paved by NBR-LiG3 are evidenced by the complementary analysis from electrochemical characterizations and ^7Li nuclear magnetic resonance measurements.

These results provide not only breakthroughs for mass production but also rational guideline to design all-solid-state electrodes toward practical ASLBs. I believe that further investigation about compatible combinations of sulfide SEs with organic materials will contribute to understand complex chemical phenomena (e.g., reactivity, solubility, and stability) of sulfide SEs, providing creative opportunities for architecting electrodes as well as motivation and insights for a new knowledge in various battery systems.

……..……..

Keywords: Lithium ion batteries, All-solid-state batteries, Sulfide solid electrolytes, Solvate ionic liquids, All-solid-state electrodes, Hybrid

Contents

List of figures

SE. (c) half-cell comprised of multi SEs (yellow and green particles). Li-In is used as counter electrode. Reproduced with permission.[65] Copyright 2014, Elsevier.

Figure 9. Dissolution test of sulfide SEs with G3-based liquids ([Li(G3)x]TFSI, $1 \leq x$). Direct observed results of LPS or LGPS with G3, $Li(G3)_4$, and Li(G3) after kept for 7d. All the liquid samples are transparent originally. Reproduced with permission.[38] Copyright 2015, Wiley-VCH.

Figure 10. Comparative study to estimate an amount of dissolved species from SEs to liquids. (a) UV-vis absorption spectra for LPS and LGPS. (b) Plots for weight fraction of dissolved elements for LPS and LGPS, which were calculated from ICPOES measurements. Reproduced with permission.[38] Copyright 2015, Wiley-VCH.

Figure 11. XRD patterns of LPS (or LGPS) with Li(G3) (or $Li(G3)_4$) varied by storage time. Reproduced with permission.[38] Copyright 2015, Wiley-VCH.

Figure 12. XRD patterns of LPS (or LGPS) with another type of superconcetrated LEs, $Li(AN)_2TFSI$ (LiTFSI/ACN = 1/2, referred as to $Li(AN)_2$). Reproduced with permission.[38] Copyright 2015, Wiley-VCH.

Figure 13. Schematic diagrams representing the interplay between sulfide SEs (LPS, LGPS) and G3-based liquids (G3 and $Li(G3)_xTFSI$). Reproduced with permission.[38] Copyright 2015, Wiley-VCH.

Figure 14. Physical properties of hybrid SEs (SE-LiG3). (a) photographic images of pristine powders and SE-LiG3 powders. (b) photographs of pelletized LGPS-LiG3. (c) TGA analysis results of SEs, LiG3, SE-LiG3. The weight ratio of SE to LiG3 is 9 to 1. Reproduced with permission.[38] Copyright 2015, Wiley-VCH.

Figure 15. Comparative electrochemical characterizations of LFP/Li-In half-cell at 30 °C. (a) Second cycle voltage profiles of LFP with (blue) and without LiG3 (red). (b) Cycle performance of LFP with LiG3. The rate performance is shown in the inset. Reproduced with permission.[38] Copyright 2015, Wiley-VCH.

Figure 16. Comparative electrochemical characterizations of LTO/Li-In half-cell at 30 °C. (a) Second cycle voltage profiles of LTO with (blue) and without LiG3 (red). (b) cycle performance of LTO with and without LiG3. Reproduced with permission.[38] Copyright 2015, Wiley-VCH.

Copyright 2017, the Royal Society of Chemistry.

Figure 26. Enlarge Raman spectra of pristine NBR and LPS-NBR. The weight ratio of LPS to NBR is 94.5 to 5.5. Reproduced with permission.[29] Copyright 2017, the Royal Society of Chemistry.

Figure 27. Arrhenius plots for LPS and LPS-Polymer obtained by AC impedance measurement using Li^+-blocking symmetric cell (Ti/sample/Ti). Reproduced with permission.[29] Copyright 2017, the Royal Society of Chemistry.

Figure 28. Illustration for a single-step wet-fabrication of sheet-type composite electrodes. Reproduced with permission.[29] Copyright 2017, the Royal Society of Chemistry.

Figure 29. Photographic images of sheet-type NCM electrode prepared from one-pot slurry. the (a) free-standing electrode with 4 cm^2 (b) the electrode before and after bending test. The electrode was wrapped 20 times along the 10 pi cylinder. Reproduced with permission.[29] Copyright 2017, the Royal Society of Chemistry.

Figure 30. Electron microscopic characterizations of cross-sectional sheet-type electrodes fabricated by a single-step wet-chemical route. FESEM images and corresponding EDXS elemental maps for (a) NCM622, (b) Graphite are presented. Ni and O indicate NCM622, C indicates Graphite, and P and S indicate LPS. Reproduced with permission.[29] Copyright 2017, the Royal Society of Chemistry.

Figure 31. FESEM images of LPS powders varied by the size of precursors. LPS prepared from (a) the pristine precursors (PP) and (b) the ball-milled precursors (BP). Reproduced with permission.[29] Copyright 2017, the Royal Society of Chemistry.

Figure 32. Electrochemical characterizations for the NCM622/Li-In half-cells at 30 ºC, depending on wet-chemically fabricated sheet-type electrodes using BP and PP. (a) First voltage profiles for the NCM622 electrodes prepared from BP and PP at 0.05C. (b) Rate capabilities. The cycle performance of BP-NCM622 is in the inset. (c) Discharge voltage profiles with various C-rate. (d) Nyquist plots for the NCM622 electrodes after 1st charging 4.3 V (vs. Li/Li^+). Reproduced with permission.[29] Copyright 2017, the Royal Society of Chemistry.

Figure 33. Transient voltage profiles and corresponding polarization plots acquired by GITT for NCM622/Li-In half-cell. The enlarged view in the inset points closed-circuit voltage (CCV) and quasi-open-circuit voltage (QOCV). BP-NCM622 is red and PP-NCM622 is green. Reproduced with

permission.[29] Copyright 2017, the Royal Society of Chemistry.

Figure 34. Electrochemical characterizations for the Gr/Li-In half-cells at 30 ºC, employing wet-chemically fabricated sheet-type electrode. (a) The first voltage profile for the BP-Graphite at 0.05C. (b) Rate capabilities. (b) The cycle performance at 0.1C. Reproduced with permission.[29] Copyright 2017, the Royal Society of Chemistry.

Figure 35. Comparison test about ASLBs and LIBs. First voltage profiles of (a) NCM622 and (b) Gr using different electrolytes. All the profiles were acquired at 30 ºC. The C-rates for assessment are notated in Insets. Cycling tests using liquid electrolytes were performed using 2032-type coin cells. A 1.15 M solution of $LiPF_6$ dissolved in ethylene carbonate (EC), ethylmethyl carbonate (EMC), and dimethyl carbonate (DMC) (2:5:3 v/v) with 5 wt.% fluorinated ethylene carbonate (FEC) and 0.5 wt.% vinyl carbonate (VC) as additives was used as the electrolyte. A porous polypropylene (PP)/polyethylene (PE)/PP tri-layer film (Celgard Inc.) was used as the separator. The compositions of electrodes for LIBs are followed; NCM622 : C : PVDF = 90 : 5 : 5 wt%, Gr : PVDF = 9 : 1. Reproduced with permission.[29] Copyright 2017, the Royal Society of Chemistry.

Figure 36. Photographs of (a) wet-chemically synthesized LPS and (b) NCM622 powders exposed to supernatant. (c) 1st voltage profiles of NCM622/Li-In cells at 0.1C at 30 ºC using pristine (black), pure-THF-treated (blue), and supernatant-treated bare (red). All samples were dried at 140 ºC under vacuum. The supernatant-exposed NCM622 powders were washed by pure THF before drying. Reproduced with permission.[29] Copyright 2017, the Royal Society of Chemistry.

Figure 37. Galvanostatic charge-discharge test of a rocking-chair ASLB employing single-step wet-chemically tailored sheet-type electrodes at 30 ºC and 100 ºC. (a) Cycle performance and (b) the corresponding charge-discharge voltage profiles. Reproduced with permission.[29] Copyright 2017, the Royal Society of Chemistry.

Figure 38. BP-NCM622/BP-Gr full-cell employing a thin SE-nonwoven composite film. (a) Schematic diagram. (b) Photographic images of the free-standing film-type ASLB. Reproduced with permission.[29] Copyright 2017, the Royal Society of Chemistry.

Figure 39. The first voltage profile of BP-NCM622/BP-Gr full-cell employing a thin SE-nonwoven composite film. [29] Copyright 2017, the Royal Society of Chemistry.

Figure 40. Photographic images of mixtures of LiG3 with diverse solvents (a) without LPSCl and (b)

after adding LPSCl and being kept for 12 h. Detailed information about solvents is in **Table 3**. Reproduced with permission.[39] Copyright 2019, Wiley-VCH.

Figure 41. Photographs of SE (LPSCl), NBR, and LiG3 (the top image) and after blending with DBM (the ground image). Reproduced with permission.[39] Copyright 2019, Wiley-VCH.

Figure 42. Schematic diagram illustrating compatibility with LPSCl for LiG3 diluted by various solvents varied by polarity; (a) nonpolar, (b) less polar, and (c) highly polar (or Lewis-basic) solvents. Reproduced with permission.[39] Copyright 2019, Wiley-VCH.

Figure 43. XRD results of pristine LPSCl, DBM-exposed LPSCl, and LPSCl-NBR-LiG3. Reproduced with permission.[39] Copyright 2019, Wiley-VCH.

Figure 44. Static ^{7}Li NMR spectra of LiG3 and NBR-LiG3. Reproduced with permission.[39] Copyright 2019, Wiley-VCH.

Figure 45. MAS ^{7}Li NMR spectra of LPSCl, NBR-LiG3, LPSCl-NBR-LiG3. Reproduced with permission.[39] Copyright 2019, Wiley-VCH.

Figure 46. Static ^{7}Li NMR spectra of LPSCl-NBR-LiG3, LPSCl, LiG3, NBR-LiG3. Reproduced with permission.[39] Copyright 2019, Wiley-VCH.

Figure 47. Cross-sectional FESEM image and EDXS elemental maps for LPSCl–NBR–LiG3. Reproduced with permission.[39] Copyright 2019, Wiley-VCH.

Figure 48. Photographs of Cross-sectional FESEM image and EDXS elemental maps for LPSCl–NBR–LiG3. Reproduced with permission.[39] Copyright 2019, Wiley-VCH.

Figure 49. Schematic diagram representing ^{6}Li symmetric cell (^{6}Li/LPSCl-NBR-LiGE/^{6}Li). Li^{+} conduction pathways in the LPSCl-NBR-LiG3 are shown blue arrows (1, 2). Reproduced with permission.[39] Copyright 2019, Wiley-VCH.

Figure 50. Cycling profiles of the $^{6}Li^{+}$-ion nonblocking symmetric cell (^{6}Li/LPSCl-NBR-LiG3/^{6}Li) with constant current of 50 μA. Reproduced with permission.[39] Copyright 2019, Wiley-VCH.

Figure 51. MAS ^{7}Li NMR spectra for comparative studies about LPSCl-NBR-LiG3 before and after

cycling. LPSCl and NBR-LiG3 are 2.5 ppm and -0.25 ppm, respectively. Reproduced with permission.[39] Copyright 2019, Wiley-VCH.

Figure 52. Nyquist plots for extracting interfacial resistance at LPSCl/NBR-LiG3. R_{int} (33.8 Ω cm ^{2}) was calculated by following equation; $R_{tot} = 2\cdot(R_{NBR\text{-}LiG3} + R_{int}) + R_{LPSCl}$. Reproduced with permission.[39] Copyright 2019, Wiley-VCH.

Figure 53. Photographs for sheet-type electrodes prepared by DBM-based wet-protocols (a) without NBR and (b) with NBR-LiG3. Reproduced with permission.[39] Copyright 2019, Wiley-VCH.

Figure 54. Electrochemical characterizations for the NCM622/Li-In half-cells at 30 °C, depending on sheet-type NCM622 electrodes fabricated by DBM-based slurry with NBR (black) and NBR-LiG3 (blue). The first-cycle voltage profiles are shown. Reproduced with permission.[39] Copyright 2019, Wiley-VCH.

Figure 55. The first-cycle voltage profiles for NCM622 and NCM711. These profiles are obtained by using conventional LEs. Cycling tests using liquid electrolytes were performed using 2032-type coin cells. A 1 M solution of $LiPF_6$ dissolved in ethylene carbonate (EC), ethylmethyl carbonate (EMC), and dimethyl carbonate (DMC) (4:3:3 v/v, Panax Inc.) was used as the electrolyte. A porous polypropylene (PP)/polyethylene (PE)/PP tri-layer film (Celgard Inc.) was used as the separator. The compositions of electrodes for LIBs are followed; NCM : C : PVDF = 90 : 5 : 5 wt%. Reproduced with permission.[39] Copyright 2019, Wiley-VCH.

Figure 56. Comparative electrochemical characterization of NCM622/Li-In half-cell at 30 °C, depending on sheet-type NCM622 electrodes fabricated by DBM-based slurry with NBR (black) and NBR-LiG3 (blue). (a) Rate capability, the cycle performances at 0.2C (0.52 mA cm^{-2}) are shown in the inset. (b) Nyquist plots obtained after charging at 4.3 V (vs. Li/Li^+). Reproduced with permission.[39] Copyright 2019, Wiley-VCH.

Figure 57. The subsequent cycling performance of NCM622 electrode with NBR-LiG3 for the data shown in **Figure 56a**. (a) The cycle data at 30°C and 60°C, (b) the voltage profiles at 30 °C (4^{th}) and 60 °C (32^{th}), tested at 0.2C both. Reproduced with permission.[39] Copyright 2019, Wiley-VCH.

Figure 58. Transient voltage profiles and polarization plots acquired by GITT for NCM622/Li-In half-cell. NCM622 electrode with NBR (black) and NBR-LiG3 (blue). Reproduced with permission.[39] Copyright 2019, Wiley-VCH.

List of tables

Nomenclature

LIB	Lithium-ion battery
ASLB	All-solid-state lithium-ion battery
LE	Liquid electrolyte
SE	Solid electrolyte
SEI	Solid electrolyte interphase
RT	Room temperature
NMP	N-Methyl-2-pyrrolidone
SIL	Solvate ionic liquid
LiG3	Li(G3)TFSI
G3	Triethylene glycol dimethyl ether
LiTFSI	Lithium bis(trifluoromethanesulfonyl)imide
LFP	$LiFePO_4$
LP	Liquid-phase synthesis
NCM622	$LiNi_{0.6}Co_{0.2}Mn_{0.2}O_2$
Gr	Graphite
NBR	Nitrile-butadiene rubber
PVC	Polyvinyl chloride
DBM	Dibromomethane
LPSCl	Li_6PS_5Cl
LCO	$LiCoO_2$
LPS	Li_3PS_4
LPSCl	Li_6PS_5Cl
LGPS	$Li_{10}GeP_2S_{12}$
ACN	Acetonitrile
THF	Tetrahydrofuran
HSAB	hard and soft acids and bases
LPS	Li_3PS_4
NBR	Nitrile butadiene rubber
SBR	Styrene butadiene rubber
XRD	X-ray diffraction
FESEM	Field-emission scanning electron microscopy
EDXS	Energy dispersive X-ray spectroscopy
HRTEM	High-resolution transmission electron microscopy
ED	Electron crystallography pattern
TGA	Thermogravimetric analysis
NMR	Nuclear magnetic resonance
MAS	Magic angle spinning
LTO	$Li_4Ti_5O_{12}$
NCM711	$LiNi_{0.7}Co_{0.15}Mn_{0.15}O_2$
GITT	Galvanostatic intermittent titration technique

1. Introduction

Demands for electrical energy have been increased drastically since the second industrial revolution, which is driving force to the development of diverse energy conversion and storage devices (e.g., capacitors, batteries, and fuel cells) for efficient energy usage. In particular, lithium-ion batteries (LIBs) have been considered as the most promising energy storage system owing to their outstanding energy density with 4 V-class reachability, comparing with others based on aqueous electrolytes.[1] The development of active materials (e.g., $LiCoO_2$ (LCO) and graphite (Gr)) and the understanding of solid electrolyte interphase (SEI) derived by organic liquid electrolytes (LEs) in contact with electrodes allowed LIBs to be operable in the range of 2.5 - 4.5 V.[2-4] It made LIBs to be successfully commercialized in the early 1990s.[2-4] Although gradual progress for materials and electrode engineering has enabled LIBs to achieve much higher energy density while widening applications of them from portable devices to electric vehicles, safety concerns originate from intrinsically flammable LEs always have threatened large scale applications of LIBs.

In this regard, all-solid-state lithium-ion batteries (ASLBs) using inorganic solid electrolytes (SEs) have been suggested as a prospective alternative because inorganic SEs are thermally stable without leakage problems and have the potential for achieving high energy density through the bi-polar stacking with ultra-high mass loading electrodes.[5-7] Moreover, inorganic SEs are possible to work at wide temperature compare to that of the LEs. Indeed, they give exceptionally high Li^+ transference number, thus, have an advantage in the aspects of charge transport at the electrode/SE interface.[5, 7, 8] If SEs offer enough Li^+ conductivity of more than 1 mS cm^{-1}, ASLBs would acquire the potential to outperform conventional LIBs based on LEs (~ 10 mS with Li^+ transference number of 0.2 – 0.4). In this reason, SE is prime factor for developing ASLBs. Among the various candidates, sulfide SEs are promising in the development for practical ASLBs because they offer high Li^+ conductivity (max. 25 mS cm^{-1} at room temperature) with great device integration. [7, 9, 10]

Unfortunately, they have severe handicap regarding chemical compatibility toward polar environments. Generally, highly Li^+ conductive sulfide SEs (Li_3PS_4 (LPS): ~1 mS cm^{-1},[11] $Li_7P_3S_{11}$: max. 17 mS cm^{-1},[12] Li_6PS_5X (LPSCl, X= Cl, Br, I): > 1 mS cm^{-1}, [13-15] $Li_{10}GeP_2S_{12}$ (LGPS) derivatives: max. 25 mS cm^{-1} [9, 16]) are composed of thiophosphates (e.g., PS_4^{3-} and $P_2S_7^{4-}$). Thus, the electrophile P in thiophosphates is easily invaded by strong Lewis-basic solvents (e.g., water, acetonitrile (ACN), tetrahydrofuran (THF)) including lone-pair electrons at highly electronegative elements (e.g., O and N), resulting in undesired dissolutions or irreversible side reaction as shown in **Figure 1**. The only some non (or less) polar solvents, such as toluene and xylene, are available to be compatible with sulfide SEs (**Figure 1b**). [17-18]

To avoid these problems, P-free sulfide SEs have been designed and developed rationally, such as xLiI-(1-x)Li_4SnS_4 (0.4 mS cm^{-1} for x=0.4),[19] $Li_{3+x}Ge_xAs_{1-x}S_4$ (1.1 mS cm^{-1} for x=1/3),[20] Na_3SbS_4 (1.1 mS cm^{-1}),[21] and $Na_{4-x}Sn_{1-x}Sb_xS_4$ (0.3 mS cm^{-1} for x=0.3)[22]. Surprisingly, these P-free sulfide SEs proved not only excellent air stability but also solution-processability based on highly Lewis-basic solvents, highlighting the exceptional chemical stability compared with typical sulfide SEs containing thiophosphates.[19, 21-23] These phenomena are nationalized by the hard and soft acids and bases (HSAB) theory. [5, 23] It assigns "hard" or "soft" to chemical species. Hard is small and high charge state and weakly polarizable, while soft is opposite concepts. According to the HSAB theory, similar species tend to interact much favorably. Sn, As, Sb, and Ge are a softer base than P, thus, they have a higher affinity for S, compared with P. The one part of periodic table for understanding HSAB theory at a glance is depicted in **Figure 2**. This might account for the better chemical stability of P-free sulfide SEs toward Lewis-basic agents. However, applications of P-free sulfide SEs are very restricted because heavy transition metals as a central atom in the building units (e.g., MS_4^{4-}: M = Ge and Sn, MS_4^{3-}: M = As and Sb) undermine electrochemical stability below ~2 V (vs. Li/Li$^+$ or Na/Na$^+$) while being reduced.[7]

The interaction between sulfide materials having P-S bonds and Lewis-basic agents doesn't necessarily mean it's negative. In fact, there were some positive cases in which sulfide SEs were synthesized from wet-chemical route enabled by SE precursors (e.g., Li_2S and P_2S_5) and THF (or ACN).[24-25] In case of liquid-phase synthesis (LP), partially dissolved SE precursors react in THF (or ACN), producing intermediate precipitants and supernatant.[26] After reaction in LP, subsequent drying and heat-treatment below 250 °C formulate final products (β-LPS: 0.2 mS cm^{-1} and $Li_7P_3S_{11}$: 1.2 mS cm^{-1}).[24, 26] Although wet-synthetic chemistries hardly have been revealed, the key of as-discussed researches is closely interrelated with solubility for precursors. These protocols provide new opportunities for developing new materials (e.g., $Li_7P_2S_8I$: 0.6 mS cm^{-1}, Li_4PS_4I: 0.12 mS cm^{-1}),[27-28] mass production, [25, 29] morphology control,[29-30] and advanced applications.[29, 31]

Progress in the development of sulfide SEs have been also expanded to applications for electrodes as well as search for new materials or enhancing (electro)chemical characteristics. To reduce interfacial resistance originated from incomplete ionic contacts between sulfide SEs and active materials, several sulfide SEs coated on active materials. The first attempt for sulfide SE coating onto active materials was investigated by pulsed laser deposition method.[32] Subsequently, solution-processable LiI-Li_4SnS_4 enabled by methanol (or water) provided the advanced applications and the insight regarding importance of ionic contacts within electrodes.[19, 33] Solution-processable electrolytes were further discovered such as Li_6PS_5X (X = Cl, Br) using ethanol,[34] Na_3SbS_4 using water,[21] and HT-Li_7PS_6 using THF and ethanol.[35] Unfortunately, although solution-processable SEs (or sulfide SE solution) have the promising potential to be applied in the practical applications for ASLBs, there were considerable issues derived by reactive sulfide solution as followed; (i) active materials would be corrupted by specific

solvents (or sulfide solution),[29, 33] (ii) reactive sulfide solution occurred the corrosion of the Al current collectors.[34]

Aforementioned the renaissance of sulfide SEs generally have handled only aspects for materials to cope with limitations of solid ionic conductors. However, practical techniques for ASLBs such as scalable fabrication protocols and electrode designs have not been developed extensively despite first-reported sulfide SE (glass Li_2S-P_2S_5-LiI) already achieved enough Li^+ conductivity of 1 mS cm^{-1} at room temperature (RT) in the 1981.[36] Notably, the LCO electrode employing LGPS (12 mS cm^{-1} at 27 ^oC) showed below par capacity of over 120 mA h g^{-1} at 14 mA g^{-1} compared to that of ones using conventional LEs (approximately 140 mA h g^{-1} at 266 mA g^{-1}), which implies importance about electrode engineering.[16, 37] Inevitably formed void space (or pores) and insufficient electric pathways in the ASLBs contribute to increase internal resistance, resulting in disappointing performance. Moreover, most of researches in the sulfide ASLBs field didn't deviate from manually mixed small-scale electrodes because poor and sensitive chemical stability of sulfide SEs hinders methodology for developing processability.[5, 7] Thus, challenges for sheet-type electrodes in the sulfide ASLBs have been still remained.[7] In this point, mechanically compliant organic materials can assist in the development of sulfide ASLBs in terms of performance and practical fabrications, which is in is indispensable.

In my doctoral thesis, tactical hybrid strategies for combining sulfide SEs and various organic materials (e.g., polymeric binders, organic solvents, LEs) to cope with engineering issues for bulk-type ASLBs employing sulfide SEs are suggested.[29, 38-39] My thesis comprises three parts; first, excellently compatible LEs with sulfide SEs are reported.[38] From the trend regarding stability of sulfide SEs varied by concentration of LEs, rational guideline for quasi-sulfide SEs is presented. In additions, unprecedented performance of carbon-coated $LiFePO_4$ (LFP) composite electrodes employing solvate ionic liquids (SIL)[40] indicates the importance of ionic contacts within the all-solid-state electrode particularly. Second, wet-chemically tailored sheet-type electrodes from one-pot slurries comprised of SE precursors, active materials, binders, conducive additives are demonstrated.[29] The hybridization of LP for sulfide SEs with slurry-based fabrication process using polymeric binders provides new chance for sheet-type ASLBs. Additionally, the effects about the size of SEs and reactive sulfide solution on the electrochemical performance are investigated. The third part is for slurry-fabricable Li^+-conductive polymeric binders enabled by SIL.[39] A series of processes for developing wet-slurry protocols to accommodate Li^+-conductive binder provide rational guideline for fabricating sheet-type electrodes in the development of bulk-type ASLBs. From the complementary analysis by electrochemical characterizations and ^7Li NMR measurements, the facilitated Li^+-contacts at interfaces paved by NBR-SILs are verified. Moreover, it rendered state-of-the-art areal capacity of 7.4 mA h cm^{-2} with remarkable high mass loading (45 mg cm^{-2}).

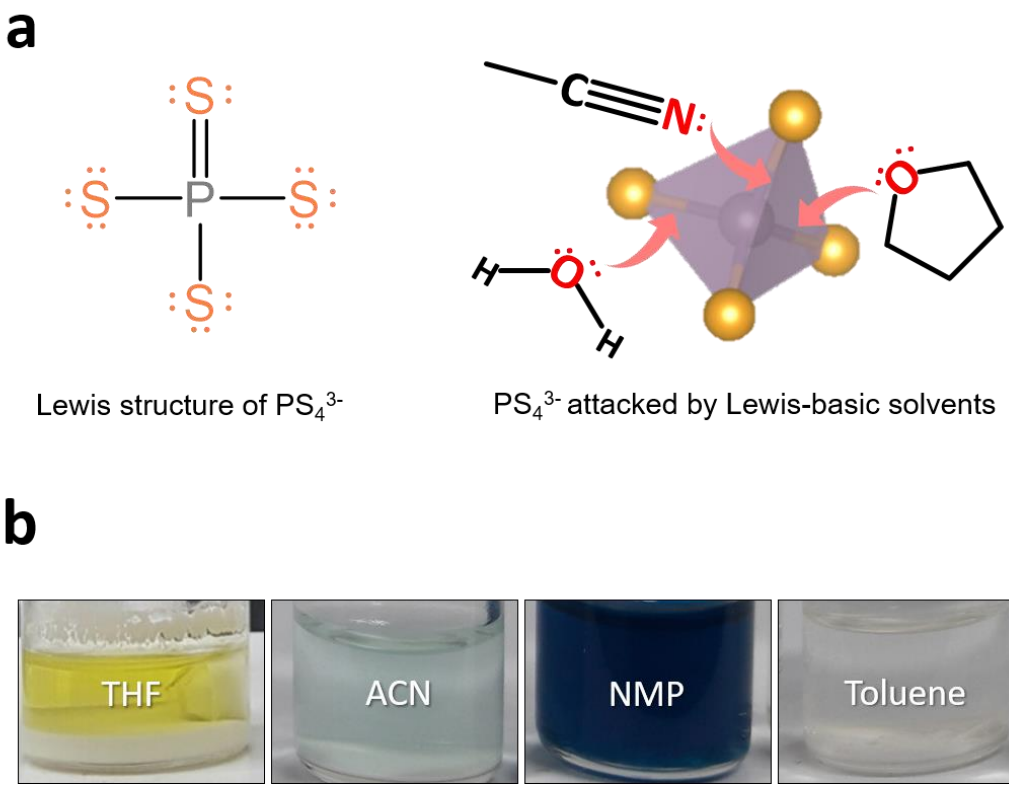

Figure 1. Schematic diagrams for (a) Lewis-structure of thiophosphate (PS_4^{3-}) and its chemical stability against Lewis-basic solvents, (b) photographs for dissolution test of sulfide SEs with various organic solvents. THF is tetrahydrofuran, ACN is acetonitrile, and NMP.

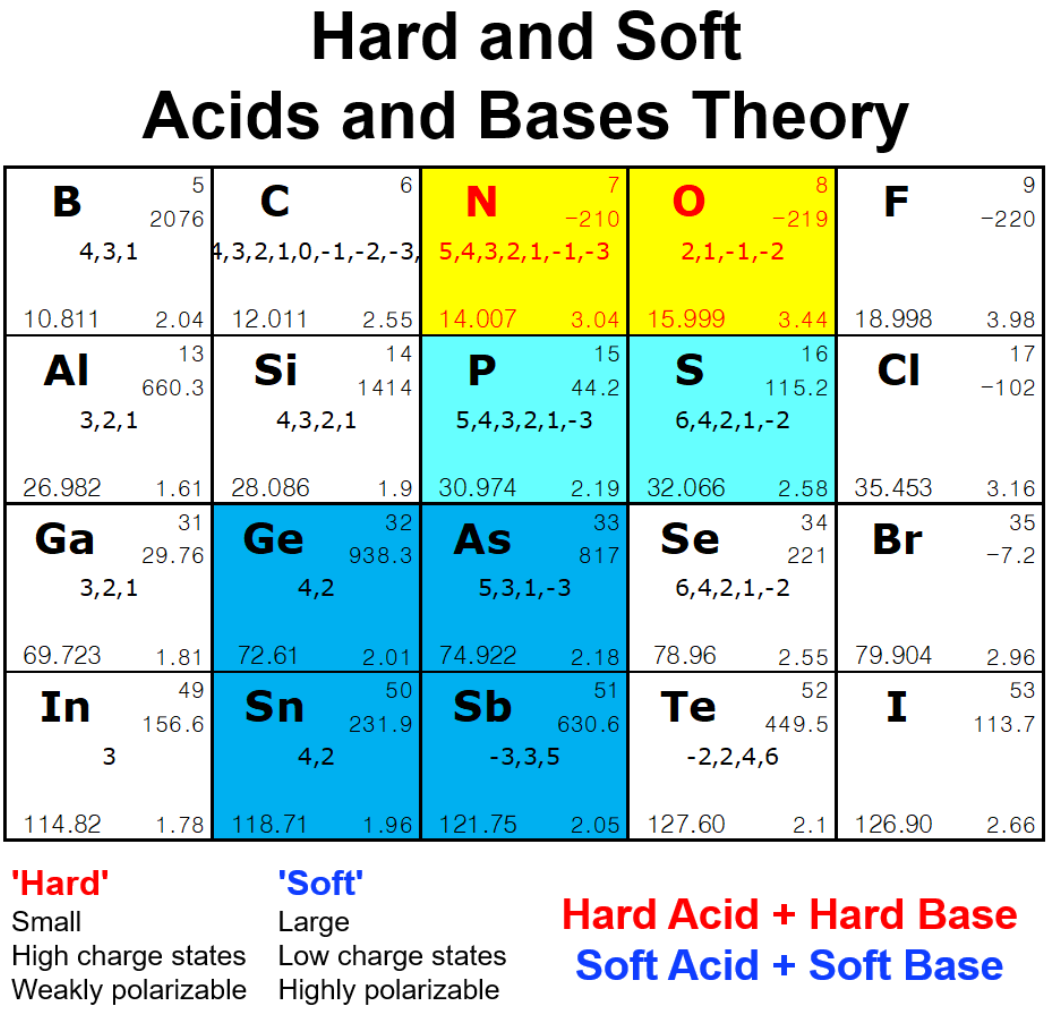

Figure 2. Periodic table for illustrating HSAB theory; shaded area indicates highly electronegative elements in Lewis-basic solvents (yellow), elements for thiophosphate (cyan), and central atoms for P-free sulfide SEs (blue). According to HSAB theory, (Ge, As, Sn, Sn)-S bonds are favorable than P-S bond.

2. Background

2.1 Principle of rechargeable lithium-ion batteries

Basically, rechargeable batteries convert chemical energy stored in electrodes to electrical energy during discharge. Charge is an opposite concept. Rechargeable LIBs consist of cathode, anode, LE, and separator as shown in **Figure 3.**[1] In the LIB field, cathode is where reduction occurs and anode is where oxidation occurs during discharge. Typically, $LiMO_2$ (M= Co, Ni, Mn) and Gr are used as cathode and anode, respectively. LE is Li^+-conductive solution consisting of aprotic polar organic solvents (e.g., ethylene carbonate, propylene carbonate, and etc.) and Li salts (e.g., $LiPF_6$, LiTFSI (lithium bis(trifluoromethanesulfonyl)imide)), which works as only ion conducting bridge between cathode and anode. Electrolytes between cathode and anode must be electronic insulator to avoid internal short-circuit. The separator is porous membrane as a physical barrier between cathode and anode, preventing internal short-circuit also. In the charge process, $LiMO_2$ (M= Co, Ni, Mn) is oxidized by losing electron and Li^+ while Gr is reduced by adopting Li^+ and electron (**Figure 3**). The discharge process changes reverse.

During the charge and discharge, LEs are decomposed owing to wide potential gap overwhelming electrochemical windows of LEs. Fortunately, decomposed products are ionically conducting with negligible electronic conductivity, which are called as SEI, suppressing continuous decomposition of LEs. The SEI is enabler to realize 4 V-class batteries.[1-3]

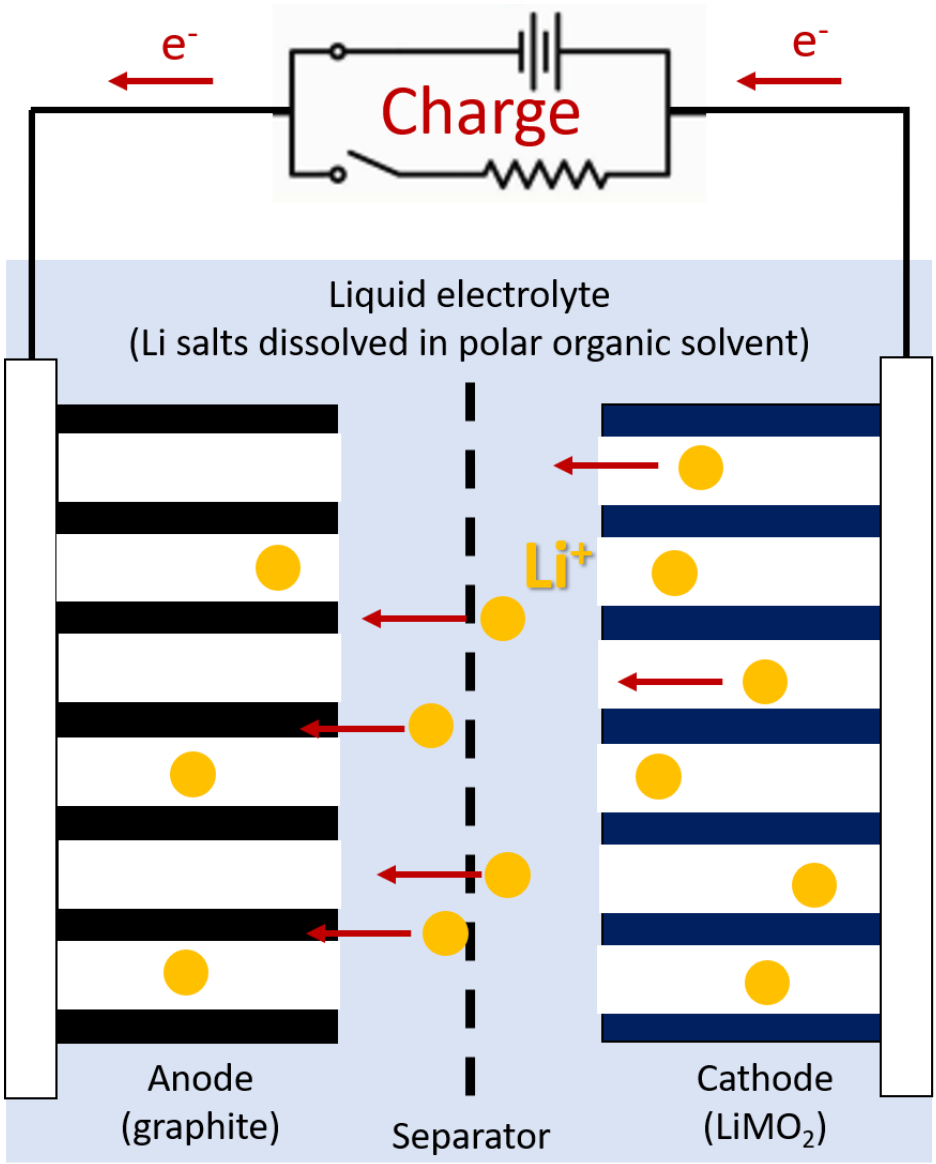

Figure 3. Graphical illustration for rechargeable LIBs.

2.2 Bulk-type all-solid-state lithium-ion batteries

ASLBs replacing flammable LEs with inorganic SEs are classified into the configurations, such as thin-film ASLBs and bulk-type ASLBs as shown in **Figure 4.** The thin-film ASLBs (**Figure 4a**) are assembled by vacuum deposition process and restricted to small-scale applications, for instance microelectric devices and smart cards. Although $Li_{3.3}PO_{3.9}N_{0.17}$ used in thin film ASLBs exhibited very lower Li^+ conductivity of 0.002 mS cm^{-1} at RT, a few micrometer in the thickness of SE layers enables to achieve very high conductance with low cell resistance.[41 42] However, owing to difficulty for massive accumulation, high price and low energy density of thin film ASLBs make hurdle to apply large scale applications such as energy storage systems and electric vehicles.

In sharp contrast, bulk-type ASLBs (**Figure 4b**) are made up particulate mixture and fabricated by pressing. They have the potential for achieving high energy density through bi-polar stacking with ultra-high mass loading electrodes (**Figure 5**). It is much suitable to demands for future electrifications.[9 39] For the bulk-type ASLBs, noticeable differences compared with conventional LIBs (**Figure 1**) are follows: (i) electrodes include SE powders since they were fabricated, compared to the injection of LEs into the as-prepared cathode/separator/anode in the conventional LIBs. (ii) void space (or pores) in the bulk-type ASLBs are inevitably formed, in contrast to perfectly filled LIBs by wetting of LEs. Importantly, these points should be contemplated to design all-solid-state electrodes. For the effective utilization, almost monolith structure is required because pores decrease effective electric pathways within the ASLBs.[7, 43] Especially, in the perspective of the electrodes, ionic contacts between SEs and active materials must be optimized since SE powders are difficult to fully enclose on the surface of active materials.[19, 38] For the high energy density, optimal portion of active materials to SEs should be considered. Furthermore, the thickness of SE layer must be reduced as much as possible.[6]

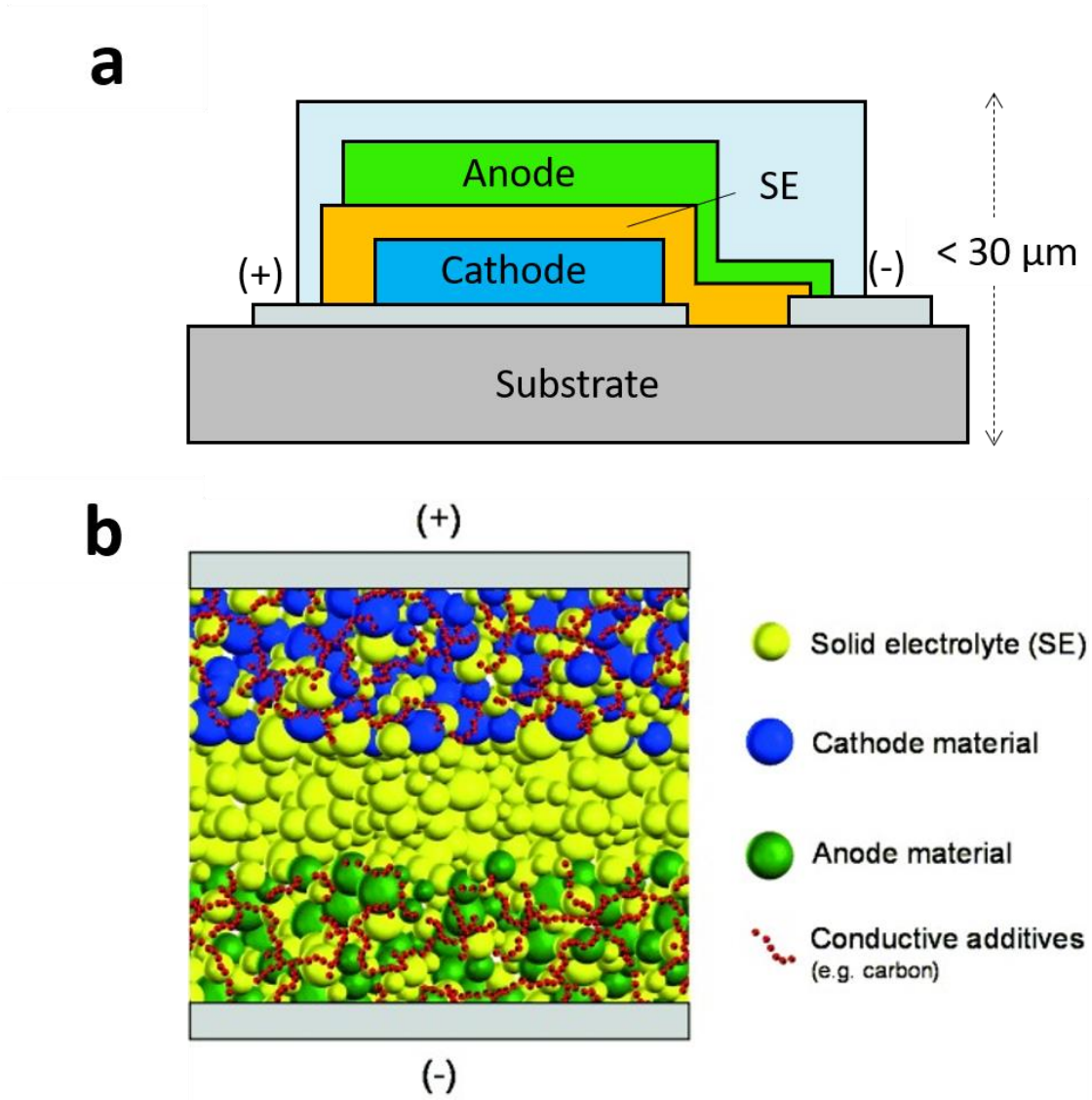

Figure 4. Schematic diagram for ASLBs. a) thin-film ASLBs. b) bulk-type ASLBs. Reproduced with permission.[5] Copyright 2015, Wiley-VCH.

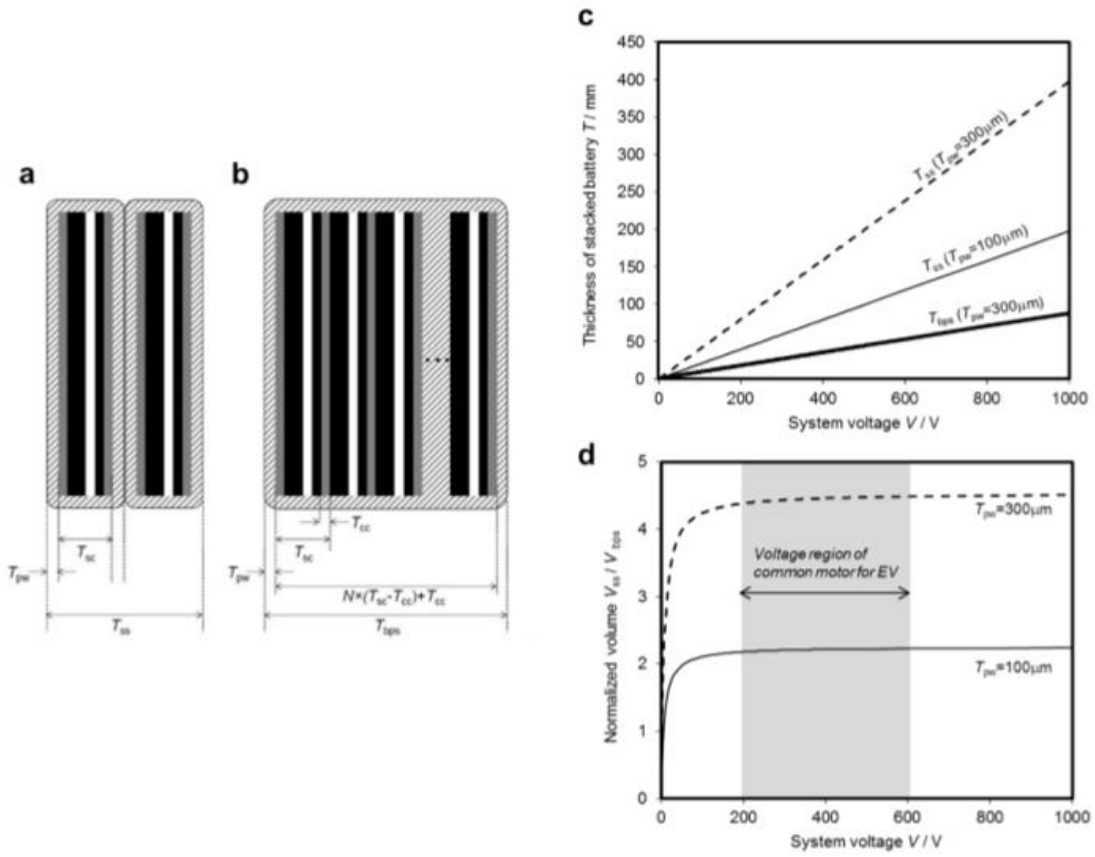

Figure 5. Volume efficiency of bi-polar stacking cells compared with sing-cell stacked system. Schematic diagrams for (a) sing-cell stacked batteries and (b) bi-polar stacking cells. (c) Battery system voltage varied by number of repeat units. (d) corresponding volume efficiency of bi-polar system to single-cell stacked system as a function of thickness of package (T_{pw}). Detailed information described in reference 9. Reproduced with permission.[9] Copyright 2016, Nature Publishing Group.

2.2.1 Sulfide solid electrolytes

To date, a plenty of SEs have been reported and they are categorized by their chemical compositions (or building units), for example, sulfides, oxides, halides, borohydrides, polymers (**Figure 6**).[2, 7, 10, 44-47] Among them, sulfide SEs have been suggested highly competitive in the development of bulk-type ASLBs due to their high ionic conductivity and great device integration (**Figure 7**).[7, 10] Several important classes are followed by: (i) Glass-ceramic $x\mathrm{Li_2S}$-$(100-x)\mathrm{P_2S_5}$ ($50 \leq x \leq 80$) exhibit Li^+ conductivity of around 1 mS cm^{-1},[11, 48] which are further evolved by introducing polarizable LiX (X= Br, I).[49] (ii) $Li_{10}GeP_2S_{12}$-structured derivatives (max. 25 mS cm^{-1}) shows state-of-the-art Li^+ conductivity,[9, 16] (iii) solution-processable Li_6PS_5X (X= Cl, Br) shows over 1 mS cm^{-1}.[34, 50-51] Their structure and (electro)chemical characteristics are strongly related to configurations of several polyhedron (e.g., PS_4^{3-}, $P_2S_7^{4-}$, $P_2S_6^{4-}$, MS_4^{4-}).[23, 47, 52-53] As well as high Li^+ conductivity of sulfide SEs, their deformable mechanical properties are also contributed to develop bulk-type ASLBs.[54] Young's moduli of sulfide SEs (18 – 25 GPa) are between oxide ceramics ($Li_7La_3Zr_2O_{12}$: 92 GPa, Li_2O-SiO_2 glasses: 70 – 80 GPa, Li_2O-P_2O_5: 50 GPa) and typical polymers (1 – 6 GPa), indicating an advantage for fabricating bulk-type ASLBs.[54] A sintering procedure at elevated temperature is necessary for all-solid-state electrodes employing oxide SEs (**Figure 7b**), but, it accompanies undesired side reaction with active materials.[55-56] In contrast, sulfide SEs can make at least ionic pathways in the electrodes by just cold-pressing (**Figure 7c**).[43, 57] In summary, high Li^+ conductivity and deformable mechanical properties of sulfide SEs contribute to lead promising electrochemical performance although drawbacks of sulfide SEs, such as intrinsic narrow electrochemical windows and poor air stability, are still remained.[19, 52, 58-59]

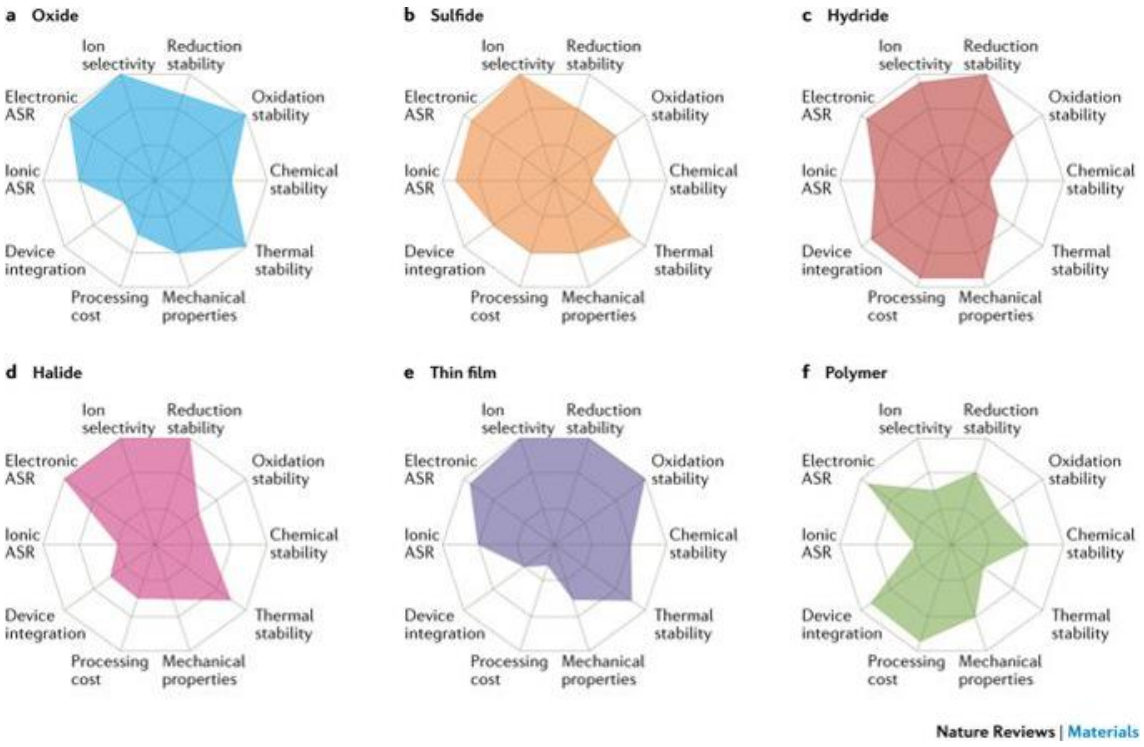

Figure 6. Rador plots of promising SEs. (a) inorganic oxide SEs, (b) inorganic sulfide SEs, (c) borohydride SEs, (d) halide SEs, (e) inorganic SEs for thin file ASLBs, (f) polymer SEs. Reproduced with permission.[10] Copyright 2017, Nature Publishing Group.

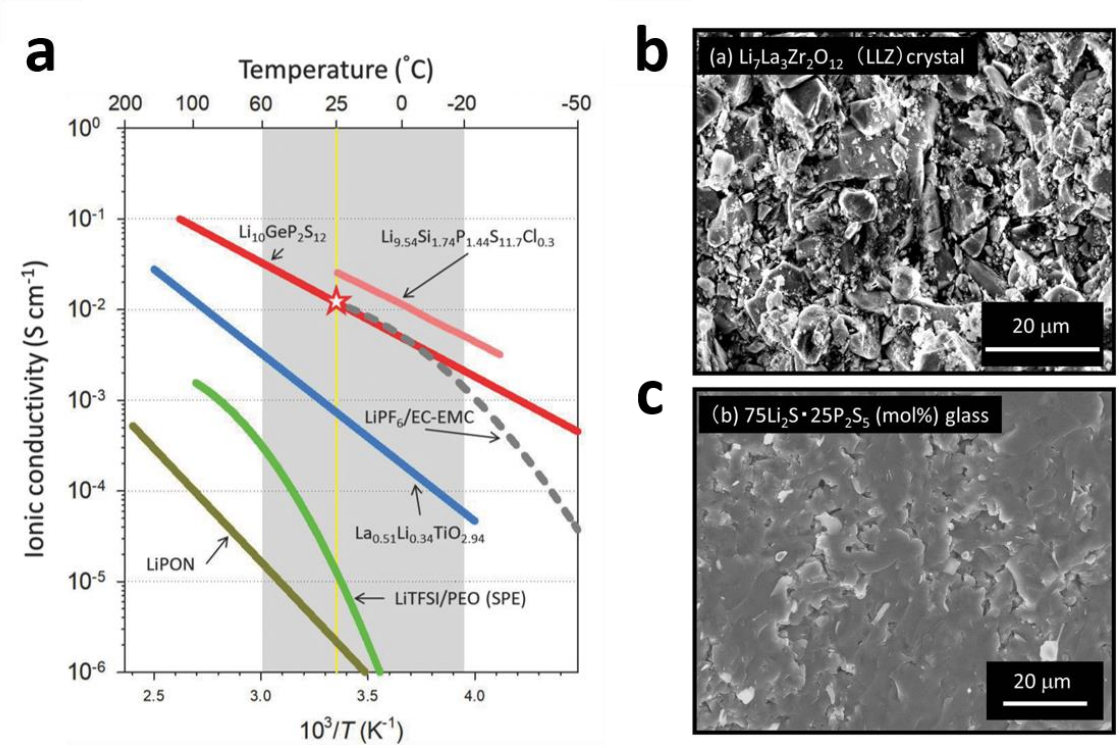

Figure 7. (a) Arrhenius plots of Li+ conductivities for representative SEs. Reproduced with permission.[7] Copyright 2018, Wiley-VCH. Cross-sectioned SEM images of SE pellets fabricated by cold-pressing at 370 MPa. (b) $Li_7La_3Zr_2O_{12}$ and (c) glass $75Li_2S$-$25P_2S_5$. Reproduced with permission.[43] Copyright 2013, Nature Publishing Group. Deformable sulfide SEs are formed to much densified pellet, comparing with oxide one.

2.2.2 Configurations of bulk-type all-solid-state lithium-ion batteries

A rocking-chair bulk-type ASLB fastened by a pressurizing jacket is shown in **Figure 8a**. For the half-cell test, Li-In electrodes having flat plateau at 0.62 V (vs. Li/Li^+) in the range of $0 \leq x \leq 1$ of the Li_xIn are selected as a counter electrode to avoid short-circuit caused by the dendritic Li (**Figure 8b**).[49, 60-62]

Typically, high pressure (< 70 MPa) has been applied under the operation of ASLBs to retain close contacts between active materials and SEs because contacts loss originated from volume changes of active materials during repeated cycling occurs degraded performance (**Figure 8a**).[63-64] Further breakthrough to down external pressure should be considered because it is hard to apply large areal applications. The interplay of the different materials within composite electrode influences on chemo(mechanical) characteristics in the bulk-type ASLBs. There might be marginal room for improvement enabled by mechanically compliant organic materials.

Owing to particulate structure of bulk-type ASLBs, multiple SEs are available to construct novel architecture as shown in **Figure 8c**, in contrast to conventional LIBs using only one LE.[5] Considering (electro)chemical properties or compatibility between active materials and SEs, optimal configurations could be reasonably designed. Hereafter, "bulk-type ASLB" is abbreviated to just "ASLB".

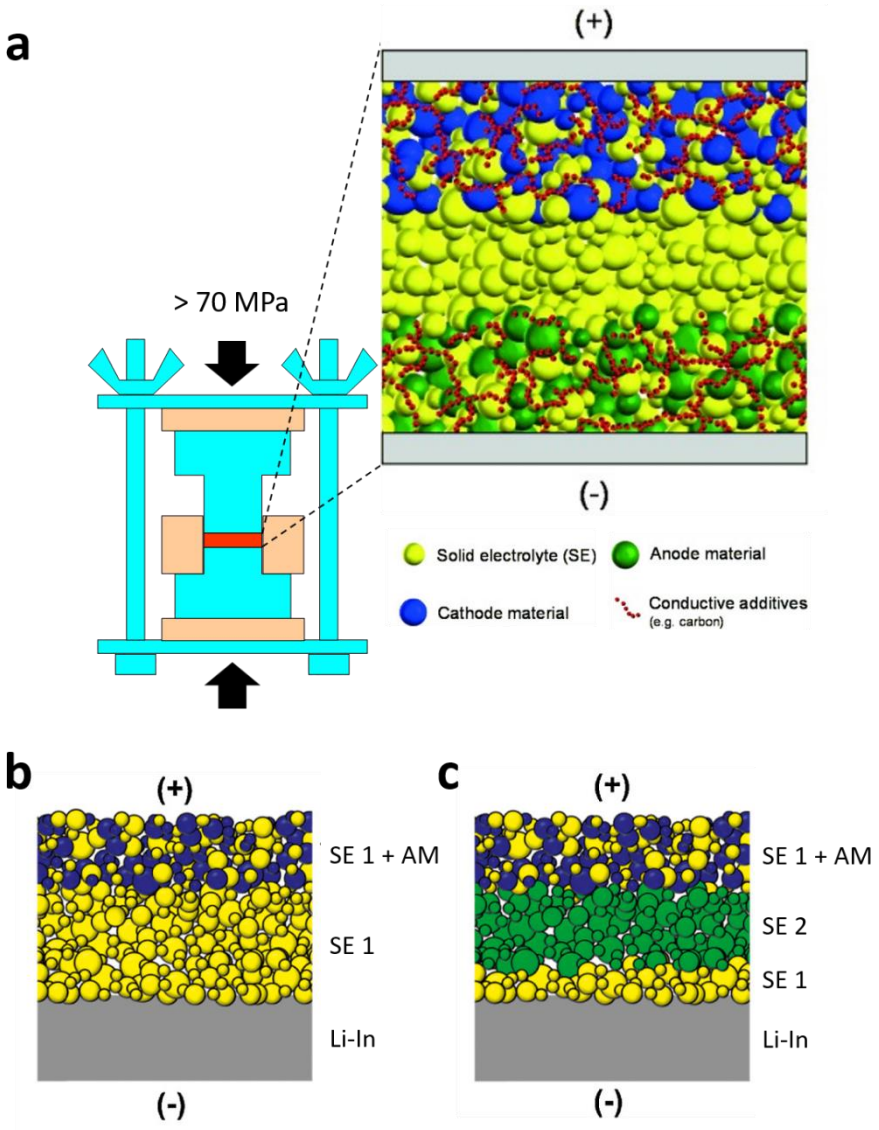

Figure 8. Schematic diagrams to illustrate configurations of bulk-type ASLBs. (a) a rocking-chair bulk-type ASLB fastened by a pressurizing jacket. Applied pressure is approximately 70 MPa. Reproduced with permission.[5] Copyright 2015, Wiley-VCH. (b) simple configuration for half-cell employing single SE. (c) half-cell comprised of multi SEs (yellow and green particles). Li-In is used as counter electrode. Reproduced with permission.[65] Copyright 2014, Elsevier.

2.2.3 Issues and challenges about sulfide all-solid-state electrodes

Understanding of electrochemical stability of SEs and interface issues where SEs in contacts with active materials is prerequisites to achieve optimal performance of ASLBs. For stable and convincing performance, electrochemical windows of SEs should be in line with operating voltage of electrodes and robust buffering phase should lie on interface between SEs and active materials.[32, 58, 65-66] However, experimental results and theoretical calculations have reported on intrinsically narrow electrochemical windows for sulfide SEs, recently. [58, 65-67] For example, (i) Li_6PS_5Cl in the $LiCoO_2$ electrode are spontaneously decomposed while forming P-$[S]_n$-P and cobalt sulfides during the charging process,[66-67] (ii) $Li_{10}GeP_2S_{12}$-deriveties in contact with Li metal suffer from continuous decomposition as a function of time.[68-69] Their subsequent stability is strongly affected by electric characteristics of decomposed products. A good interphase between SEs and active materials are ionically conducting and electronic insulating. In this regard, various coating materials comprised of Li^+ ionic conductors and protective technologies have been developed and certainly applied to ASLBs.[66]

Not only interfacial stability but also effective ionic contacts with active materials is also important. [7] Insufficient ionic surface coverage of active materials in the ASLBs decreases kinetics for electrochemical reactions, leading to lower utilization of electrodes.[18, 39] In this reason, entirely monolith electrodes are required to compensate insufficient ionic contacts between SEs and active materials. In addition, there were some negative cases in which conductive additives disturb facile ionic pathways between active materials and SEs, while they offer essential electronic pathways to active materials. [38, 70] Hence, all-solid-state electrodes consisting of too much carbon would exhibit below-par performance, compared with the conventional LIBs. It is important to balance ionic- and electronic- pathways within the electrodes. In other word, highly electronic conducting materials have a benefit in designing ideal electrodes.[57]

In the practical point of view, fabrication of scalable sheet-type electrodes is essential and inevitable. Slurry-mixed electrodes including a small amount of polymeric binders is common solution to fabricate sheet-type electrodes with processability. Unfortunately, poor chemical stability of sulfide SEs had impeded in the development of slurry process for sulfide SEs, hence, dry-mixed electrodes prepared by manual mixing have been widely used to explore ASLBs.[5, 32-33, 59, 65-67] Even if conventional dry-mixed electrodes have advantages to explore basic (or fundamental) issues easily, it is difficult to mass production owing to their fragility.[6]

Since the first demonstration of sheet-type electrodes enabled by nonpolar xylene and NBR (nitrile butadiene rubber) in 2014, [17] several succeeding studies were reported that electrically insulating polymeric binders caused disappointing performance.[18, 71-72] However, slurry process based on nonpolar solvents (toluene and xylene) and rubber-type binders (NBR and SBR) has been in a stalemate because chemical instability of sulfide SEs restricted available candidates.[73]

3. Experimental

3.1 Preparation of materials

To prevent air exposure, all procedures were conducted in glove filled by Ar. Residual water in the solvents was removed by molecular sieve or CaH_2 (95%, Sigma Aldrich) before used.

3.1.1 Sulfide solid electrolytes

LPS (Li_3PS_4) was prepared from Li_2S (99.9%, Alfa Aesar) and P_2S_5 (99.9%, Sigma Aldrich). The stoichiometric mixtures of precursors were mechanically milled by a planetary ball mill (Pulverisette 7PL; Fritsch GmbH) with Ar-sealed zirconia vial (80 mL) and zirconia balls of 115 g and heat-treated at 240 ºC for 1 h under vacuum. LGPS ($Li_{10}GeP_2S_{12}$) was obtained by heat treatment of a pelletized stoichiometric mixture of Li_2S, P_2S_5, and GeS_2 (99.9%, American Elements) at 550 °C for 10 h under vacuum. LPSCl (Li_6PS_5Cl) was prepared by a planetary ball mill and subsequent heat treatment at 550 ºC for 5 h under Ar atmosphere. The stoichiometric mixtures of Li_2S, P_2S_5, and LiCl (99.99%, Sigma Aldrich) were ball-milled at 600 rpm for 10 h in with a zirconia vial (80 mL) with zirconia balls. β-LPS powders was synthesized *via* wet-chemical routes using tetrahydrofuran (THF, 99.9%, anhydrous, Sigma Aldrich). The stoichiometric mixtures of Li_2S and P_2S_5 were stirred in THF at 30 ºC for 9 h, followed by drying (80 ºC, for 2 h) and subsequent heat treatment (150 ºC, for 1 h) under vacuum. LPS-polymer samples were acquired from same wet-chemical method for β-LPS except for that 5.5 wt% polymers were added in reacting batch. Polymers were NBR (nitrile-butadiene rubber, Sigma Aldrich) and PVC (polyvinyl chloride, Sigma Aldrich).

3.1.2 Solvate Ionic Liquids

For [Li(glyme)$_x$]TFSI (x = 1, 4), the stoichiometry mixtures of LiTFSI (Lithium bis(trifluoromethanesulfonyl)imide, 99%, Sigma Aldrich) and purified G3 (triethylene glycol dimethyl ether, 99%, Sigma Aldrich) were stirred for 24 h at ambient temperature. At x = 1, [Li(glyme)$_x$]TFSI turned into SILs having an ionic-liquid-like behaviors.

3.2 Materials characterizations

The powder X-ray diffraction (XRD) patterns were collected by using a D8-Bruker Advance diffractometer or MiniFlex600 equipped with Cu Kα radiation (1.54056 Å) at 40 kV and 40 mA. To avoid air exposure, samples were sealed by Be window and mounted on the instruments. The field-emission scanning electron microscopy (FESEM) image and energy dispersive X-ray spectroscopy (EDXS) elemental maps were acquired by S-4800 (Hitachi) or JSM-7000F (JEOL). The high-resolution transmission electron microscopy (HRTEM) images and electron crystallography patterns (ED) were

collected by JEM-2100F (JEOL) with 200 kV and 0.105 mA. Raman spectra were obtained by using Alpha300S (Witec Instrument) equipped a 532 nm Nd-YAG laser and homemade holder to prevent air exposure. Thermogravimetric analysis (TGA) were conducted by using Q50 (TA Instrument Corp.) and Ar carrier gas. UV-vis molecular absorption spectra were collected by Cary 5000 (Agilent Technologies). The static and magic angle spinning (MAS) ^{7}Li NMR spectra were recorded using a Varian VNMRS 600 with 1.6 mm MAS HXY triple-resonance probe at Larmor frequencies of 233 MHz. The spinning rate was 25 kHz for MAS ^{7}Li NMR. LiCl used for a reference.

3.3 All-solid-state electrodes fabrication

The dry-mixed electrode has advantages to explore basic considerations in the development of ASLBs, but it is hard to scalable production in terms of large areal processability. On the other hand, the slurry-mixed electrode is prepared from particulates with binder solution, forming a sheet on current collectors.

3.3.1 Dry-mixed electrode

The composite electrodes including active materials, SEs, or carbon additives were prepared by manual mixing for 20 min.

3.3.2 Slurry-mixed electrode

Slurries consist of active materials, SEs, polymeric binders, processing solvents, carbon additives, or SILs were blended by Thinky mixer (AR-100) at 2000 rpm for 5 min. As-prepared slurries were coated on current collector (Al for cathode, Ni for anode) *via* doctor-blade method, followed by drying under vacuum.

3.4 Electrochemical characterizations

3.4.1 All-solid-state cell assembly

To fabricate ASLBs, 150 mg of SE powders (LPS or LGPS or LPSCl) were pelletized by hydraulic press at 70 MPa at RT to form SE layer. The as-prepared composite electrodes for cathode and anode (or Li-In electrode) were loaded on each side of the SE layer. Finally, the tri-layers were pelletized at 370 MPa at RT. The Diameter in pelletizers (Ti) and a mold (polyaryletheretherketone) was 13 mm. The as-fabricated all-solid-state cells were fastened by a pressurizing jacket as shown in **Figure 8**.

3.4.2 Electrochemical impedance spectroscopy

AC impedance data were collected by VSP-300 (Biologics) or Iviumstat (IVIUM Technologies Corp.) with an amplitude of 10 (or 14.1) mV in range of 1.5 MHz to 10 mHz. Nyquist plots for ASBL half-cells were acquired after charging to terminal voltage and rest for 3 h.

3.4.3 Galvanostatic charge/discharge test

For $LiFePO_4$ (LFP) electrodes, they were examined in the rage of 2.5 – 4.0 V (vs. Li/Li^+) at 30 ºC. 1C was 150 mA g^{-1}. For $Li_4Ti_5O_{12}$ (LTO) electrodes, they were examined in the rage of 1.0 – 2.5 V (vs. Li/Li^+) at 30 ºC. 1C was 170 mA g^{-1}. For $LiNi_{0.6}Co_{0.2}Mn_{0.2}O_2$ (NCM622) or $LiNi_{0.7}Co_{0.15}Mn_{0.15}O_2$ (NCM711) electrodes, NCM were examined in the rage of 3.0 – 4.3 V (vs. Li/Li^+) at 30 (or 60) ºC. 1C was 174 mA g^{-1} for NCM622 and 196 mA h g^{-1} for NCM711. For graphite electrodes, they were examined in the rage of 0.005 – 2.0 V (vs. Li/Li^+) at 30 ºC. 1C was 360 mA g^{-1}. Detailed information of electrodes for ASLBs is summarized in **Table 1**.

3.4.4 Galvanostatic intermittent titration technique

Galvanostatic intermittent titration technique (GITT) was conducted to extract polarization of electrodes and calculate ionic contact area between NCM622 and SE. By subtracting the closed-circuit voltage (CCV) from quasi-open-circuit voltage (QOCV) in the transient voltage profiles, the polarization curves were extracted. To comparative study of ionic percolations in the electrodes, the ionic surface coverage of NCM622 was obtained by the **Equation 1**.

$$\text{Surface coverage [\%]} = \frac{S_{\mathrm{SE}}}{S_{\mathrm{NCM}}} = \frac{2m_{\mathrm{NCM}}\cdot\Delta E_{\mathrm{S}}\cdot V_{\mathrm{m}}}{S_{\mathrm{NCM}}\cdot M_{\mathrm{NCM}}\cdot\Delta E_{\mathrm{t}}\cdot(\pi D\cdot\tau)^{0.5}}$$

(Equation 1)

S_{SE}: ionic contact area between active materials and SEs

S_{NCM}: surface area of NCM powders obtained by the N_2 adsorption-desorption isotherm (0.64 m^2 g^{-1})

m_{NCM}: mass of NCM in the electrodes

ΔE_S: voltage change at steady state

V_m: molar volume of NCM (20.29 cm^3 mol^{-1})

M_{NCM}: molecular weight of the host NCM622 (90.13 g mol^{-1})

ΔE_S: transient voltage change

D: Li^+ diffusion coefficient of NCM obtained from the GITT result of NCM/Li cells using liquid electrolytes

τ: pulse duration (60 s)

Project	Active material	Composition (weight ratio)	Mass loading [mg cm^{-2}]	Note	Figure
1[a)]	$LiFePO_4$	37.7 : 56.6 : 0.0 : 5.7	2.84	LGPS	
		37.7 : 50.9 : 5.7 : 5.7	2.84	LGPS	
	$Li_4Ti_5O_{12}$	49.8 : 49.8 : 0.0 : 0.5	3.75	LPS	
		49.8 : 44.8 : 5.0 : 0.5	3.75	LPS	
2[b)]	$LiNi_{0.6}Co_{0.2}Mn_{0.2}O_2$	70.0 : 27.5 : 1.5 : 1.0	2.76	NBR	
		70.0 : 27.5 : 1.5 : 1.0	2.76	PVC	
	Graphite [b)]	50.0 : 47.5 : 2.5 : 0.0	1.86	NBR	
3[c)]	$LiNi_{0.6}Co_{0.2}Mn_{0.2}O_2$	70.0 : 27.5 : 0.0 : 1.5 : 1.0	15		
		70.0 : 26.5 : 1.0 : 1.5 : 1.0	15		
		70.0 : 24.0 : 3.5 : 1.5 : 1.0	15		
	$LiNi_{0.7}Co_{0.15}Mn_{0.15}O_2$	80.0 : 17.5 : 0.0 : 1.5 : 1.0	45		
		83.0 : 13.7 : 1.6 : 0.7 : 1.0	30		
		80.0 : 15.0 : 2.5 : 1.5 : 1.0	45		

Table 1. Specifications of electrodes. [a)] active material : LGPS (or LPS) : LiG3 : C, [b)] active material : β-LPS : NBR (or PVC) : C, [c)] active material : LPSCl : LiG3 : NBR: C

4. Results and discussion

4.1 Hybrid sulfide solid electrolytes employing solvate ionic liquids

The electrochemical performance of ASLBs is strongly governed by a heterogenous interface where the surface of active materials is enclosed by SEs.[5, 7] Deformable sulfide SEs can easily form 2-dimensional contacts with active materials through simple cold-pressing without hot sintering, resulting in approved performance compare to that of oxide counterparts.[43, 54] Even if sulfide SEs are considered as enough deformable materials, fabrication of monolithic electrodes is restricted owing to an intrinsic attribute of the solid. For this reason, the reversible capacities of ASLBs employing sulfide SEs have appeared to be much lower than those obtained from conventional LIBs. There is clearly room for improvement.

In this regard, hybrid configurations comprised of sulfide SEs with a small amount of LE could be suggested a general solution because a soft and fluidal LE compensate insufficient ionic pavement in the electrodes while filling void space.[74-75] However, there are no any reports about hybrid configurations based on sulfide SEs because of highly incompatible nature of the sulfide materials toward conventional LEs that are Li salt dissolved organic solvents. To develop hybrid ASLBs based on sulfide SEs, the following contradictory situations should be handled: (i) sulfide SEs dissolve or react with polar Lewis-basic solvents. (ii) Solvents for common LEs have highly polar with Lewis-basic functional groups to dissolve Li salt. These troublems led me to recent research addressing alternative LEs to suppress polysulfide dissolution in Li–S batteries.[76-79] According to prior literatures, polysulfide dissolution was suppressed by abnormally high concentrated electrolytes. Especially, SILs, the equimolar complex of Li salt and glyme (linear ether), have an excellent effect in suppressing polysulfide dissolution.[76-78] Also, their unexpected oxidative stability and thermal stability are noticeable.[40]

In this section, the excellent stability of sulfide SEs with SILs and applications of LiG3-LPS (or LGPS) for bulk-type ASLBs are demonstrated. The compatibility of sulfide SEs toward glyme-based LEs varied by concentration are investigated by multiple ways *via* direct observations, XRD, UV-vis, and EIS. LiG3 is an enabler to compensate insufficient ionic contacts within ASLBs, leading to dramatically improved capacity for LFP electrodes.

4.1.1 Compatibility test for hybridization

For a systematic investigation of the interplay between sulfide SEs toward glyme-based LEs, three liquid samples were prepared; (i) G3 (triglyme or triethylene glycol dimethyl ether), (ii) $Li(G3)_4TFSI$ ($LiTFSI/G3 = 1/4$, $Li(G3)_4$), (iii) Li(G3)TFSI ($LiTFSI/G3 = 1/4$, Li(G3). LPS (1.0 mS cm^{-1}) and LGPS (6.0 mS cm^{-1}) are selected as a model SE.

To check feasibility about combining sulfide SEs and glyme-based LEs, dissolution test was assessed. The change in color directly indicated that both LPS and LGPS were dissolved into glyme-based liquids except for only LiG3 (**Figure 9**). The G3, one of liner ethers, are well known as good solvent for LEs due to its higher donor ability of oxygens to Lewis-acidic Li^+,[80] which also implies the possibility of dissolution (or reaction) problems with sulfide materials. In this regard, the dissolution of sulfide SEs into glyme-based liquids is acceptable. Unprecedentedly, sulfide SEs (LPS and LGPS) have negligible solubility in the LiG3, which implies their excellent chemical compatibility. For comparison studies about the trends observed in **Figure 9**, UV–vis molecular absorption spectroscopy and ICPOES carried out. In the **Figure 10**, the results of UV–vis spectra and weight fraction of dissolved elements (obtained by ICPOES) are consistent in the direct observation. Notably, dissolution of sulfide SEs was decreased as an increase in concentration of Li salt (LiTFSI). In addition, solubility for LGPS is lower than LPS.

Corresponding their phase analyses were conducted using XRD as depicted in **Figure 11**. Only hybrid SEs employing LiG3 were remained their original crystal structure without significant impurities, even after kept for 2 days. For the sulfide SEs with $Li(G3)_4$, LPS-$Li(G3)_4$ exhibited intense unknown peaks compared with LPS-$Li(G3)_4$, indicating that the stability of LPS toward the $[Li(glyme)_x]TFSI$ ($x > 4$) is inferior to that of LGPS. The same trend regarding poor stability of the LPS compared to that of the LGPS was also revealed in another case of solvent-salt complex (or superconcentrated LE), $Li(AN)_2TFSI$ as shown in **Figure 12**.

Preceding observations regarding compatibility of sulfide SEs in contact with glyme-based liquids varied by concentration might be rationalized by **Figure 13**. Strongly Lewis-basic oxygen in G3 prefers to interact with electrophile, which results in nucleophilic attack to electrophile P-S (or Ge-S) bonds (**Figure 1**) while accompanying dissolution problems (**Figure 9, 10**). In the case of increasing concentration of Li^+, interaction between Lewis-basic oxygen in G3 and sulfide SEs become weak owing to the strong complexation of glyme with Li salts in the $[Li(G3)]^+$, leading to significantly suppressed dissolution at the case of LiG3. In particular, a negligible free-solvent in SILs enables great compatibility of sulfide SEs. Furthermore, the better stability of LGPS than LPS might be accounted for HSAB theory (**Figure 2**, see the intro section).

Although SIL (LiG3) is chemically stable to sulfide SEs, strong advantages (e.g., thermal stability, no leakage, and etc.) of sulfide SEs could be degraded by adding LiG3. **Figure 14** compares the appearance of the pristine SE and hybrid SE containing 10wt% of LiG3 as well as thermal stability assessed by TGA. Hybrid SEs still kept powder-like behaviors (**Figure 14a, b**) and moderate thermal stability at least 130 °C due to ionic-liquid-like behavior of SILs (**Figure 14c**). The hybrid SEs were prepared by mechanical milling

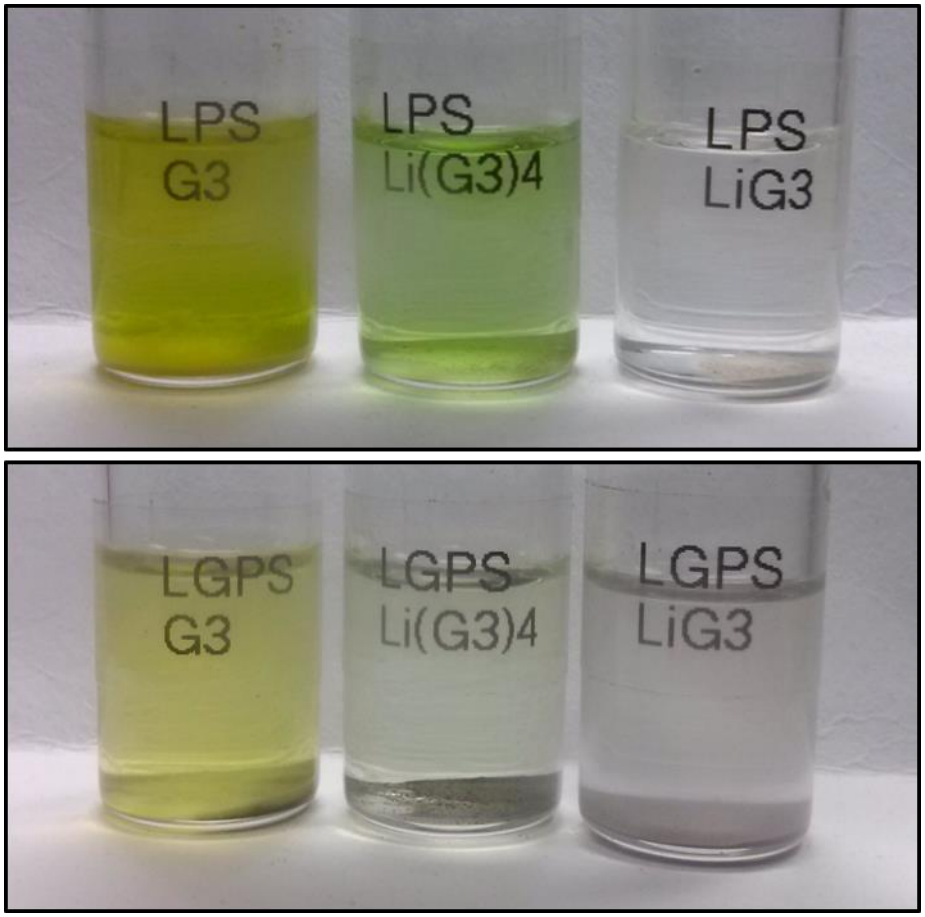

Figure 9. Dissolution test of sulfide SEs with G3-based liquids ([Li(G3)x]TFSI, $1 \leq x$). Direct observed results of LPS or LGPS with G3, $Li(G3)_4$, and Li(G3) after kept for 7d. All the liquid samples are transparent originally. Reproduced with permission.[38] Copyright 2015, Wiley-VCH.

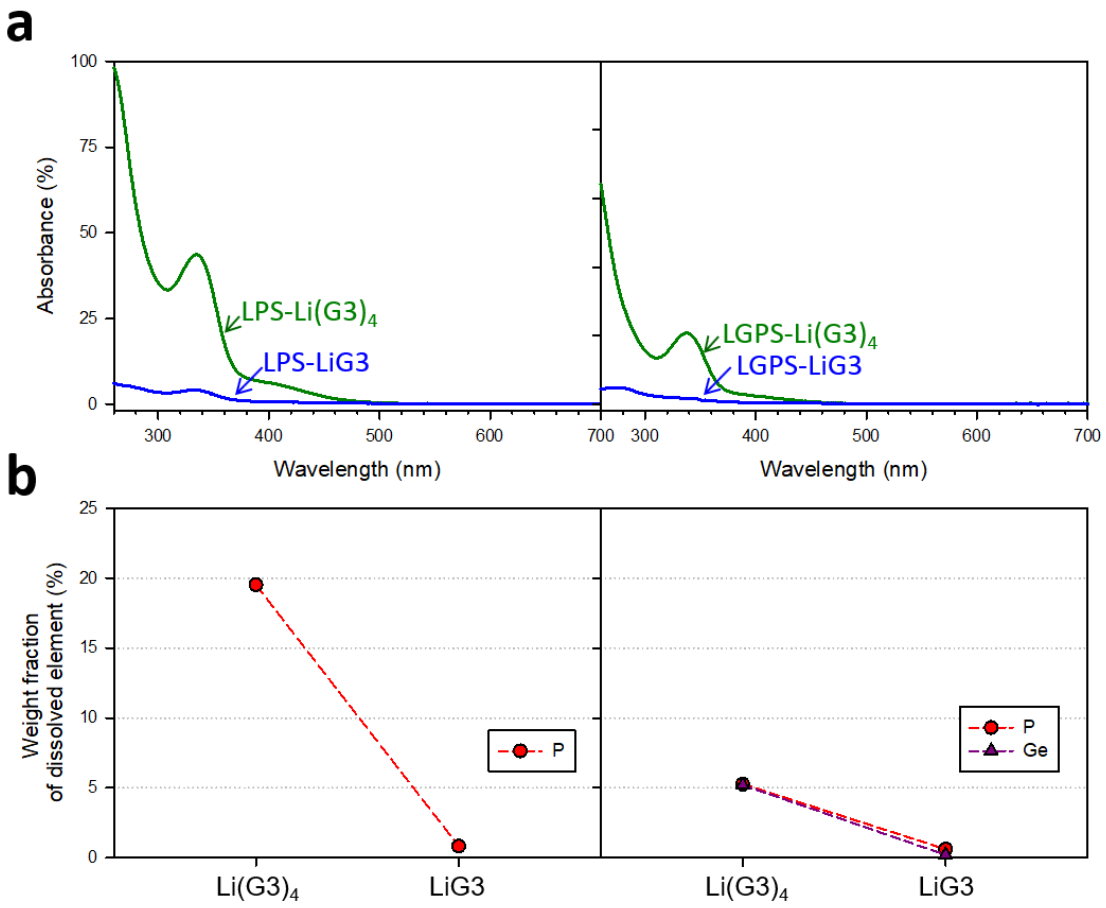

Figure 10. Comparative study to estimate an amount of dissolved species from SEs to liquids. (a) UV-vis absorption spectra for LPS and LGPS. (b) Plots for weight fraction of dissolved elements for LPS and LGPS, which were calculated from ICPOES measurements. Reproduced with permission.[38] Copyright 2015, Wiley-VCH.

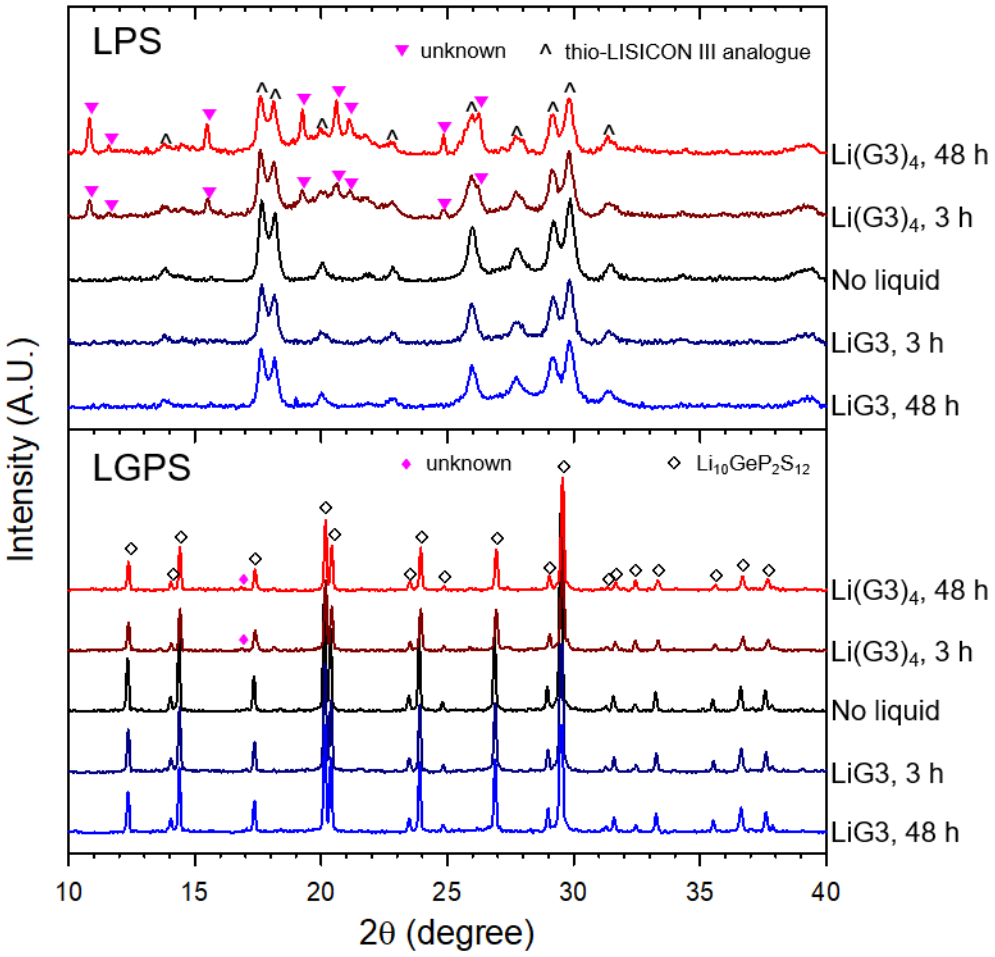

Figure 11. XRD patterns of LPS (or LGPS) with Li(G3) (or $Li(G3)_4$) varied by storage time. Reproduced with permission.[38] Copyright 2015, Wiley-VCH.

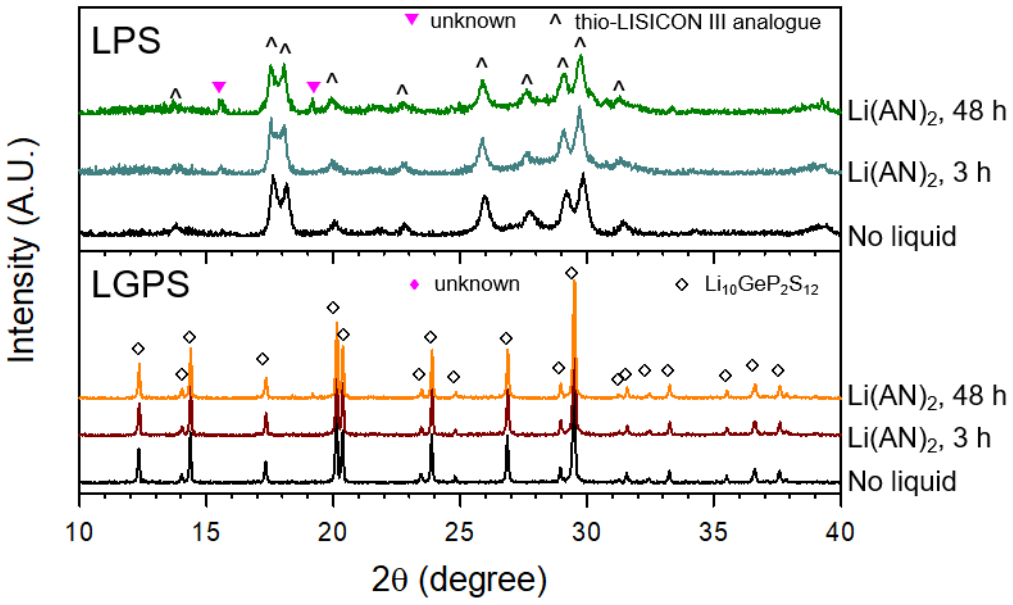

Figure 12. XRD patterns of LPS (or LGPS) with another type of superconcetrated LEs, $Li(AN)_2TFSI$ (LiTFSI/ACN = 1/2, referred as to $Li(AN)_2$). Reproduced with permission.[38] Copyright 2015, Wiley-VCH.

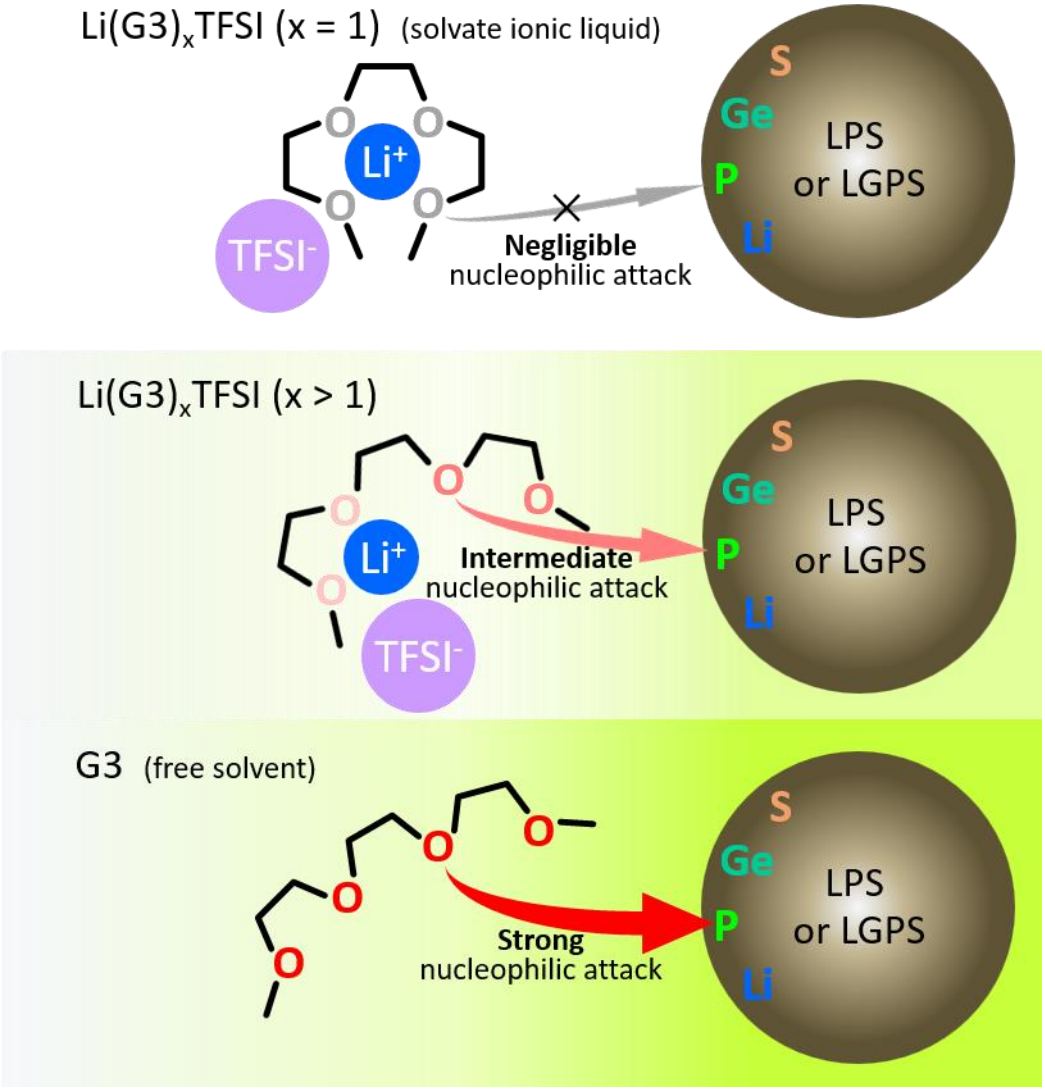

Figure 13. Schematic diagrams representing the interplay between sulfide SEs (LPS, LGPS) and G3-based liquids (G3 and $Li(G3)_xTFSI$). Reproduced with permission.[38] Copyright 2015, Wiley-VCH.

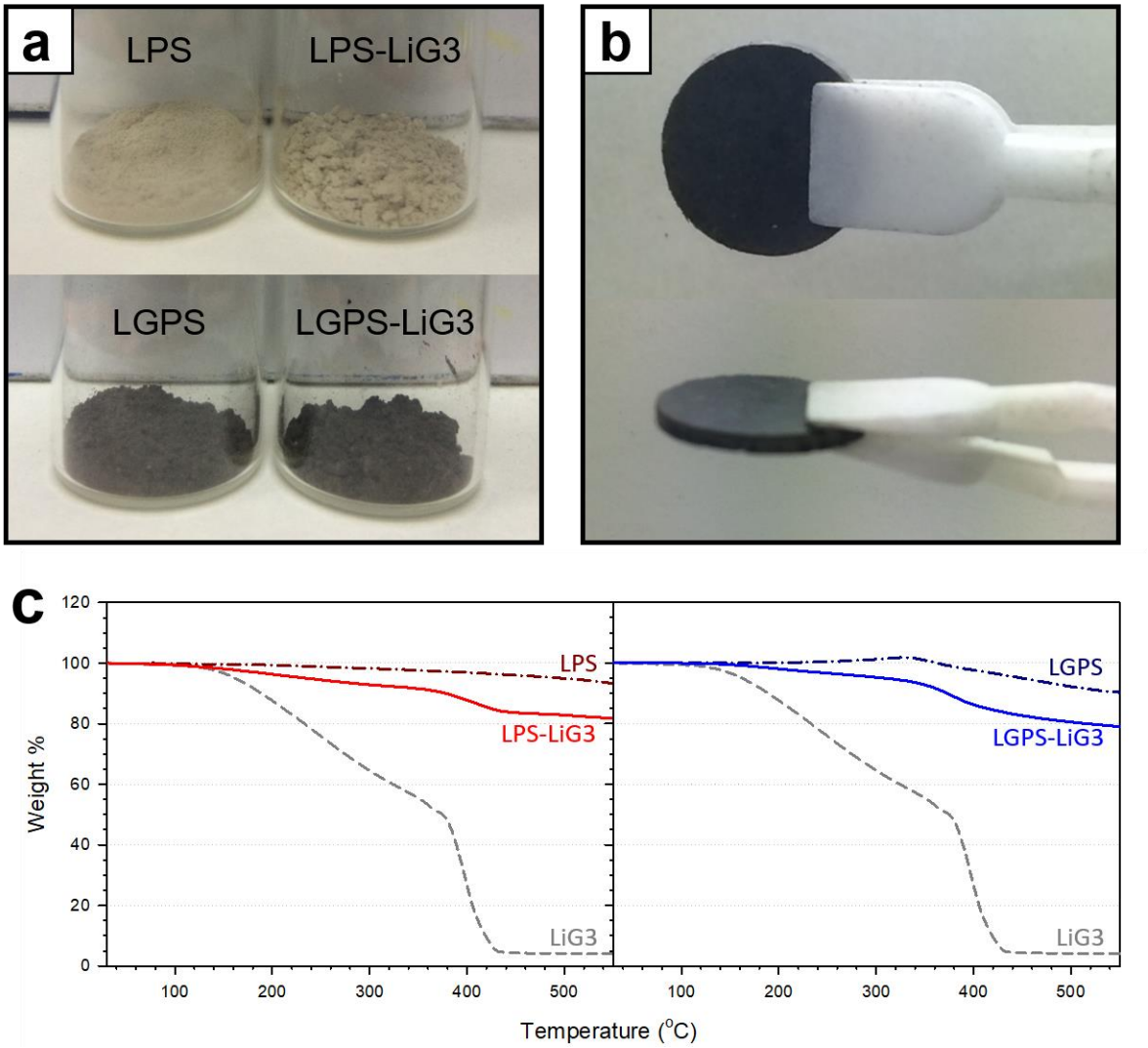

Figure 14. Physical properties of hybrid SEs (SE-LiG3). (a) photographic images of pristine powders and SE-LiG3 powders. (b) photographs of pelletized LGPS-LiG3. (c) TGA analysis results of SEs, LiG3, SE-LiG3. The weight ratio of SE to LiG3 is 9 to 1. Reproduced with permission.[38] Copyright 2015, Wiley-VCH.

4.1.2 Electrochemical characterization

The electrochemical performance of ASLBs employing LiG3 was evaluated by using LFP electrodes. Detailed information for electrodes and test conditions are summarized in **Table 1** and **experimental section**, respectively. Surprisingly, LFP electrode with LiG3 (5.7 wt%) shows a reversible capacity of 144 mA h g^{-1} at 0.1C (17 mA g^{-1}), in contrast to negligible capacity obtained from without LiG3 (**Figure 15**). A similar achievement was also confirmed in the case of LTO/Li-In half cells. The LTO electrode with LiG3 (5 wt%) exhibited 1.5 times higher a reversible capacity (127 mA h g^{-1}), compared with 89 mA h g^{-1} at 0.2C (35 mA g^{-1}) for without LiG3 (**Figure 16**).

As shown in **Figure 17** for representing the microstructure of the composite electrodes, there are inevitably formed void spaces (or pores) because cold-pressing is insufficient to fabricate monolithic electrodes. Porosities, calculated from specific densities per measured densities (**Table 2**), for each electrodes support **Figure 17**. As expected, the porosities of electrode (40.4% for LFP and 27.5% for LTO) were remarkably decreased by introducing LiG3 (28.8% for LFP with LiG3 and 20.8% for LTO with LiG3). These results imply that LiG3 wets or occupies the surroundings of the pores, resulting in improved effective ionic contacts between the active materials and SEs (**Figure 17**). This is reason why ASLBs including LiG3 outperformed without LiG3.

A control experiment was conducted to reveal the extremely inferior performance of LFP in ASLBs. It is common sense that LFP is usually treated by carbon coating due to its severely low electric conductivity. Carbon coating layers on LFP was verified by HRTEM and corresponding EDXS (**Figure 18**). These carbon layers on LFP act as a physical barrier blocking Li^+ conduction between LFP and SE. To verify a side effect of carbon layer on LFP in the ASLBs, two symmetric Li-ion blocking cells without and with LiG3 were prepared and tested by AC impedance method (**Figure 19**). Cell configurations are Ti/LGPS/C/LGPS/Ti and Ti/LGPS/(C-LiG3)/LGPS/Ti, respectively. Artificial carbon layer (2-3 nm) sandwiched by two LGPS layer was fabricated from C sputtering on one side of cold-pressed LGPS pellet. For the Ti/LGPS/(C-LiG3)/LGPS/Ti, as-prepared carbon layer at the surface of LGPS pellet was wetted by LiG3 of 5 μL. In **Figure 19b**, a symmetric cell without LiG3 (Ti/LGPS/C/LGPS/Ti) displayed meaningless noisy signal, in sharply contrast to clear semicircle with Warburg tail obtained for a symmetric cell with LiG3 (Ti/LGPS/C-LiG3/LGPS/Ti). These results strongly support that LiG3 paves the ionic conduction pathways in between the LFP and SE domains.

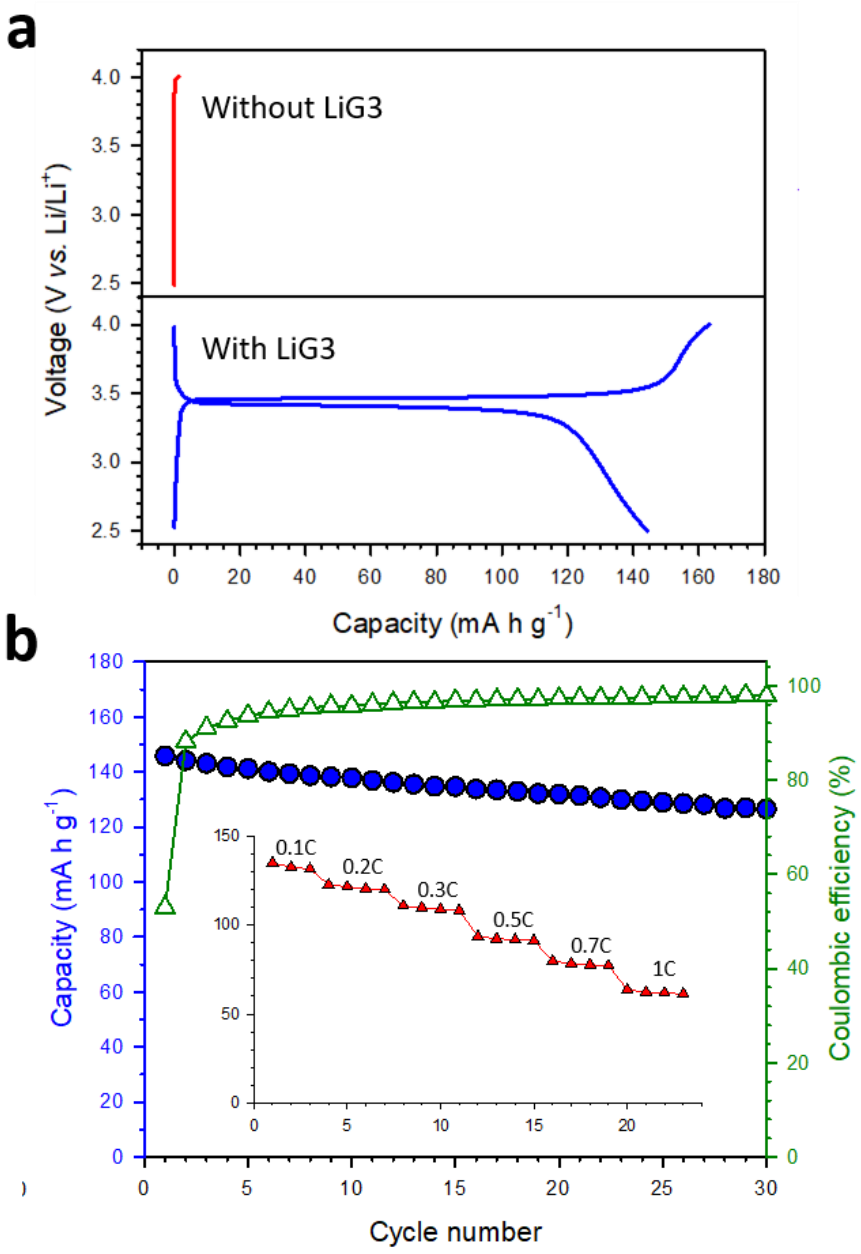

Figure 15. Comparative electrochemical characterizations of LFP/Li-In half-cell at 30 °C. (a) Second cycle voltage profiles of LFP with (blue) and without LiG3 (red). (b) Cycle performance of LFP with LiG3. The rate performance is shown in the inset. Reproduced with permission.[38] Copyright 2015, Wiley-VCH.

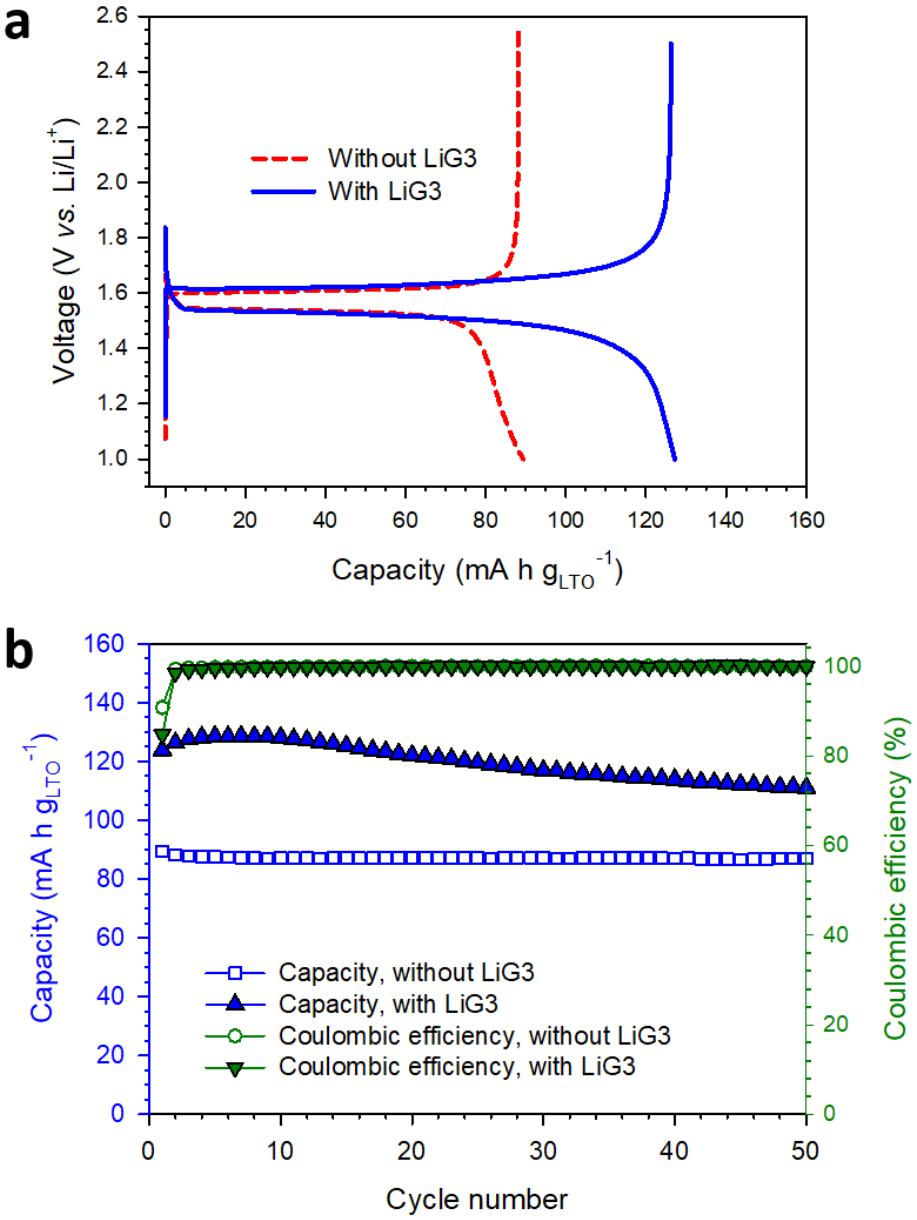

Figure 16. Comparative electrochemical characterizations of LTO/Li-In half-cell at 30 °C. (a) Second cycle voltage profiles of LTO with (blue) and without LiG3 (red). (b) cycle performance of LTO with and without LiG3. Reproduced with permission.[38] Copyright 2015, Wiley-VCH.

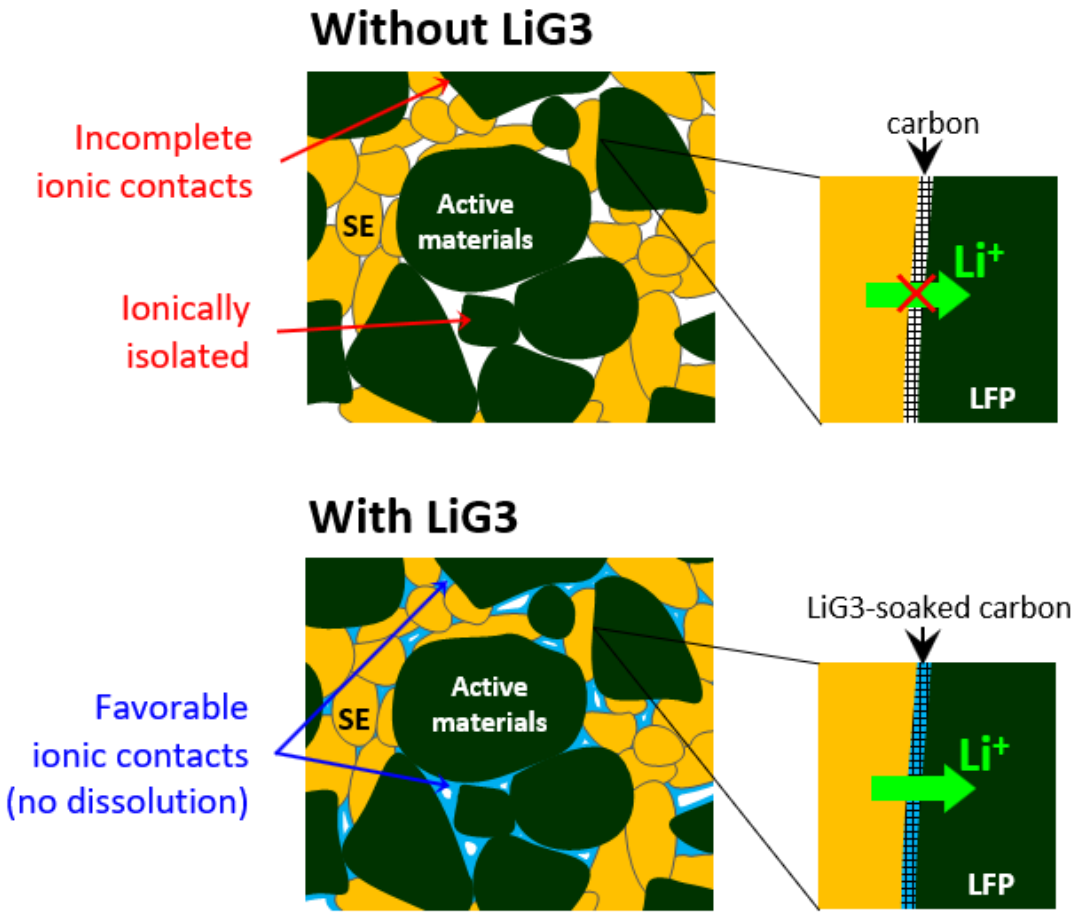

Figure 17. Illustrations for the composite electrodes without and with LiG3, respectively. The LiG3 compensates imperfect solid-solid contacts through filling or paving void spaces. For an intuitive explanation, carbon additives in the composite electrode are omitted. Reproduced with permission.[38] Copyright 2015, Wiley-VCH.

Electrode	Weight ratio [wt%]	Volume of LiG3 [μL cm^{-2}]	Porosity [%]
LTO	49.8:49.8:0.5 (LTO:LPS:C)	-	27.5
LTO with LiG3	49.8:44.8.0.5:5.0 (LTO:LPS:C:LiG3)	0.52	20.2
LFP	37.7:56.6:5.7 (LFP:LGPS:C)	-	40.4
LFP with LiG3	37.7:50.9:5.7:5.7 (LFP:LGPS:C:LiG3)	0.30	28.8

Table 2. Porosities of composite electrodes without and with LiG3. Porosity of samples are calculated by following:

Porosity [%] = $100 - 100\sum(A_i M/\rho_i)/[(\pi/4)\cdot D^2\cdot t]$

A_i: weight fraction of i in the composite

M: weight of the pellet

D: diameter of the pellet

t: thickness of the pellet

ρ_i: apparent density (ρ_{LPS} = 1.87 g cm^{-3}, ρ_{LGPS} = 2.035 g cm^{-3}, ρ_{LiG3} = 1.46 g cm^{-3}, ρ_C = 2.0 g cm^{-3}, ρ_{LTO} = 3.5 g cm^{-3}, ρ_{LFP} = 3.6 g cm^{-3})

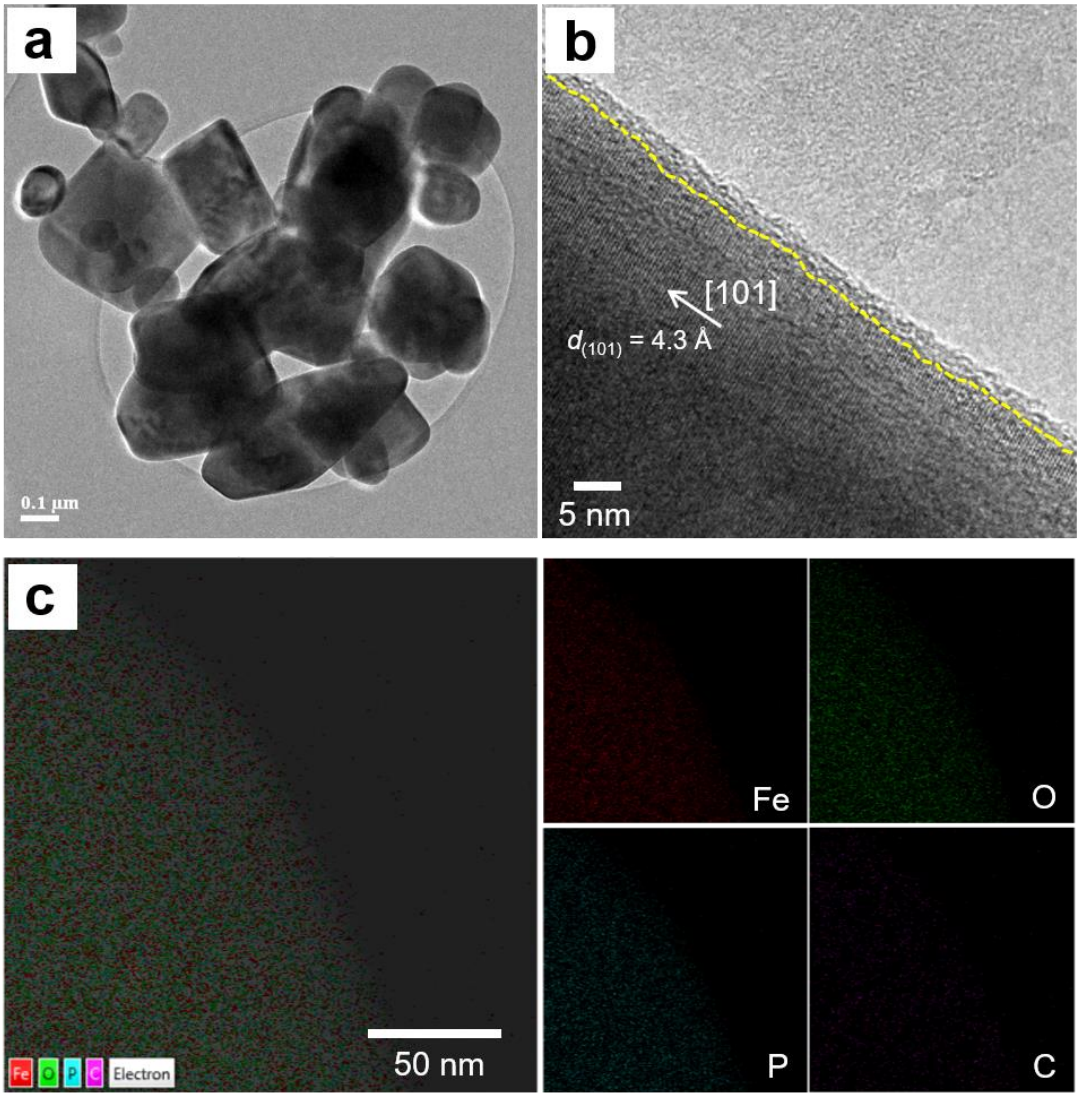

Figure 18. HRTEM images for LFP powders. (a) and (b) are bright-field image. Amorphous carbon layers (less than 2 nm) is observed. (c) corresponding elemental mapping of LFP. Notably, homogeneously distributed C (purple) are closely match to elements of LFP, indicating uniform carbon coating on the LFP particle. Reproduced with permission.[38] Copyright 2015, Wiley-VCH.

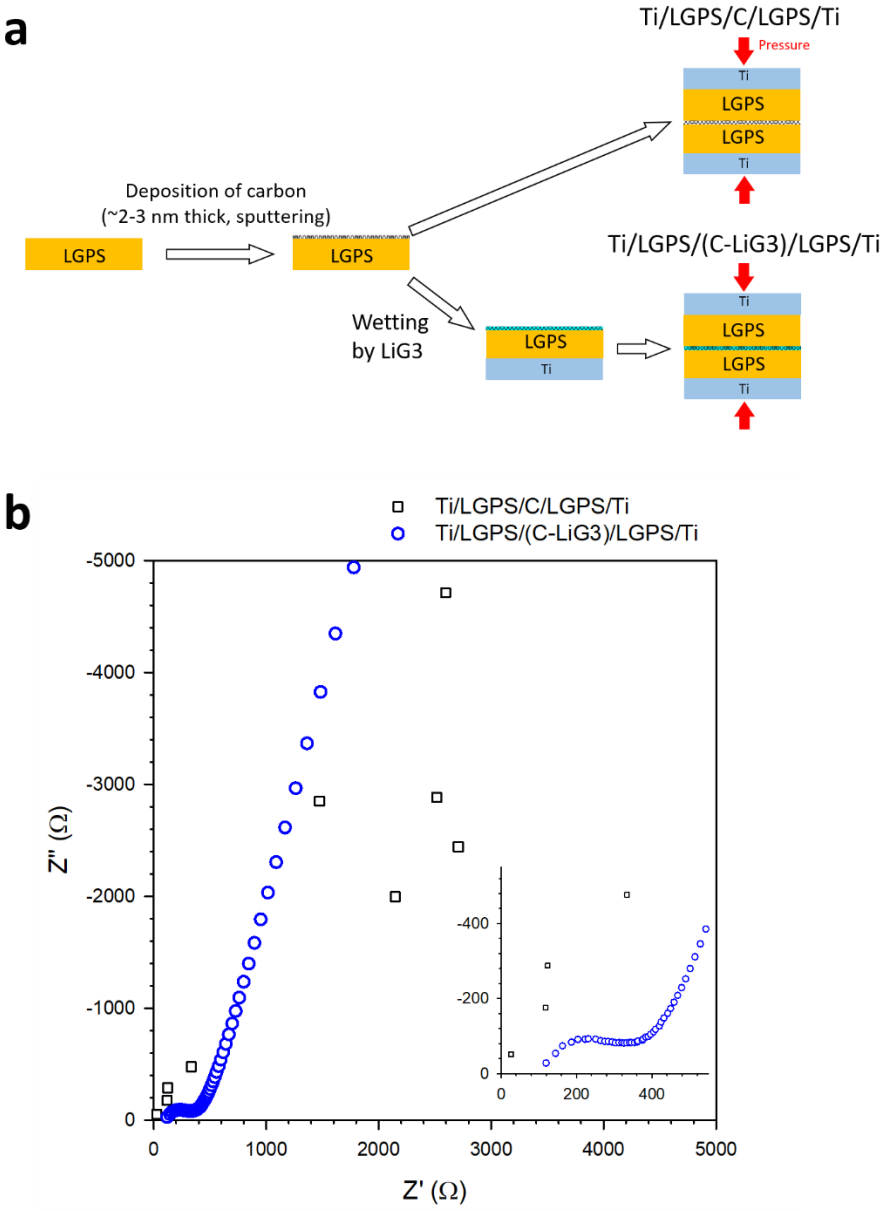

Figure 19. (a) sequence diagrams representing the preparation of Li-ion blocking symmetric cells (Ti/LGPS/C/LGPS/Ti and Ti/LGPS/(C-LiG3)/LGPS/Ti). (b) Nyquist plots for two symmetric cells. Enlarged plots at high frequency are in the insetst. Reproduced with permission.[38] Copyright 2015, Wiley-VCH.

4.2 Sheet-type electrodes fabricated by wet-chemical route

The mass productive technologies for the ASLBs need to be more agonized to realize practical ASLBs. In the aspect of a fabrication protocol, sheet-type electrodes tailored by slurry-process rather than dry-mixed electrodes are much suitable to apply practical applications such as large-format batteries. For the materials, morphology-controllable or scalable routes for SEs are also necessary. Unfortunately, severe dissolution problems of sulfide SEs have limited to choose processing solvents and polymeric binders for slurry-process. In this reason, only nonpolar solvents and rubber-type binders have been considered for slurry-process comprising sulfide SEs,[18, 72-73] which restricted many options for creative electrode engineering.

To date, the development of sulfide SEs have tended to make progress *via* solid-state synthetic routes (mechanical milling and heat-treatment) in order to explore new compositions,[9, 16, 81-82] overlooking new synthetic protocols. Recently, β-Li_3PS_4 (β-LiPS) was reported to be prepared by liquid-phase synthesis. In case of the liquid-phase synthesis (LP), SE precursors (Li_2S and P_2S_5) react in solvents (e.g., THF or ACN), producing intermediate precipitants and supernatant. Final products were obtained by drying and heat-treatment.[24-26, 30] Notably, these wet-chemically prepared SEs are usually crystallized at lower temperature (less than 250 °C), which inhibits particulate segregations and allows to control their morphology.[24-26, 30] These wet-chemical routes enabled by moderately polar solvents, expanding polymer candidates, offer new chance to electrode engineering.[31]

In this section, scalable single-step fabrication of sheet-type electrodes for ASLBs using a one-pot slurry consisting of THF, SE precursors, active materials (NCM622 or graphite), THF-soluble polymeric binders (NBR and PVC) are reported. Additionally, the reliance of the electrochemical performance on the particle size of the SE precursors and polymeric binders are investigated.

4.2.1 Compatibility test for hybridization

Firstly, three model samples (LPS, LPS-NBR, and LPS-PVD) were prepared to estimate their chemical compatibility during wet-chemical process. Polymers of 5.5 wt% were blended with LPS. As shown in **Figure 20**, LPS and LPS-NBR kept a white after HT at 80 °C and 140 °C, compared to a violet LPS-PVC treated at 140 °C. It directly implies chemical changes in the LPS-PVC. For the LPS-PVC, dehydrochlorination of PVC with releasing HCl was confirmed by Raman spectroscopy, proved by the formation of a C=C double bond (**Figure 21**). [83-84] On the other hand, NBR is thermally stable up to 300 °C, confirmed by TGA (**Figure 22)**. In **Figure 23**, Raman spectra for NBR and NBR treated at 140 °C are in consistent with TGA result (**Figure 22**). Further analyses of three model samples obtained by wet-chemical routes carried out to comparative study through XRD measurement and Raman spectroscopy (**Figure 24, 25**). The XRD patterns of them closely match to β-Li_3PS_4, reported by C.

Liang, without distinct impurities as shown in **Figure 24**.[24] Additionally, Raman spectra of them exhibits characteristic signal of thiophosphate (PS_4^{3-}, 421 cm^{-1}) in LPS.[47] Notably, only LPS with PVC display slightly lower intensities in XRD (**Figure 24**) and distinctly different peaks in Raman result (**Figure 25**). These undesired Raman signals of LPS-PVC originated from thermally decomposed PVC as discussed in **Figure 21**. Released HCl from PVC at elevated temperature might react with sulfide SEs and hinder the crystallization of LPS. In the **Figure 26**, enlarged Raman spectra of LPS-NBR and pristine LPS exhibits the maintenance of NBR in the LPS-NBR. **Figure 27** represents an Arrhenius plot of Li^+ conductivities of LPS (0.20 mS cm^{-1}), LPS-NBR (0.11 mS cm^{-1}), and LPS-PVC (0.1 mS cm^{-1}). Owing to Li^+ insulating property of polymer, the ionic conductivity of LPS decreased to around half. From the complementary analysis of model materials to clarify compatibility of wet-chemical routes employing polymeric binders (NBR and PVC), wet-chemical routes employing NBR as well as THF was demonstrated.

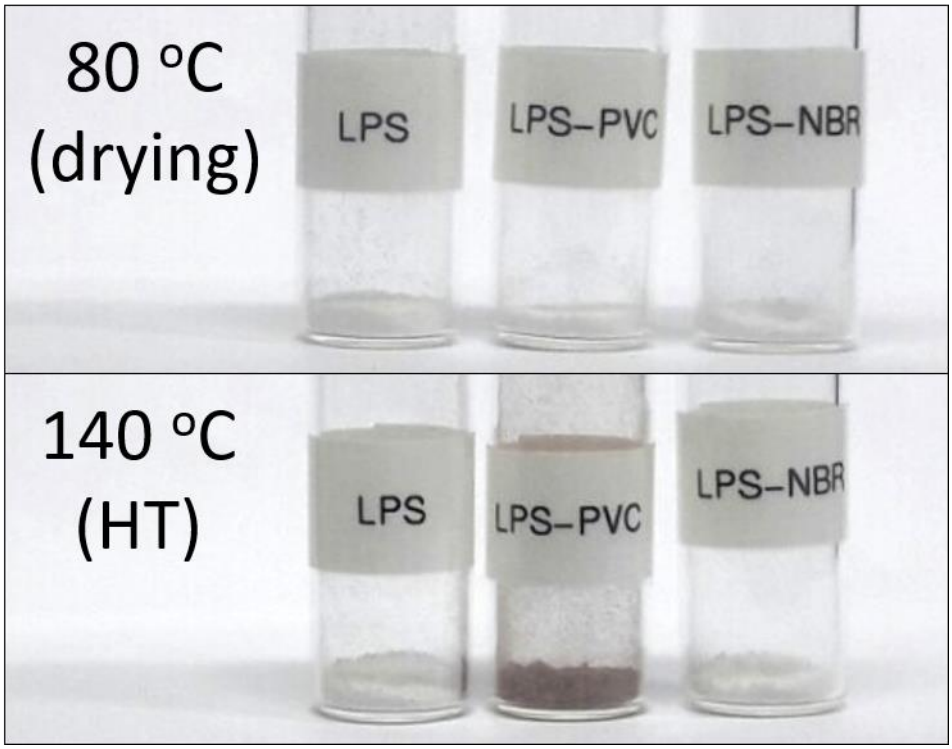

Figure 20. Direct observation of LPS-polymer composite prepared by the wet-chemical route using THF. Photographic images of model samples (LPS-polymer) after HT at 80 ºC and 140 ºC. Reproduced with permission.[29] Copyright 2017, the Royal Society of Chemistry.

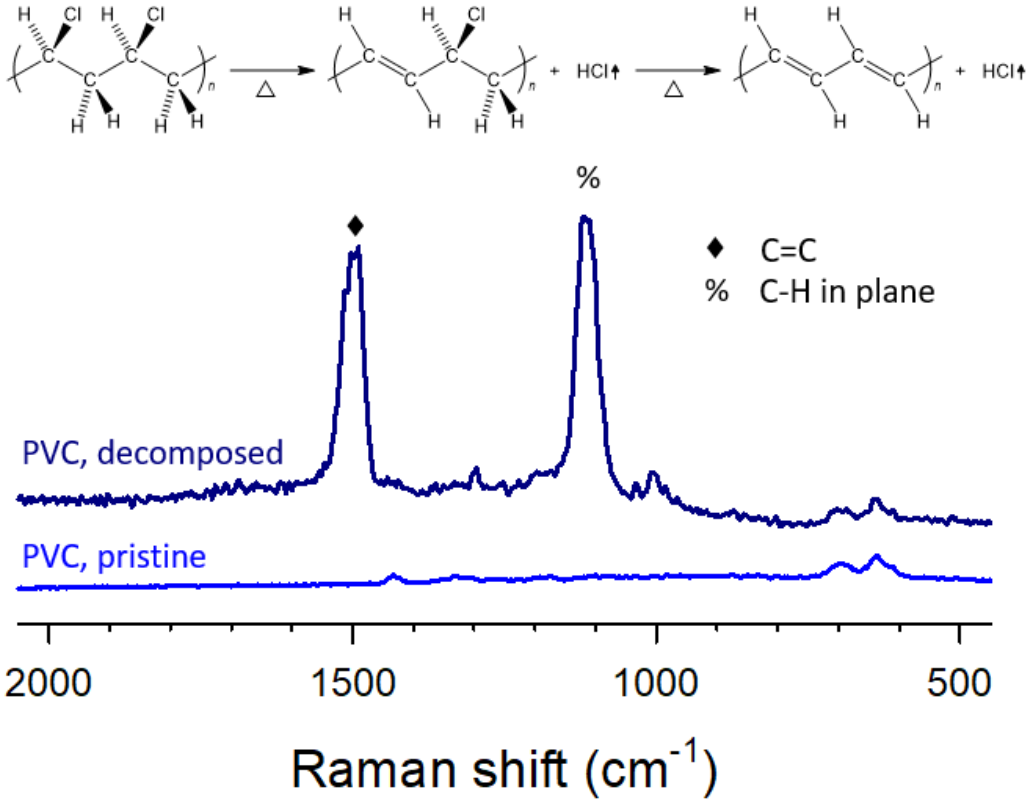

Figure 21. Raman spectra for pristine PVC and decomposed PVC. Schematic diagram of dehydrochlorination of PVC is shown in the inset. Reproduced with permission.[29] Copyright 2017, the Royal Society of Chemistry.

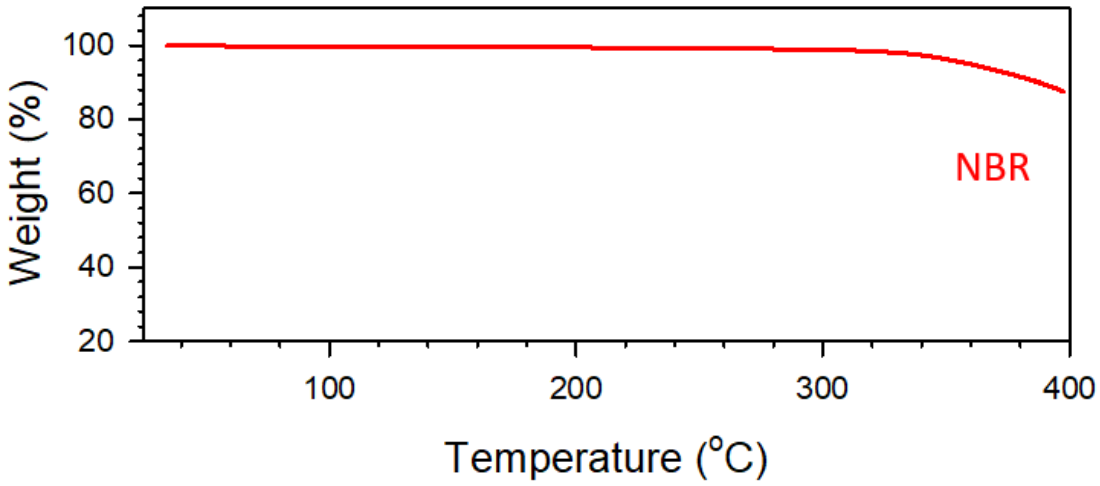

Figure 22. TGA result for NBR under Ar. Reproduced with permission.[29] Copyright 2017, the Royal Society of Chemistry.

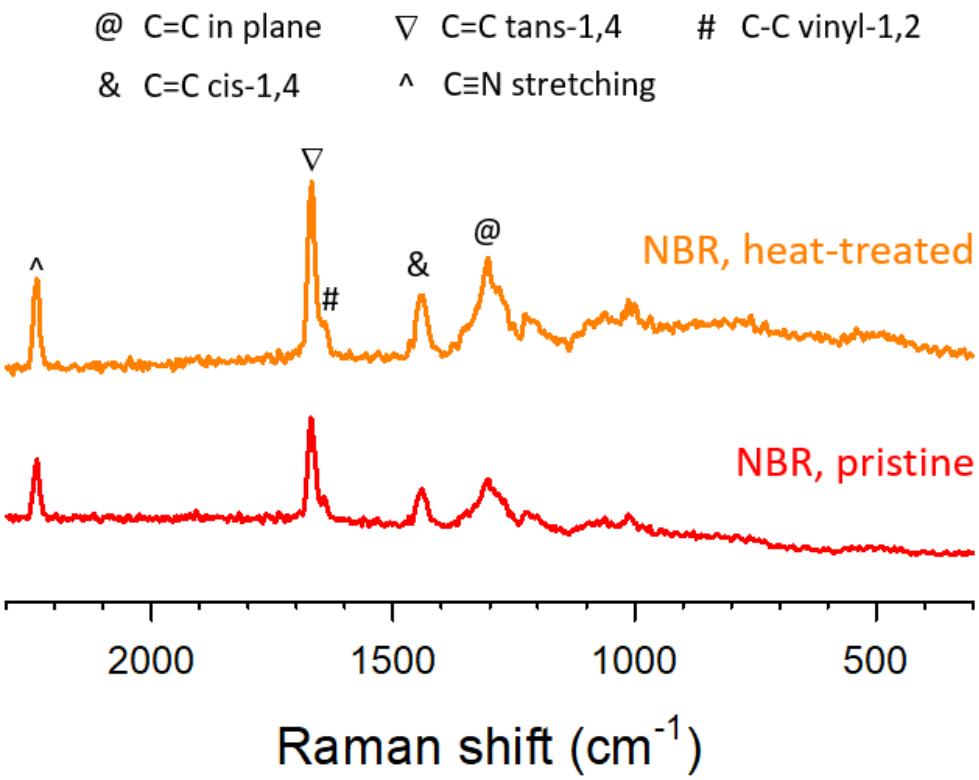

Figure 23. Raman spectra for pristine NBR and heat-treated NBR. The heat-treated NBR was prepared from dried NBR solution (dissolved in THF) AT at 140 °C. Reproduced with permission.[29] Copyright 2017, the Royal Society of Chemistry.

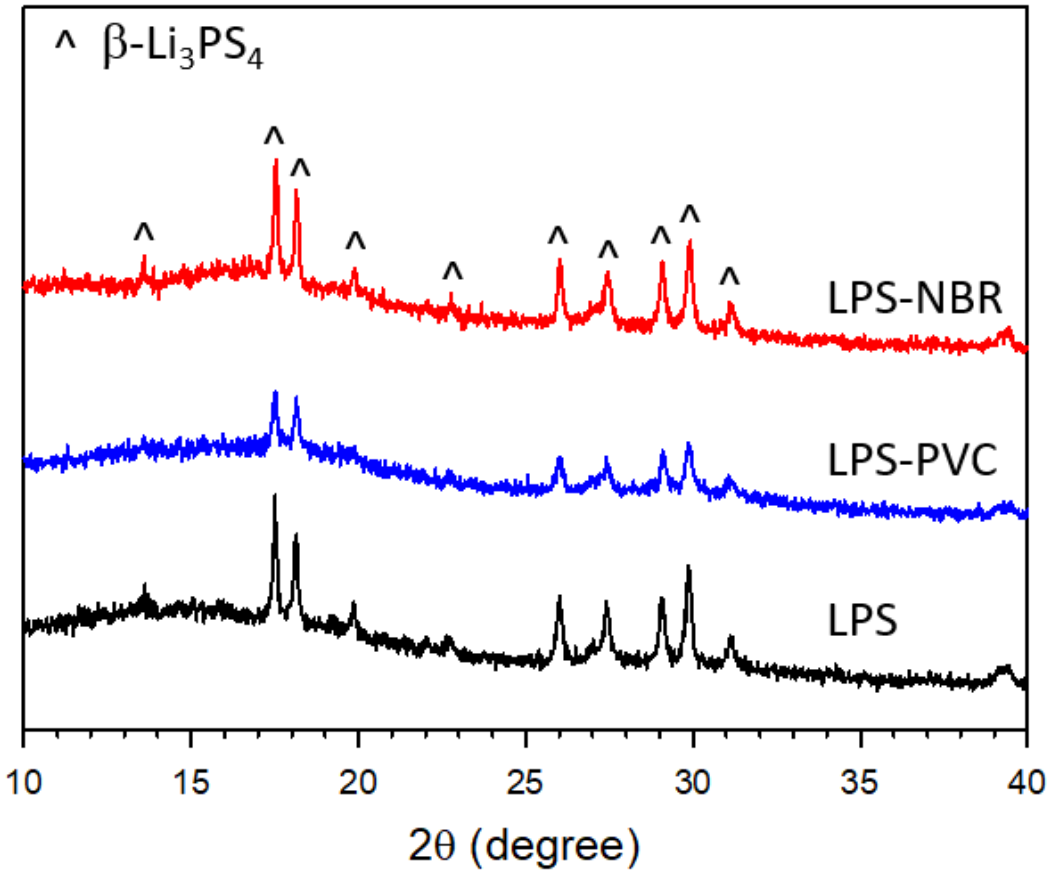

Figure 24. Characterizations of LPS and LPS-Polymer prepared *via* wet-chemical routes using THF. XRD patterns display their phase mainly agree with β-Li_3PS_4. Reproduced with permission.[29] Copyright 2017, the Royal Society of Chemistry.

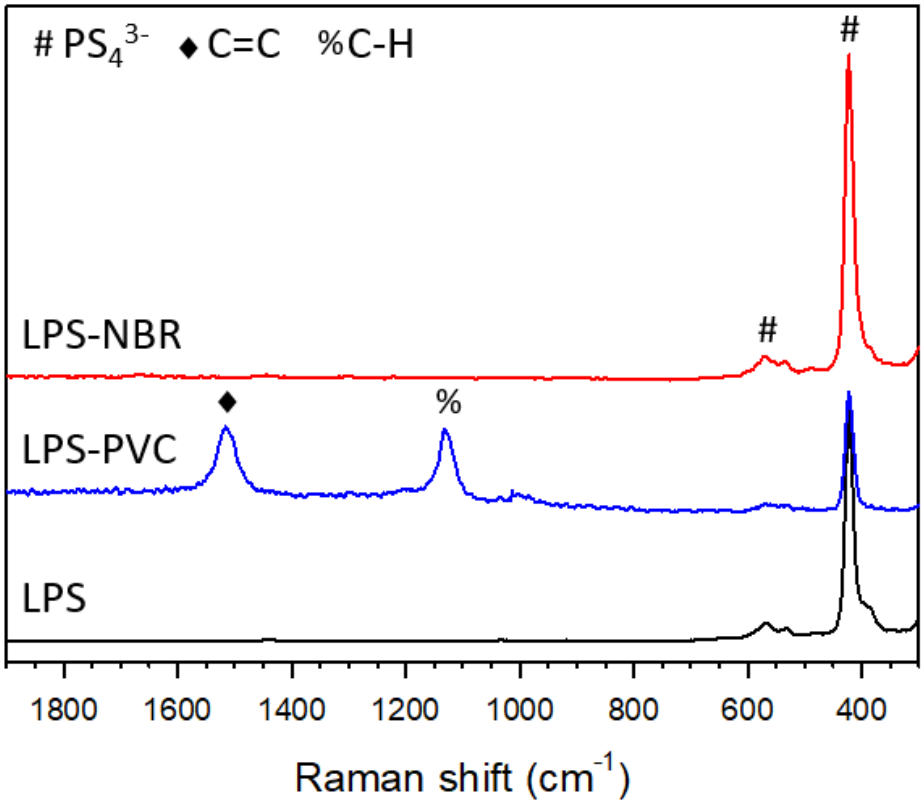

Figure 25. Raman spectroscopy results of LPS and LPS-Polymer to verify chemical structure and their compatibility. PS_4^{3-} (421 cm^{-1}) is significant signal for β-Li_3PS_4. Reproduced with permission.[29] Copyright 2017, the Royal Society of Chemistry.

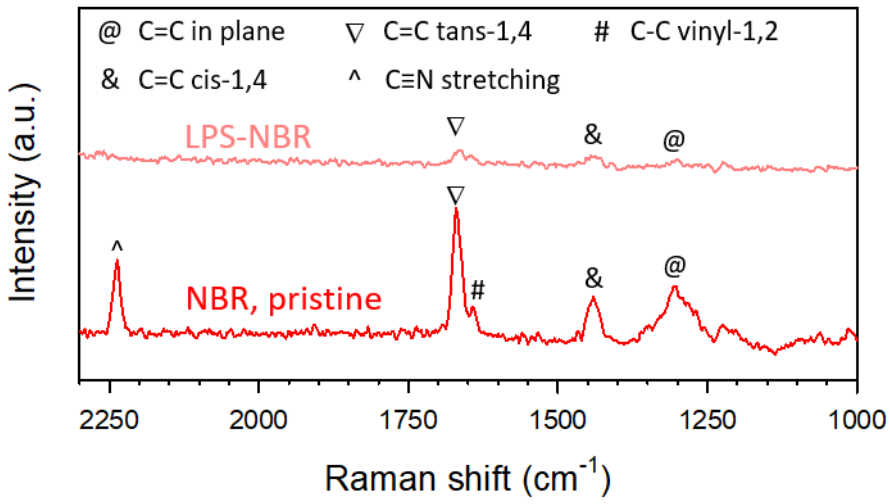

Figure 26. Enlarge Raman spectra of pristine NBR and LPS-NBR. The weight ratio of LPS to NBR is 94.5 to 5.5. Reproduced with permission.[29] Copyright 2017, the Royal Society of Chemistry.

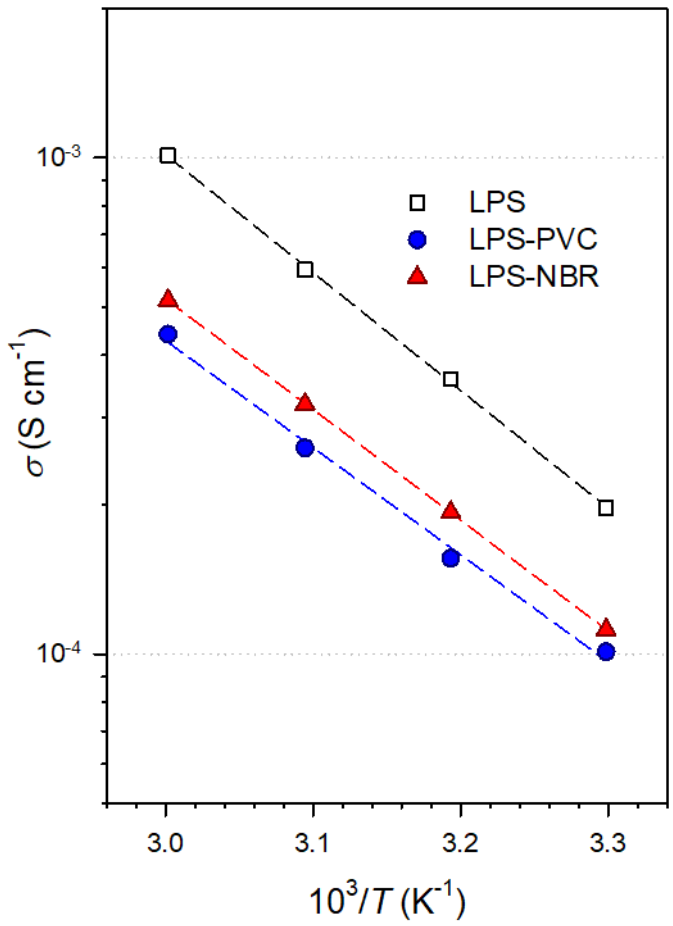

Figure 27. Arrhenius plots for LPS and LPS-Polymer obtained by AC impedance measurement using Li^+-blocking symmetric cell (Ti/sample/Ti). Reproduced with permission.[29] Copyright 2017, the Royal Society of Chemistry.

4.2.2 Wet-chemically tailored electrodes ($LiNi_{0.6}Co_{0.2}Mn_{0.2}O_2$ and Graphite)

Based on screening tests in **section 4.2.1** (Compatibility test for hybridization), sheet-type electrodes were prepared from one-pot slurries including active materials (NCM, graphite), carbon additives, NBR binder, and SE precursors (Li_2S and P_2S_5) in THF. **Figure 28** illustrates sequential procedure to prepare sheet-type electrodes tailored *via* wet-chemical route. One-pot slurries were coated on Al foil (or Ni foil) for cathodes (or anodes). SE precursors (Li_2S and P_2S_5) in one-pot slurries turned into LPS after stirring and subsequent HT at 140 ºC under vacuum. As-prepared sheet-type electrodes via single-step wet-chemical routes are uniform, scalable, and bendable as shown in **Figure 29**, emphasizing the positive role of polymeric binders. **Figure 30** shows cross-sectioned FESEM images with EDXS elemental maps of NCM622 and graphite electrodes.

While looking for optimal way to maximize electrochemical performance, we found that the size of LPS was governed by the size of precursors. In **Figure 31**, LPS using pristine precursors (PP-LPS) and LPS using ball-milled precursors (BP-LPS) are about 1 μm and 10 μm, respectively. The particle size of the SEs can affect homogeneity for slurry and uniformity for electrodes, leading to difference in the aspect of their ionic contacts or percolation.[85-86] The electrochemical performance depending of the size of precursors is discussed later.

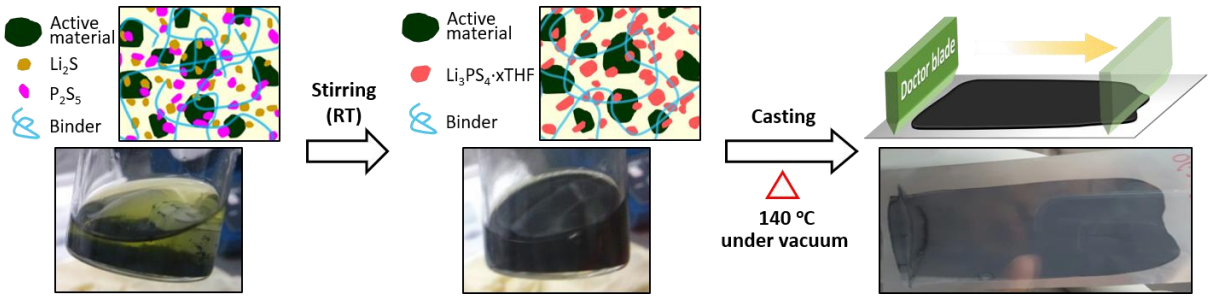

Figure 28. Illustration for a single-step wet-fabrication of sheet-type composite electrodes. Reproduced with permission.[29] Copyright 2017, the Royal Society of Chemistry.

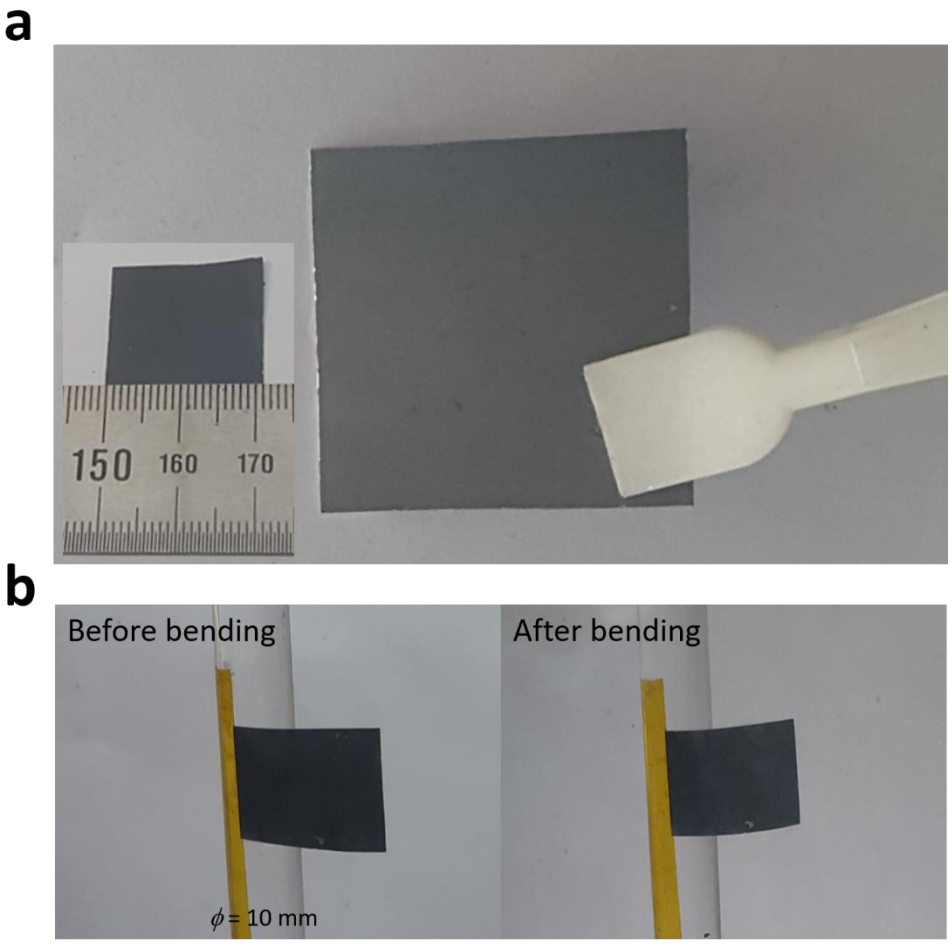

Figure 29. Photographic images of sheet-type NCM electrode prepared from one-pot slurry. the (a) free-standing electrode with 4 cm^2 (b) the electrode before and after bending test. The electrode was wrapped 20 times along the 10 pi cylinder. Reproduced with permission.[29] Copyright 2017, the Royal Society of Chemistry.

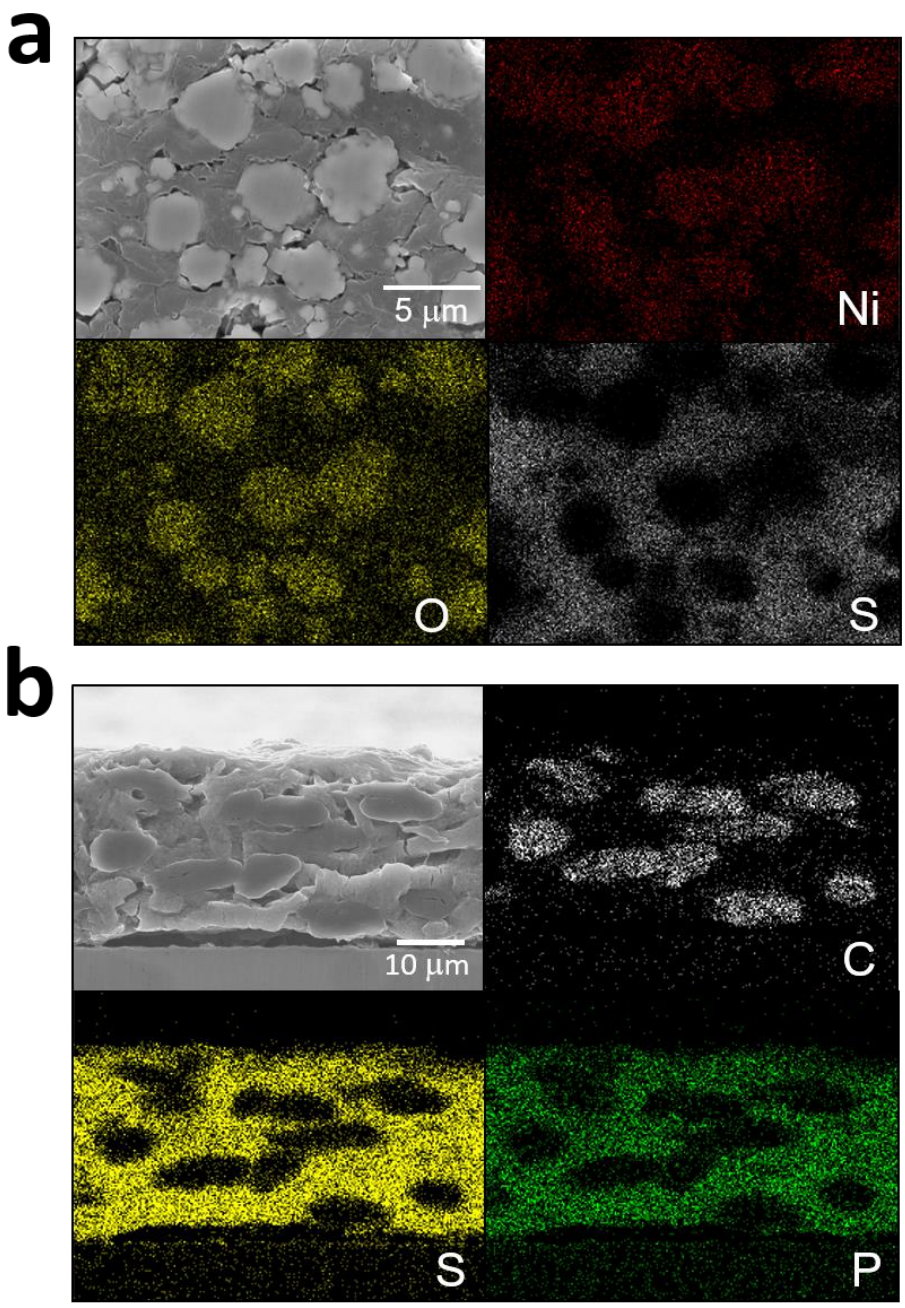

Figure 30. Electron microscopic characterizations of cross-sectional sheet-type electrodes fabricated by a single-step wet-chemical route. FESEM images and corresponding EDXS elemental maps for (a) NCM622, (b) Graphite are presented. Ni and O indicate NCM622, C indicates Graphite, and P and S indicate LPS. Reproduced with permission.[29] Copyright 2017, the Royal Society of Chemistry.

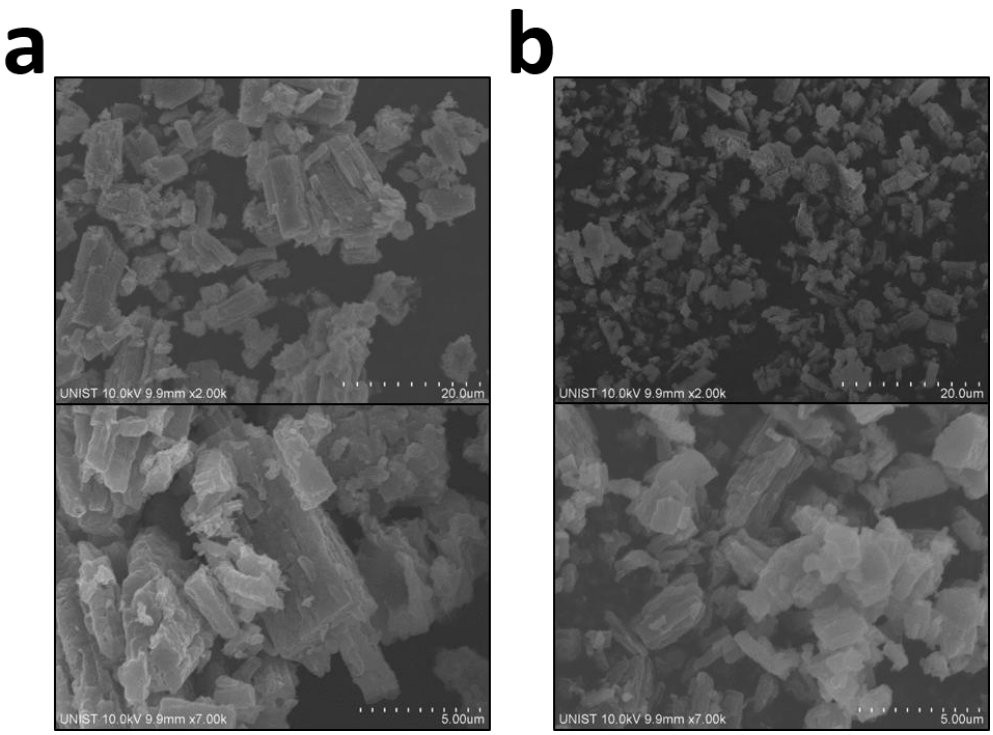

Figure 31. FESEM images of LPS powders varied by the size of precursors. LPS prepared from (a) the pristine precursors (PP) and (b) the ball-milled precursors (BP). Reproduced with permission.[29] Copyright 2017, the Royal Society of Chemistry.

4.2.3 Electrochemical characterization

Three electrodes were prepared to evaluate electrochemical performance of NCM and Gr, depending on size effect of SE. BP-NCM622 and PP-NCM622 are NCM622 electrodes prepared from ball-milled precursors (BP) and pristine precursors (PP), respectively. BP-Gr is graphite electrodes prepared from BP. Detailed information for electrodes and test conditions are summarized in **Table 1** and **experimental section**, respectively.

The electrochemical performance varied by the size of precursors were assessed NCM622/Li-In half-cell as shown in **Figure 32**. A reversible capacity of BP-NCM622 (153 mA h g^{-1}) is higher than 136 mA h g^{-1} of counterpart PP-NCM622 (**Figure 32a**), indicating that smaller SE powders is desirable to enhance ionic contacts and percolation within the electrodes. The ionic surface coverage of NCM622 surrounded by SE was extracted by GITT data (**Figure 33**, see the experimental section). The ionic surface coverage of BP-NCM622 and PP-NCM622 was 14% and 10%, respectively. A very low surface coverage value is attributed to insufficient contacts of NCM622 in contact with SE and presence of Li^+ insulating NBR as well as inevitable pores in the secondary-particle-shaped NCM622.[38, 87] The rate capabilities (**Figure 32d, c**) and the Nyquist plots (**Figure 32d**) agree with the trend in the GITT results (**Figure 33**). Comprehensive electrochemical characterizations (**Figure 32, 33**) were successfully demonstrate the size effect of SEs to wet-chemically assembled sheet-type electrodes. Graphite electrode prepared from BP-LPS was also tested at 30 ºC. The first voltage profile and cycle retention are depicted in **Figure 34**. The BP-Gr showed a great reversible capacity of 318 mA h g^{-1} with the cycle retention of 98% at 0.1C (**Figure 34**). Surprisingly, BP-Gr showed a decent performance as much as typical LIBs using LEs, in contrast to poor BP-NCM622 (153 mA h g^{-1} at 0.05C) compared with NCM622 liquid-electrolyte-cell (163 mA h g^{-1} at 0.2C), shown in **Figure 35**. The volumetric ratio of active materials to electrolytes (SE or LE) was set to unit for a fair comparison (assumption: all pores of LIB-electrode were filled by LE). In the case of NCM electrode, all-solid-state cell suffered larger polarization and didn't fully utilize even in operating at very low C-rate (0.05C). Only 90% of capacity was available, compared to that of liquid-electrolyte cell. Otherwise, graphite electrodes exhibited similar performance in both systems. This outstanding performance of BP-Gr compared to BP-NCM may be nationalized by considering several factors. First, electronic conducting graphite has the advantages for electrode utilization because it allows to form favorable ionic pathways without interruption by conducting additives.[57, 70] Seconds, there are undesirable side reactions of NCM with THF solution containing Li_2S and P_2S_5 (**Figure 36**). A control experiment confirmed that NCM622 which was exposed to a THF solution containing Li_2S and P_2S_5 (supernatant) showed a slightly inferior performance to that of pristine NCM622, evaluated by dry-mixed electrode (**Figure 36**).

Finally, rocking-chair ASLBs (BP-NCM622/BP-Gr) were fabricated and tested at 30 ºC and 100 ºC. In the **Figure 37**, a reversible capacity of the NCM622/Graphite full-cell was 131 mA h g_{NCM622}^{-1} in the voltage range of 2.50 – 4.15 V at 0.1C at 30 ºC. At extremely harsh conditions in the aspect of

temperature (100 ºC) and C-rate (15C), the full-cell assembled by wet-tailored electrodes showed impressive capacity of 110 mA h g_{NCM622}^{-1} with high coulombic efficiency (~99.9%). The cycle retention after 250 cycles, relative to the initial capacity at 100 ºC was 86%. Notably, the temperature of 100 ºC is far beyond the operating temperature limits for conventional LIBs (< 60 ºC).[7, 88]

Precedent evaluated ASLBs in this work used conventional thick SE layer (~700 μm) in between the cathode and anode, thus, the film-type rocking-chair ASLBs using a thin SE-nonwoven composite film (~70 μm) was also attempted to achieve higher energy density. The as-fabricated film-type ASLB and their appearances are presented in **Figure 38**. The first reversible capacity of this full-cell was 124 mA h g_{NCM622}^{-1} in the voltage range of 2.5 – 4.2 V at 0.025C at 30 ºC, which translates to 92 W h kg^{-1} (**Figure 39**).

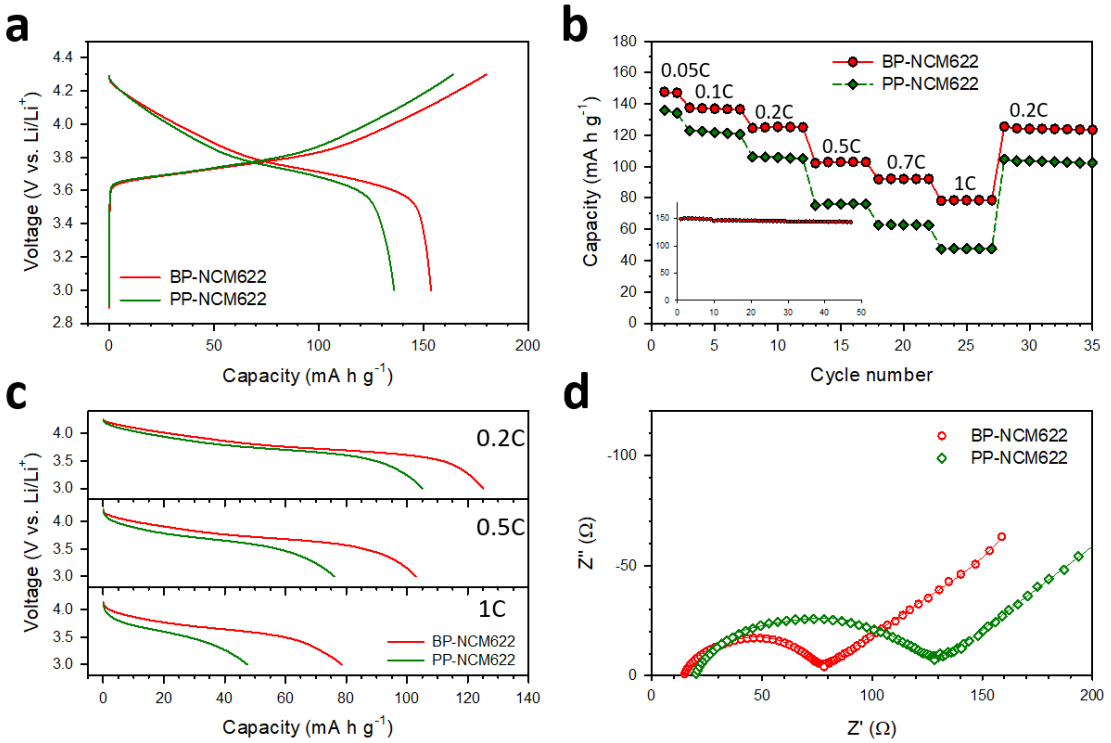

Figure 32. Electrochemical characterizations for the NCM622/Li-In half-cells at 30 ºC, depending on wet-chemically fabricated sheet-type electrodes using BP and PP. (a) First voltage profiles for the NCM622 electrodes prepared from BP and PP at 0.05C. (b) Rate capabilities. The cycle performance of BP-NCM622 is in the inset. (c) Discharge voltage profiles with various C-rate. (d) Nyquist plots for the NCM622 electrodes after 1st charging 4.3 V (vs. Li/Li^+). Reproduced with permission.[29] Copyright 2017, the Royal Society of Chemistry.

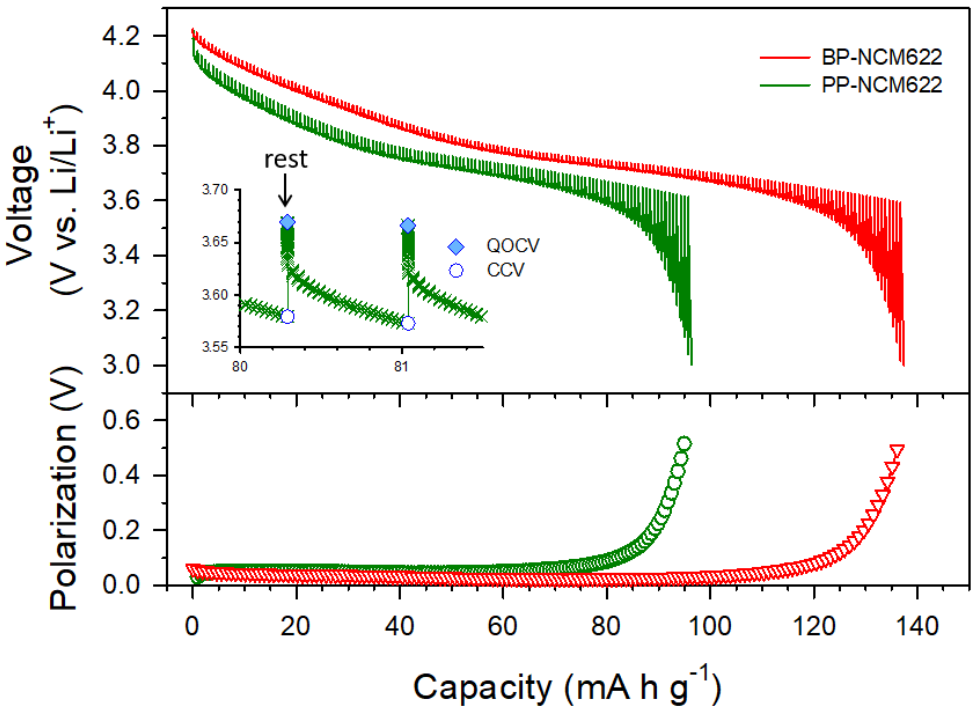

Figure 33. Transient voltage profiles and corresponding polarization plots acquired by GITT for NCM622/Li-In half-cell. The enlarged view in the inset points closed-circuit voltage (CCV) and quasi-open-circuit voltage (QOCV). BP-NCM622 is red and PP-NCM622 is green. Reproduced with permission.[29] Copyright 2017, the Royal Society of Chemistry.

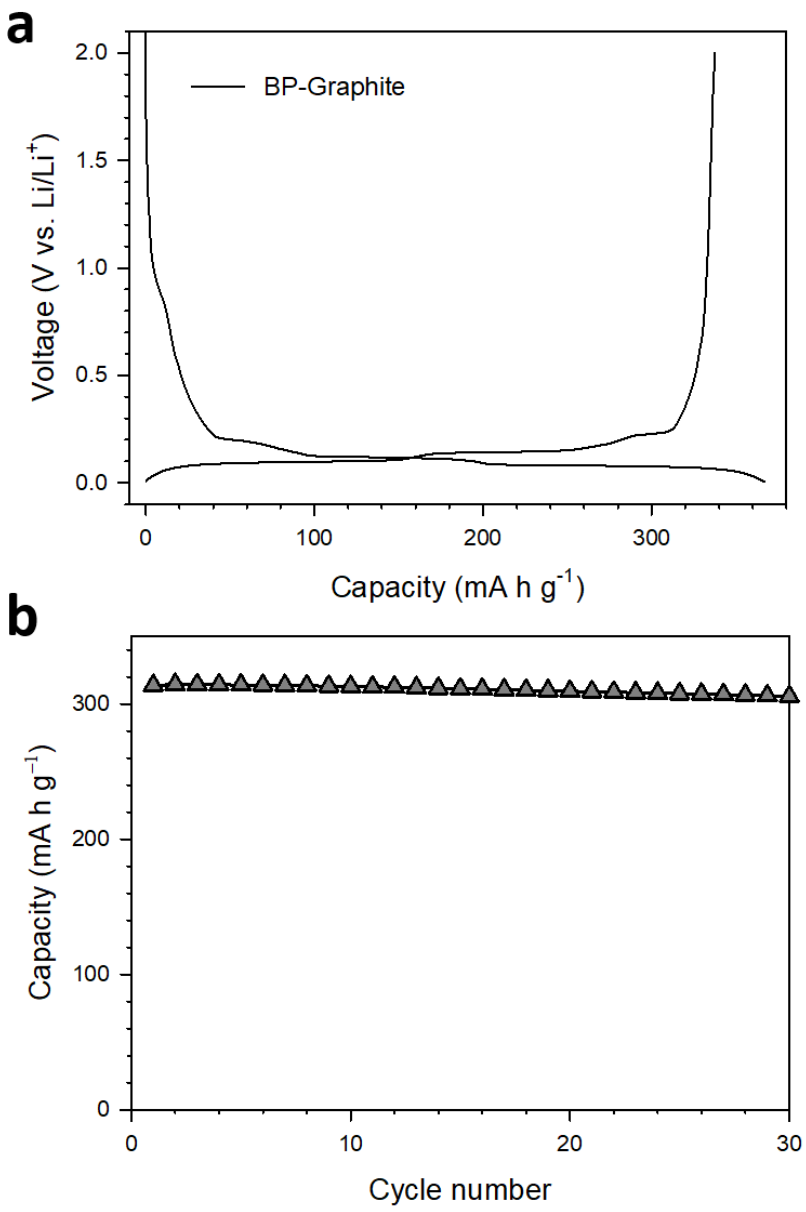

Figure 34. Electrochemical characterizations for the Gr/Li-In half-cells at 30 °C, employing wet-chemically fabricated sheet-type electrode. (a) The first voltage profile for the BP-Graphite at 0.05C. (b) Rate capabilities. (b) The cycle performance at 0.1C. Reproduced with permission.[29] Copyright 2017, the Royal Society of Chemistry.

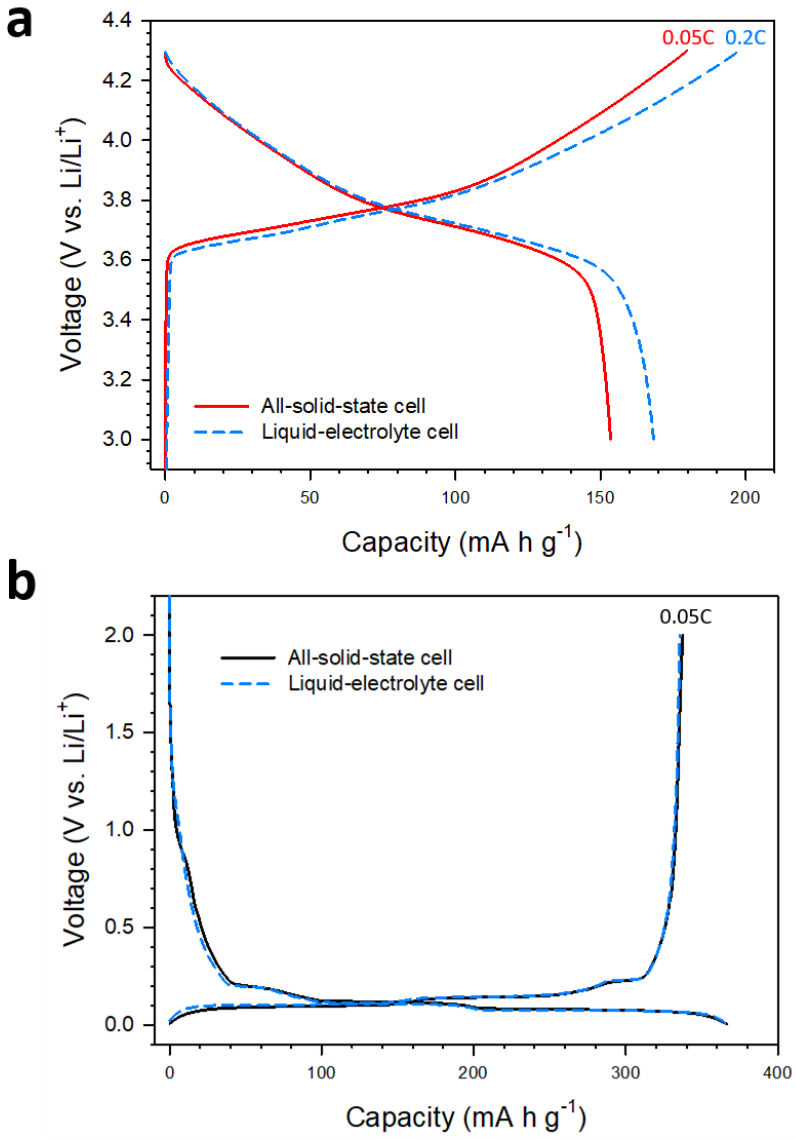

Figure 35. Comparison test about ASLBs and LIBs. First voltage profiles of (a) NCM622 and (b) Gr using different electrolytes. All the profiles were acquired at 30 °C. The C-rates for assessment are notated in Insets. Cycling tests using liquid electrolytes were performed using 2032-type coin cells. A 1.15 M solution of $LiPF_6$ dissolved in ethylene carbonate (EC), ethylmethyl carbonate (EMC), and dimethyl carbonate (DMC) (2:5:3 v/v) with 5 wt.% fluorinated ethylene carbonate (FEC) and 0.5 wt.% vinyl carbonate (VC) as additives was used as the electrolyte. A porous polypropylene (PP)/polyethylene (PE)/PP tri-layer film (Celgard Inc.) was used as the separator. The compositions of electrodes for LIBs are followed; NCM622 : C : PVDF = 90 : 5 : 5 wt%, Gr : PVDF = 9 : 1. Reproduced with permission.[29] Copyright 2017, the Royal Society of Chemistry.

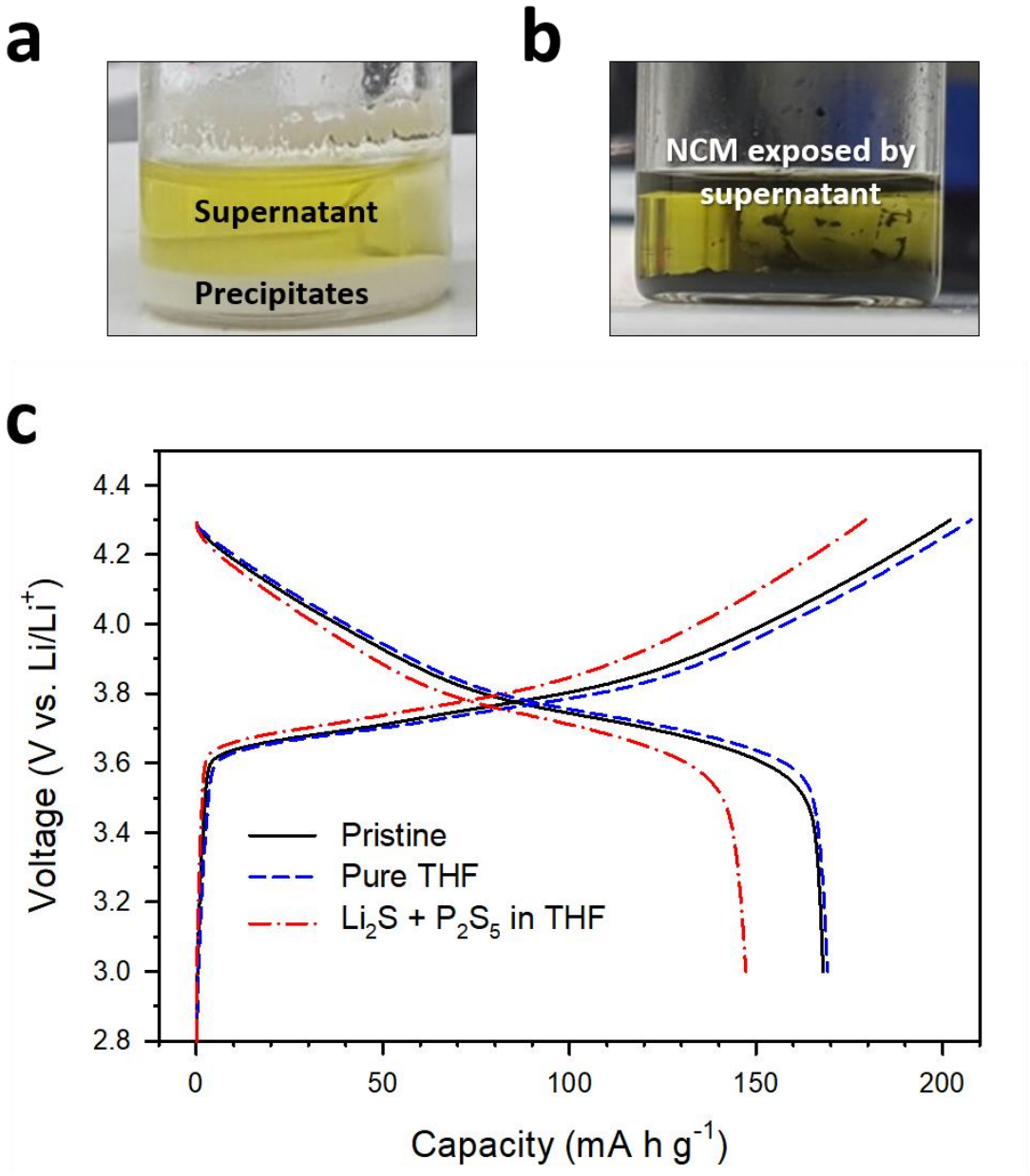

Figure 36. Photographs of (a) wet-chemically synthesized LPS and (b) NCM622 powders exposed to supernatant. (c) 1st voltage profiles of NCM622/Li-In cells at 0.1C at 30 °C using pristine (black), pure-THF-treated (blue), and supernatant-treated bare (red). All samples were dried at 140 °C under vacuum. The supernatant-exposed NCM622 powders were washed by pure THF before drying. Reproduced with permission.[29] Copyright 2017, the Royal Society of Chemistry.

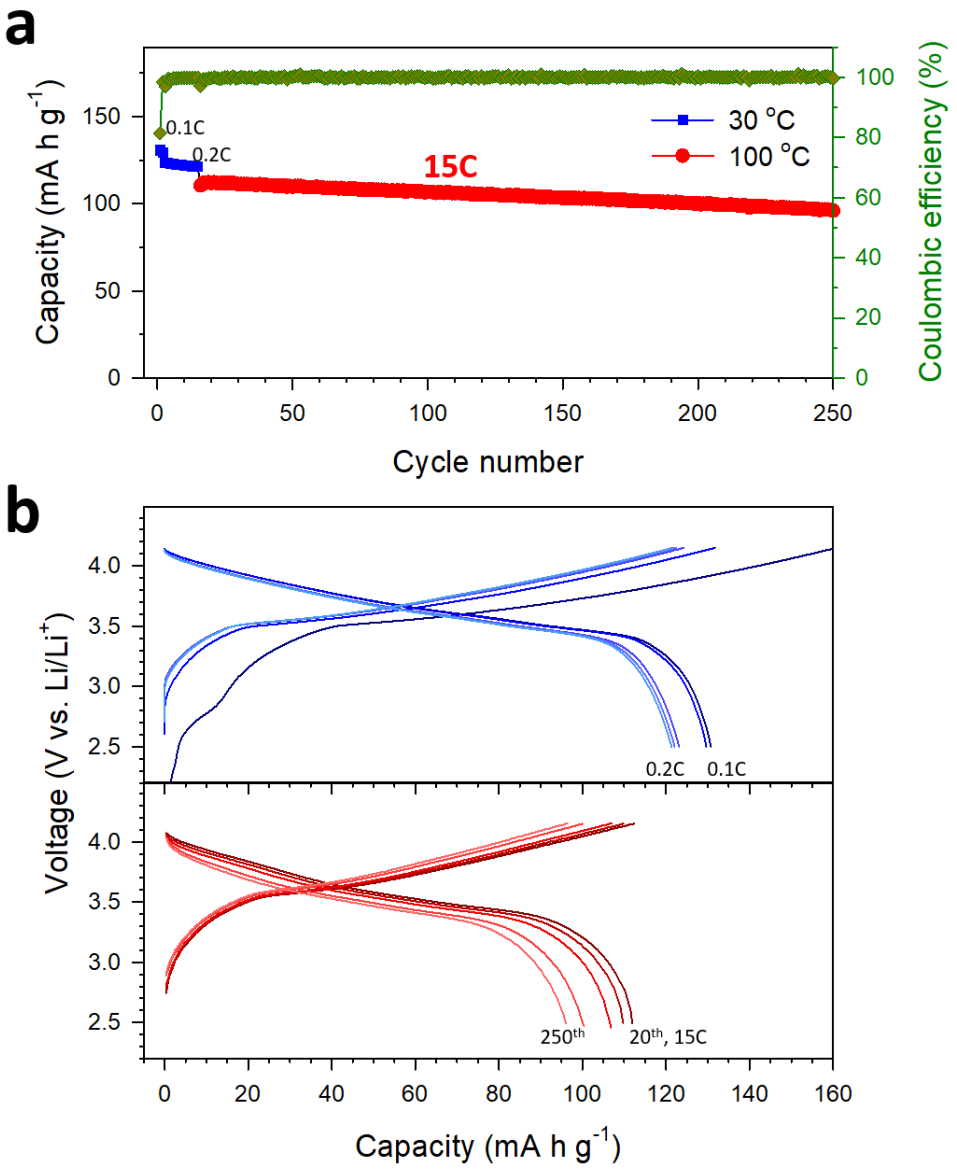

Figure 37. Galvanostatic charge-discharge test of a rocking-chair ASLB employing single-step wet-chemically tailored sheet-type electrodes at 30 °C and 100 °C. (a) Cycle performance and (b) the corresponding charge-discharge voltage profiles. Reproduced with permission.[29] Copyright 2017, the Royal Society of Chemistry.

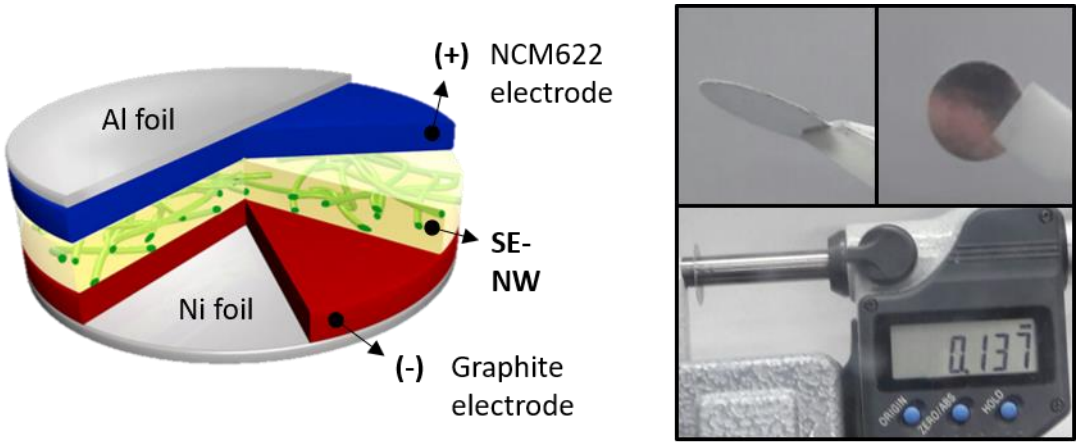

Figure 38. BP-NCM622/BP-Gr full-cell employing a thin SE-nonwoven composite film. (a) Schematic diagram. (b) Photographic images of the free-standing film-type ASLB. Reproduced with permission.[29] Copyright 2017, the Royal Society of Chemistry.

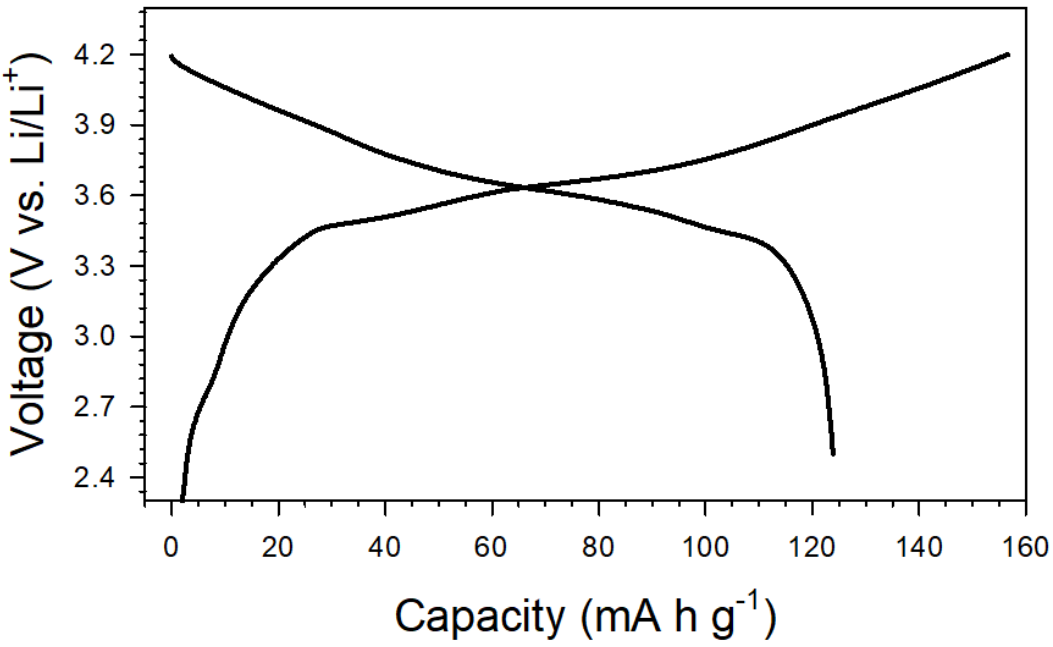

Figure 39. The first voltage profile of BP-NCM622/BP-Gr full-cell employing a thin SE-nonwoven composite film. [29] Copyright 2017, the Royal Society of Chemistry.

4.3 Slurry-fabricated Li+-conductive polymeric binders enabled by solvate ionic liquids for sheet-type electrodes

For mass production of ASLBs based on sulfide SEs, the wet-slurry process for sheet-type electrodes is imperative.[17-18] Unfortunately, the poor chemical stability of sulfide SEs, in terms of reactivity or dissolutions, severely restrict available candidates for solvents and in turn polymer binders.[29, 38]

Several challenging issues must be solved to establish universal wet-slurry protocols for sulfide based ASLBs. First, polymeric binders should be dissolved into nonpolar or less polar solvents that are inert with sulfide SEs. Second, polymeric binders should have acceptable adhesion properties with flexibility. In this regard, only rubbery binders with low glass transition temperature and nonpolar or less polar solvents to dissolve rubber have been allowed to fabricate sheet-type ASLBs based on sulfide SEs; e.g., nitrile−butadiene rubber (NBR) and xylene, styrene−butadiene rubber (SBR) and toluene. [18, 30, 72, 89]

Even if wet-slurry protocols for mechanically compliant electrodes could be developed using certain polymers and solvents, the binders interrupt Li^+-ionic contacts at interfaces, resulting in the below par electrochemical performance.[18] This problem motivates to develop Li^+-conductive hybrid electrolytes consisting of polymer electrolytes and sulfide SEs. In consideration of Li^+ conductivity and mechanical versatility, highly Li^+-conductive gel polymer electrolytes (>10^{-4} S cm^{-1}) are an appropriate candidate. However, applying gel polymer electrolytes to sulfide ASLBs is very challenging because liquid components for gel polymer electrolytes are completely antithetic to conventional wet-slurry process for sulfide SEs. Moreover, highly thermal stable gel polymer electrolytes are desired in order not to offset the advantage ASLBs. These considerations led me to my previous research addressing chemical compatibility of sulfide SEs and SILs. [90-91]

In this section, systemic approaches to cope wet-slurry process involving sulfide SEs with SILs are presented. Moreover, their electrochemical characteristics are investigated by complementary analysis to reveal ionic conduction mechanism in the complex system. Moreover, sheet-type electrodes fabricated by slurry-fabricable Li^+ conducive polymeric binders enable to achieve unprecedent state-of-the-art high areal capacity of 7.4 mA g cm^{-2}, is highlighted.

4.3.1 Compatibility test for hybridization

For designing wet-slurry process to accommodate SILs and sulfide SEs together, miscibility and dissolution test as function of polarity of solvent were tested by direct observations (**Figure 40**) and several characteristics of corresponding solvents are listed in **Table S3**. The mixtures of LiG3 and nonpolar solvents (toluene and *o*-xylene) turned into binary phase clearly (**Figure 40a**), indicating different polarity and density of them. (e.g., *o*-xylene: 0.88 g ml^{-1} and LiG3: 1.46 g ml^{-1}). Otherwise,

highly polar solvents (water, ACN, and NMP) and intermediate polarity (dichloromethane, dibromomethane (DBM), and chloroform) appeared to be miscible with LiG3 (**Figure 40a**). The trend about solubility of LiG3 into various solvents could be described by like-dissolve-like; LiG3-miscible solvents have roughly similar physical parameters compared to G3 (see **Table 3**), in particular, the DMB is the most like a G3. However, highly Lewis-basic (or highly polar) solvents showed distinct dissolution of sulfide SE, LPSCl, as expected (**Figure 40b**). From these screening tests, DBM was selected as an appropriate solvent for the ASLB slurry (**Figure 41**).

The comprehensive explanation on these observed results is illustrated in **Figure 42**. In general, polar solvents have asymmetric electronic density derived by functional groups. Especially, strong Lewis-basic (or highly polar) solvents (e.g., water, ACN, and G3) including lone-pair electrons at highly electronegative elements (e.g., O and N) react with electrophilic species (e.g., P^{5+} in sulfide SEs). In addition, strong interaction between electronegative species (e.g., O and N) in these solvents and Li^+ solvated by the G3 might cleave coordination structure of $[Li(G3)]^+$, leading to underside interplay between G3 and LPSCl. For example regarding NMP used for typical LIB slurries, the O in carbonyl group could interact with solvated Li^+,[92-93] then, adrift O in G3 could corrupt LPSCl (**Figure 42c**). Additionally, the unsaturated C in carbonyl group could be attacked by nucleophile thiophosphates (e.g., PS_4^{3-} and $P_2S_7^{4-}$) in LPSCl. This rationale is in line with the chemical incompatibility between carbonate-based LEs and polysulfides in the Li-S batteries.[94] In sharp contrast, nonpolar solvents (e.g., o-xylene) are chemically inert to LPSCl owing to their negligible donor ability, but, LiG3 is immiscible with nonpolar solvents since there are huge difference in polarity (**Table 3**). In the contradictory situation for designing wet-slurry process accommodating LiG3 and LPSCl, less polar solvents with moderately lower donor ability, especially DBM, enable to dilute LiG3 without disruption of $[Li(G3)]^+$ and be compatible with LPSCl (**Figure 42b**).

To estimate their compatibility during wet-slurry process, a model composite comprised of LPSCl, NBR, and LiG3 (referred as to "LPSCl-NBR-LiG3", weight ratio of 50:20:30) was prepared BY wet-slurry using DBM. The slurry was dried at 60 °C under vacuum for 2h. The LPSl-NBR-LiG3 composite and DBM-exposed LPSCl, obtained from same wet-slurry route, still remained the crystal structure of LPSCl without any impurities (**Figure 43**). The absence of impurities in XRD results corroborates that DBM is inert to LPSCl and $[Li(G3)]^+$, explained in **Figure 42b**.

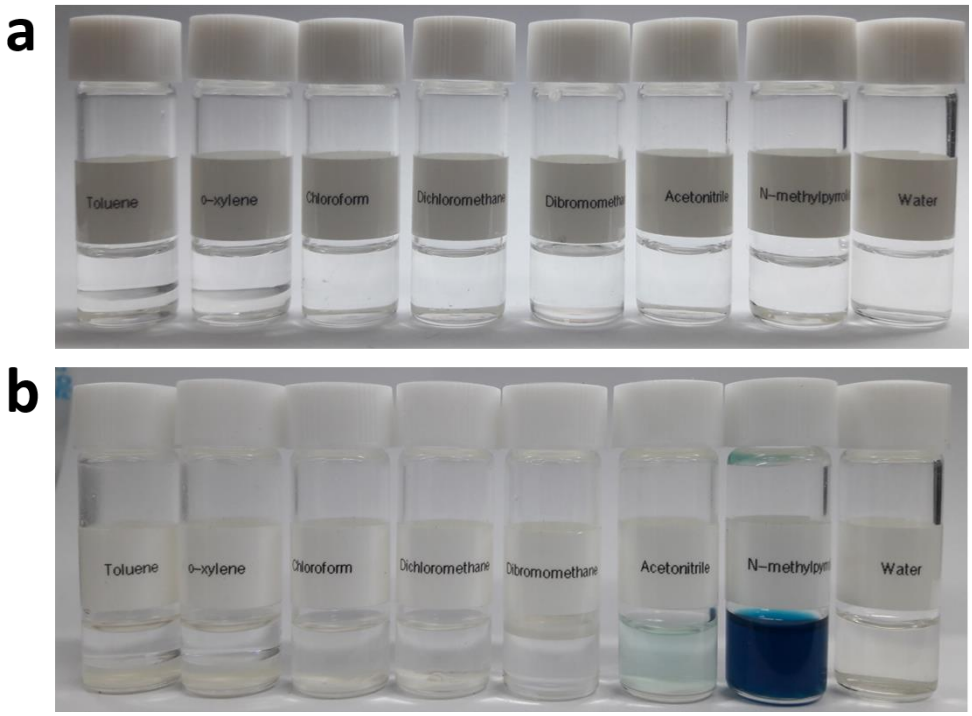

Figure 40. Photographic images of mixtures of LiG3 with diverse solvents (a) without LPSCl and (b) after adding LPSCl and being kept for 12 h. Detailed information about solvents is in **Table 3**. Reproduced with permission.[39] Copyright 2019, Wiley-VCH.

Solvent	Dielectric constant	Dipole moment [D]	Donor number [kJ mol^{-1}]	Reactivity with LPSCl	Solubility of LiG3
Water	78	1.85	75.3	O	O
NMP	32	4.09	-	O	O
Acetonitrile	36	3.9	58.6	O	O
Triethylene glycol dimethyl ether (G3)	7.5	2.16	58.6	O	O
Dichloromethane	9.1	1.6	4.2	X	O
Dibromomethane (DBM)	7.8	1.78	-	X	O
Chloroform	5.5	1.08	16.7	X	O
o-xylene	2.6	0.64	-	X	X
Toluene	2.4	0.36	0.4	X	X

Table 3. Characteristics of various solvents for wet-slurry process accommodating LiG3 with sulfide SEs. Reproduced with permission.[39] Copyright 2019, Wiley-VCH.

Figure 41. Photographs of SE (LPSCl), NBR, and LiG3 (the top image) and after blending with DBM (the ground image). Reproduced with permission.[39] Copyright 2019, Wiley-VCH.

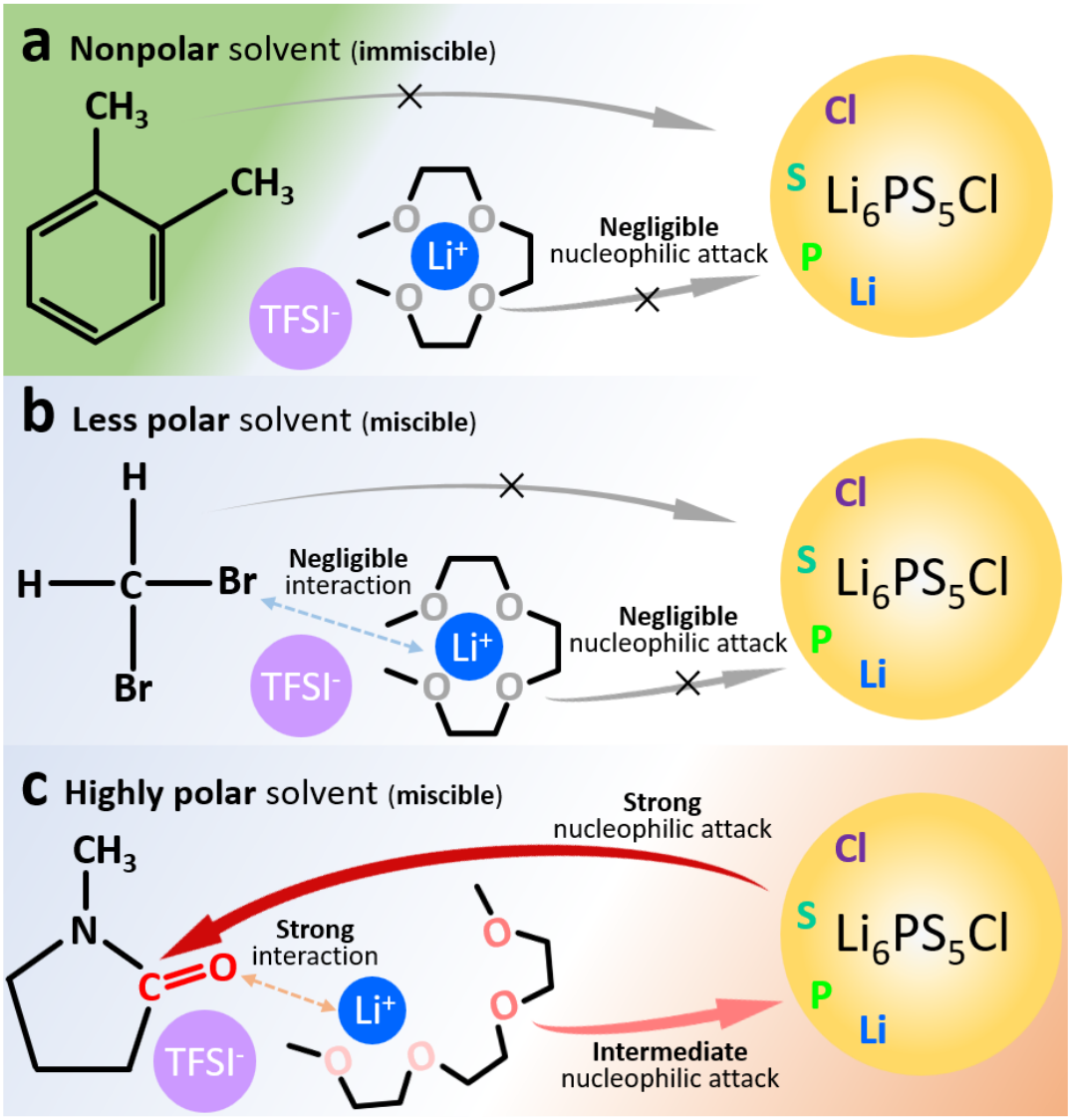

Figure 42. Schematic diagram illustrating compatibility with LPSCl for LiG3 diluted by various solvents varied by polarity; (a) nonpolar, (b) less polar, and (c) highly polar (or Lewis-basic) solvents. Reproduced with permission.[39] Copyright 2019, Wiley-VCH.

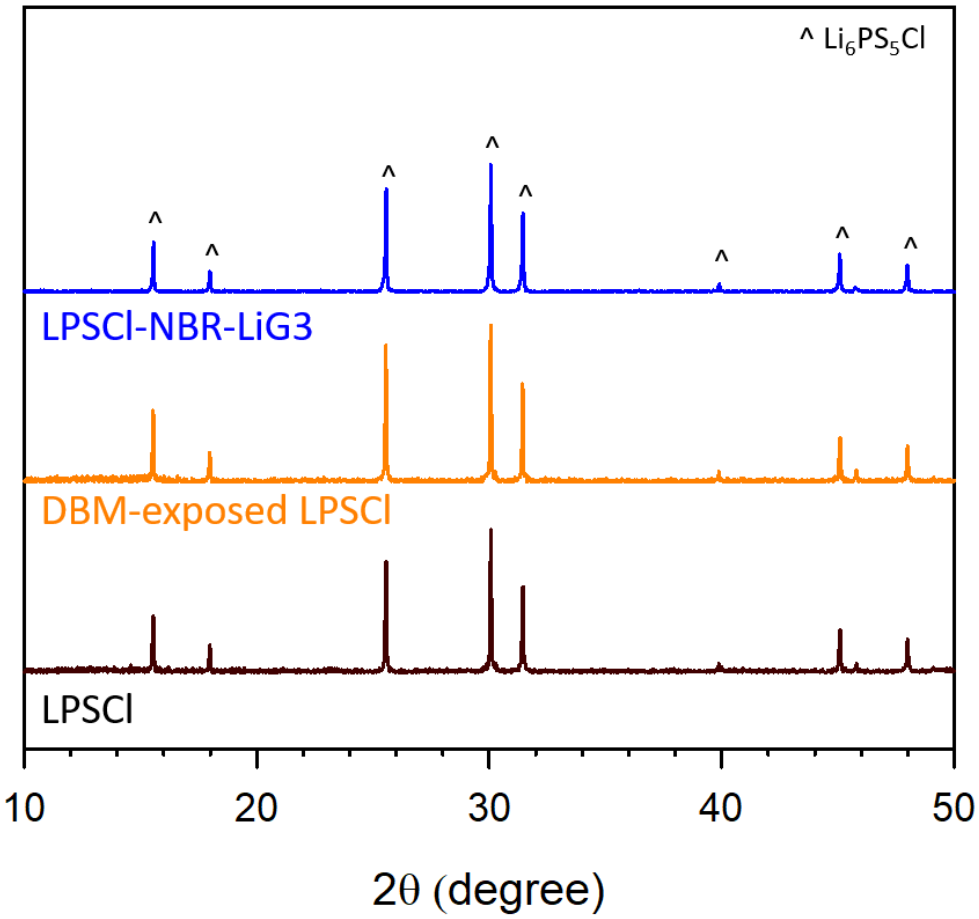

Figure 43. XRD results of pristine LPSCl, DBM-exposed LPSCl, and LPSCl-NBR-LiG3. Reproduced with permission.[39] Copyright 2019, Wiley-VCH.

4.3.2 Phase analysis and Li^+-conducting mechanism

To determine the local environment around LiG3, ^7Li NMR analyses for LiG3 and NBR-LiG3 (a composite NBR and LiG3) were conducted (**Figure 44**). A very sharp peak at -0.36 ppm was observed in the liquid-sate LiG3, meaning that Li is only shielded by O in the G3 and mobile freely in a liquid phase.[95] In contrast, NBR-LiG3 showed broaden peak, indicating reduced mobility of Li^+ due to polymer matrix. This is in line with typical phenomenon in gel polymer electrolytes when LEs is soluble into the polymer matrix.[96] Furthermore, LiG3 in the microstructure of LPSCl-NBR-LiG3 were verified by magic angle spinning (MAS) NMR measurement (**Figure 45**) because the broad peak of LPSCl (~2.5 ppm) covered other signals (LiG3 or NBR-LiG3) at static mode (**Figure 46**). By high resolution MAS NMR at 25 kHz, distinct peaks for LPSCl and NBR-LiG3 were clearly identified in the LPSCl-NBR-LiG3. It implies that liquid phase LiG3 turn into solid state while merging into NBR as forming gel polymer electrolytes. Additionally, cross-sectional FESEM and corresponding elemental maps by EDXS were acquired to double check to assign location of LiG3 in LPSCl-NBR-LiG3. In **Figure 47**, overlapped maps for C (from NBR and LiG3), F (from LiG3), N (From NBR and LiG3) except for P and S (from LPSCl) implies formation of the NBR-LiG3 gel polymer electrolyte in consistent with MAS ^7Li NMR results (**Figure 45**).

The bendable and free-standing LPSCl-NBR-LiG3 film (70μm) are presented in **Figure 48**. As shown 70-μm-thick LPSCl-NBR-LiG3 (3.3 mS cm^{-1}) exhibited 2-fold higher Li^+ conductivity compared to that of LPSCl-NBR (1.7 mS cm^{-1}). It suggests that NBR-LiG3 (0.17 mS cm^{-1}) work as a good Li^+ conductive polymeric binders. Detailed information about Li^+ conductivities of samples are summarized in **Table 4**.

To investigate Li+ conduction pathway in the composite LPSCl-NBR-LiG3, MAS ^7Li NMR analysis of Li-ion non-blocking symmetric cells using ^6Li metal electrode, ^6Li/LPSCl-NBR-LiG3/^6Li, was attempted as shown in **Figure 49**.[97-98] The as-prepared ^6Li symmetric cell was repeatedly cycled at 50 μA in opposite direction to substitute ^7Li in the sample (LPSCl-NBR-LiG3) for ^6Li. **Figure 50** shows that the alternative signs of voltage denote reversible Li striping and plating at ^6Li electrodes while replacing intrinsic ^7Li of LPSCl-NBR-LiG3 with ^6Li. After the cycling, the LPSCl-NBR-LiG3 sample was collected and subjected to the MAS ^7Li NMR measurements. MAS ^7Li NMR spectra of LPSCl-NBR-LiG3 before and after cycling is shown in **Figure 51** The overall peak intensities decreased after cycling, indicating that that Li^+ migrated through both LPSCl and NBR-LiG3 while ^7Li in the samples were partly replaced by ^6Li. Most importantly, the areal ratio of LPSCl to NBR-LiG3 was decreased from 16 to 9 after cycling, which indicate that LPSCl is dominant Li^+ pathways compared to that of NBR-LiG3 in the hybrid system. Moreover, the evidence for Li^+ conduction at LPSCl/NBR-LiG3 interface was proved by a control experiment using NBR-LiG3/LPSCl/NBR-LiG3 symmetric cell

(**Figure 52**). The interfacial resistance between LPSCl and NBR-LIG3 is 33.8 Ω cm^2, which is lower than for LiG3/Li (~150 Ω cm^2),[40] Li_3PS_4/Li (~ 100 Ω cm^2),[49]and typical LIBs (62 Ω cm^2).[99] From this result, facile Li^+ transport across the LPSCl/NBR-LiG3 interfaces was demonstrated.

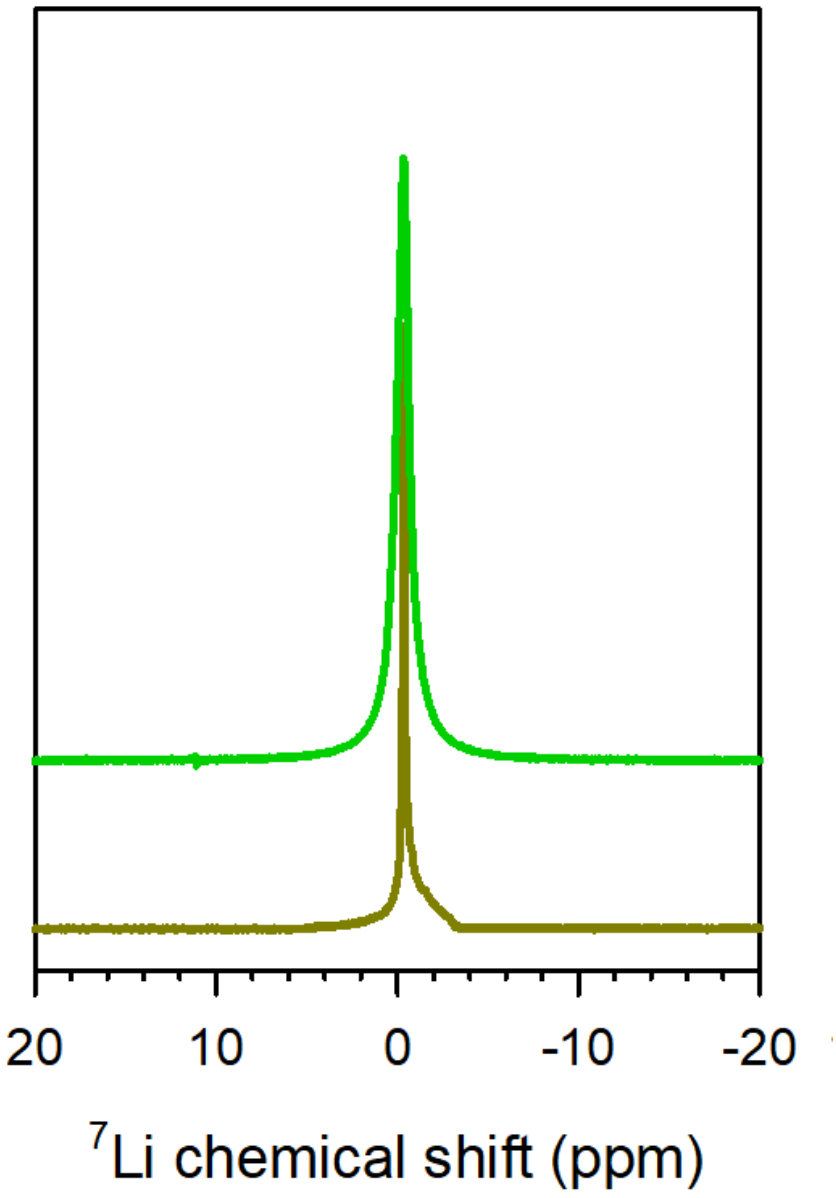

Figure 44. Static ^{7}Li NMR spectra of LiG3 and NBR-LiG3. Reproduced with permission.[39] Copyright 2019, Wiley-VCH.

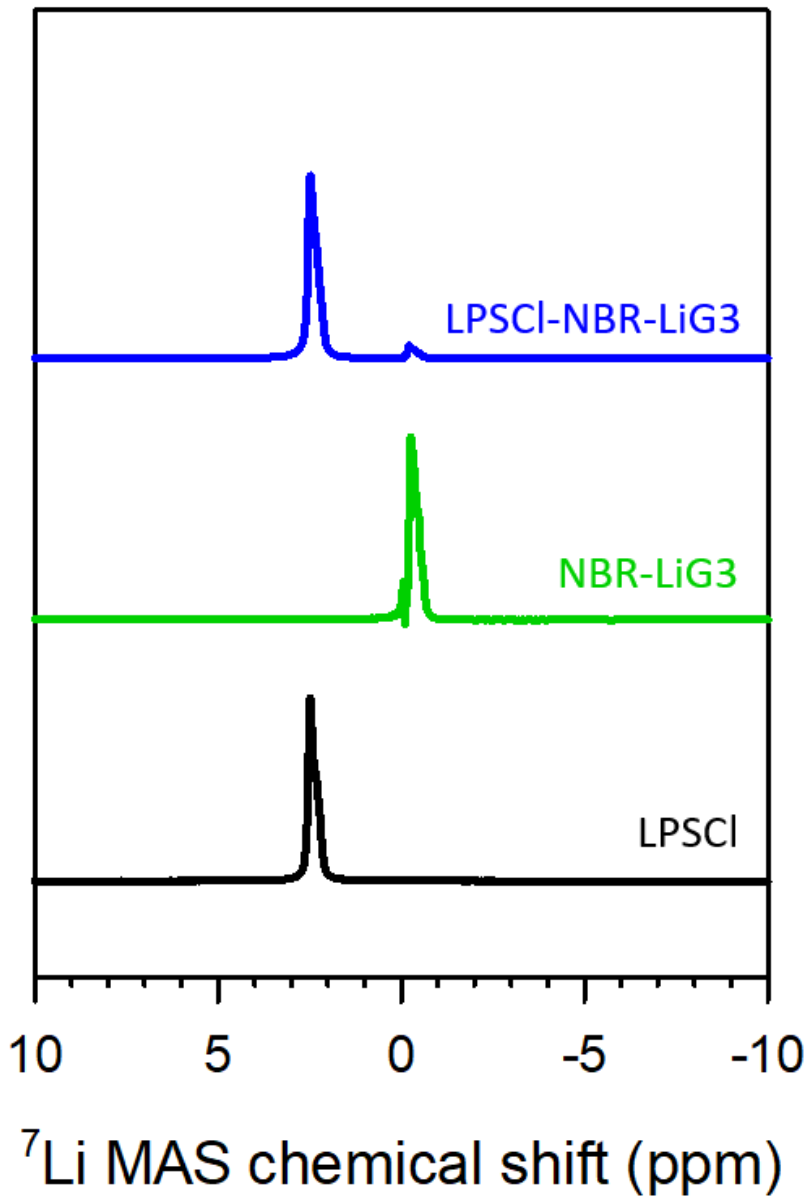

Figure 45. MAS ^{7}Li NMR spectra of LPSCl, NBR-LiG3, LPSCl-NBR-LiG3. Reproduced with permission.[39] Copyright 2019, Wiley-VCH.

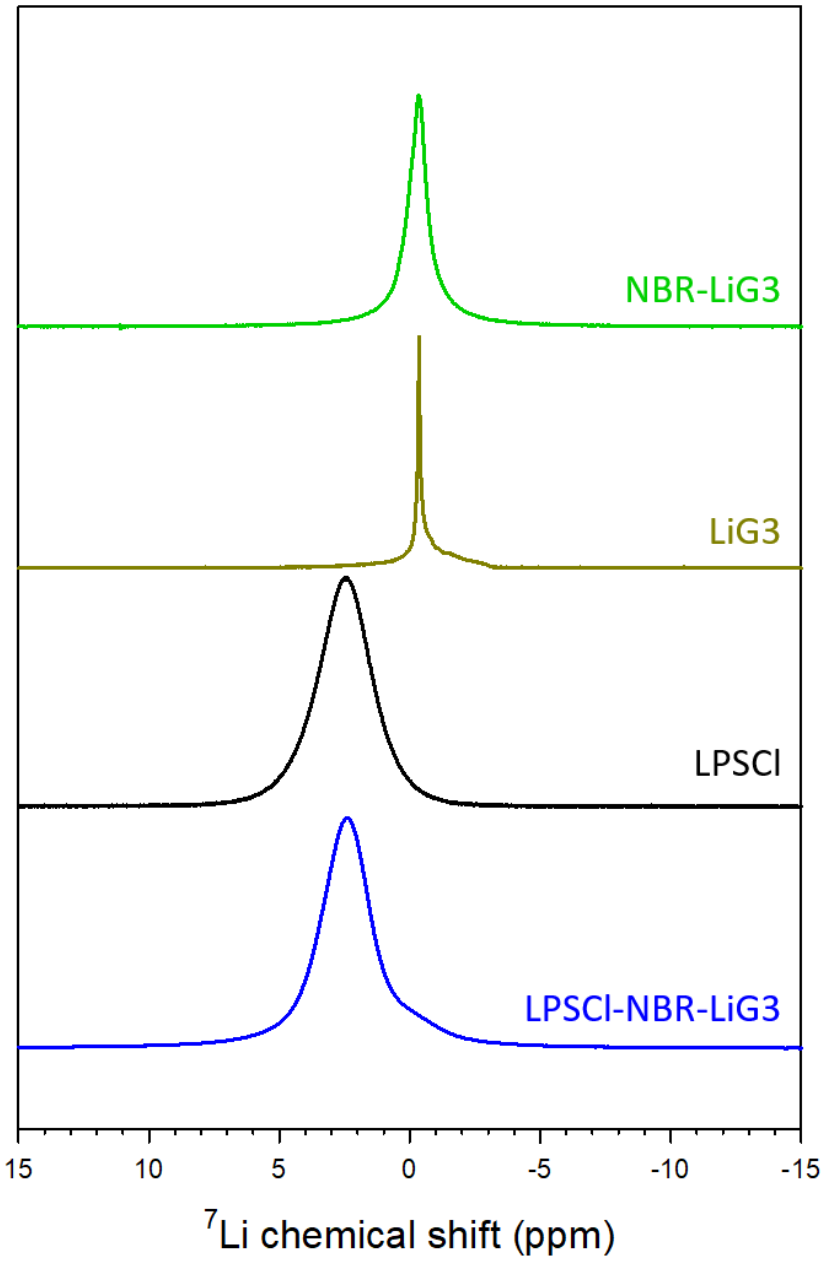

Figure 46. Static ^{7}Li NMR spectra of LPSCl-NBR-LiG3, LPSCl, LiG3, NBR-LiG3. Reproduced with permission.[39] Copyright 2019, Wiley-VCH.

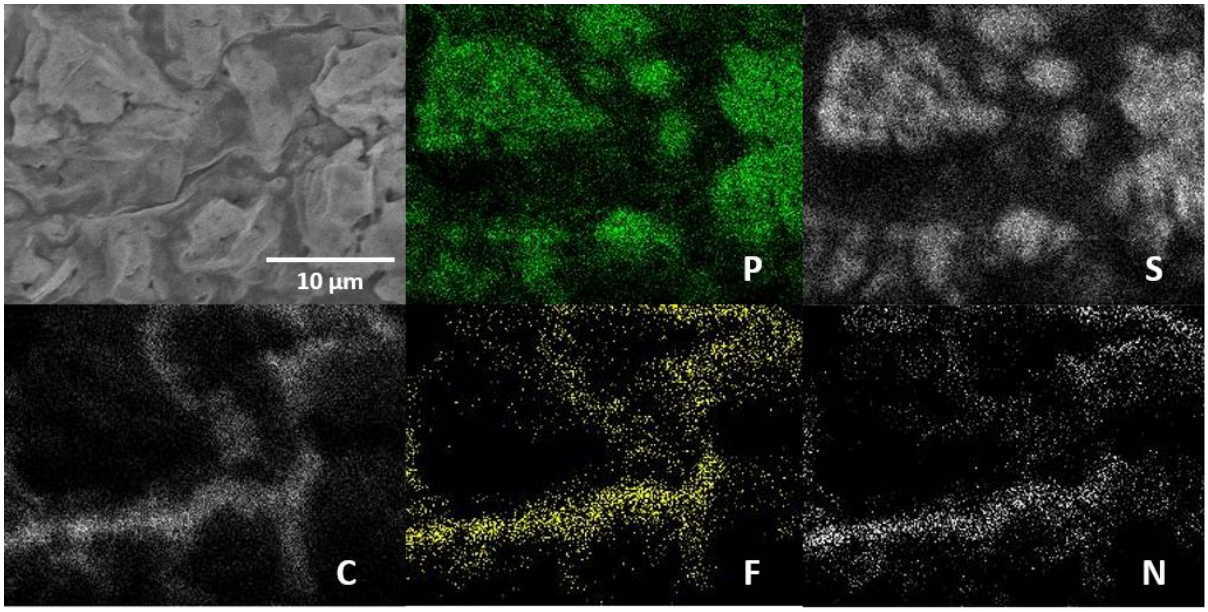

Figure 47. Cross-sectional FESEM image and EDXS elemental maps for LPSCl–NBR–LiG3. Reproduced with permission.[39] Copyright 2019, Wiley-VCH.

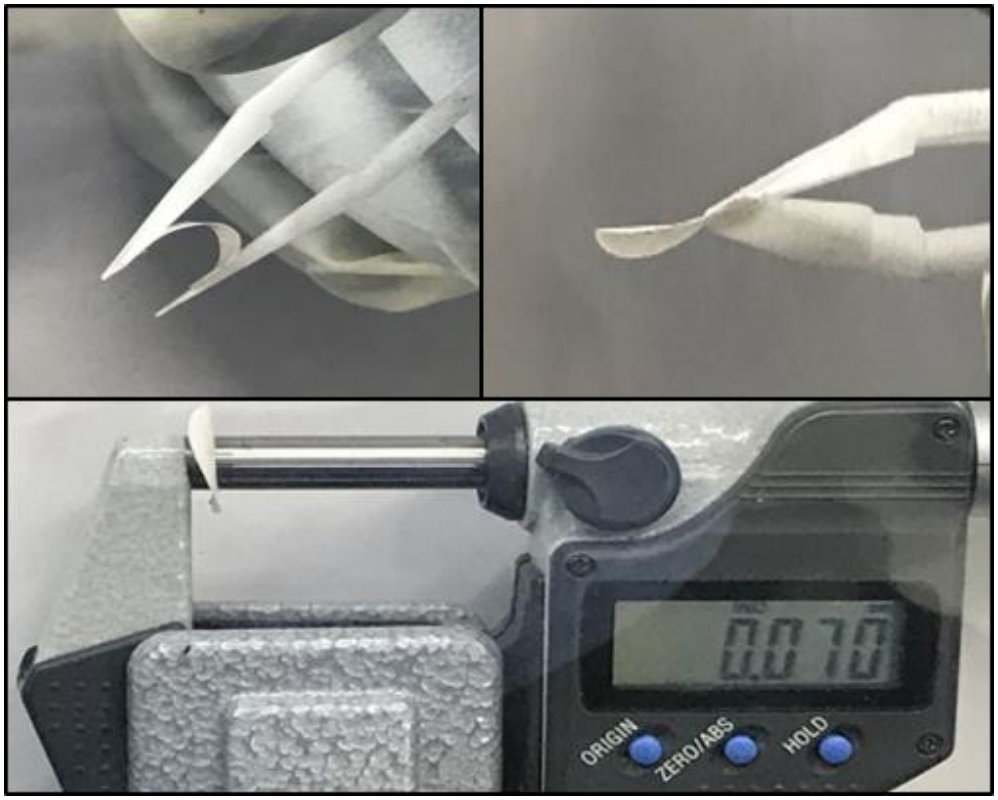

Figure 48. Photographs of Cross-sectional FESEM image and EDXS elemental maps for LPSCl–NBR–LiG3. Reproduced with permission.[39] Copyright 2019, Wiley-VCH.

Sample	Weight ratio	σ_{30} [S cm^{-1}]
LPSCl	-	4.2×10^{-3}
LPSCl-NBR-LiG3	95.0 : 1.5 : 3.5	3.3×10^{-3}
LPSCl-NBR	98.5 : 1.5	1.7×10^{-3}
LiG3	-	1.0×10^{-3}
NBR-LiG3	30 : 70	1.7×10^{-4}

Table 4. Li^+ conductivities for samples at 30 °C. Reproduced with permission.[39] Copyright 2019, Wiley-VCH.

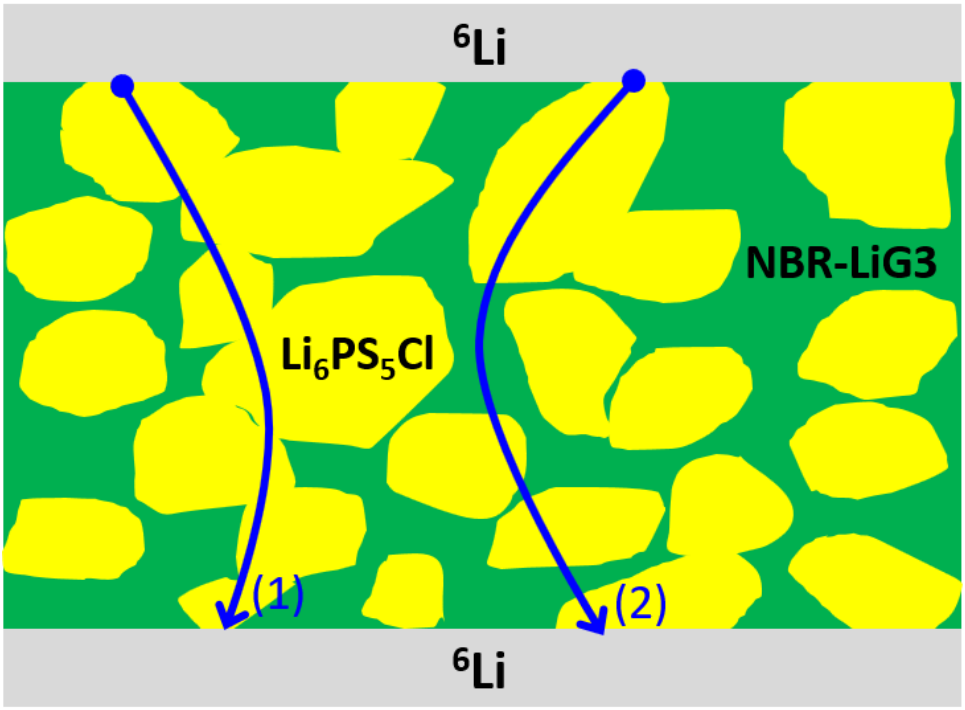

Figure 49. Schematic diagram representing ^{6}Li symmetric cell (^{6}Li/LPSCl-NBR-LiGE/^{6}Li). Li^{+} conduction pathways in the LPSCl-NBR-LiG3 are shown blue arrows (1, 2). Reproduced with permission.[39] Copyright 2019, Wiley-VCH.

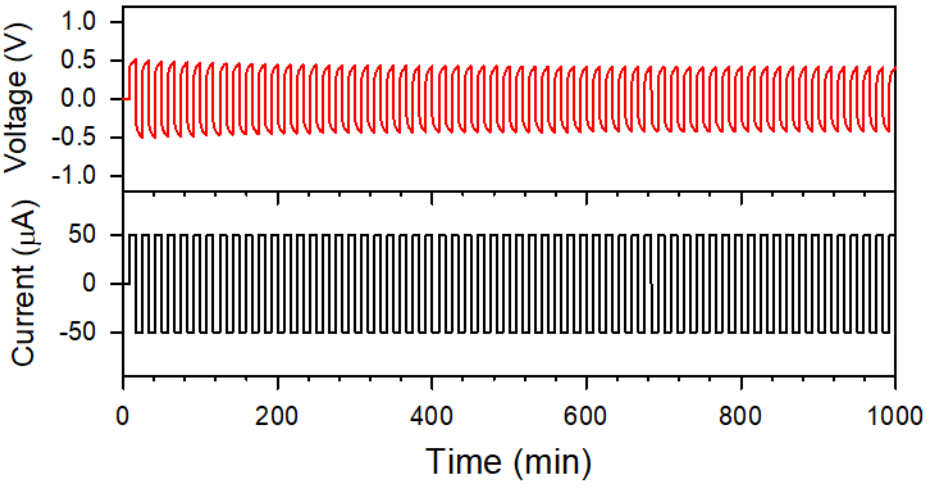

Figure 50. Cycling profiles of the $^{6}Li^{+}$-ion nonblocking symmetric cell (^{6}Li/LPSCl-NBR-LiG3/^{6}Li) with constant current of 50 μA. Reproduced with permission.[39] Copyright 2019, Wiley-VCH.

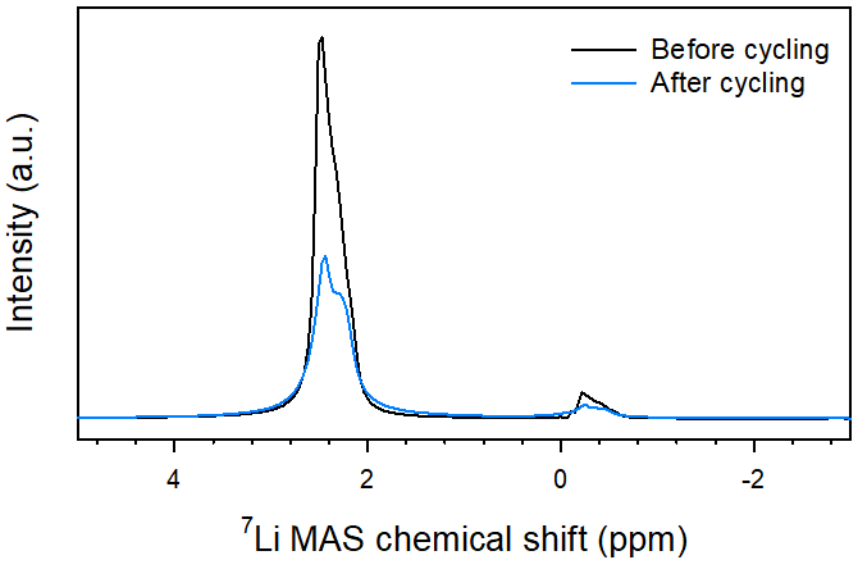

Figure 51. MAS ^{7}Li NMR spectra for comparative studies about LPSCl-NBR-LiG3 before and after cycling. LPSCl and NBR-LiG3 are 2.5 ppm and -0.25 ppm, respectively. Reproduced with permission.[39] Copyright 2019, Wiley-VCH.

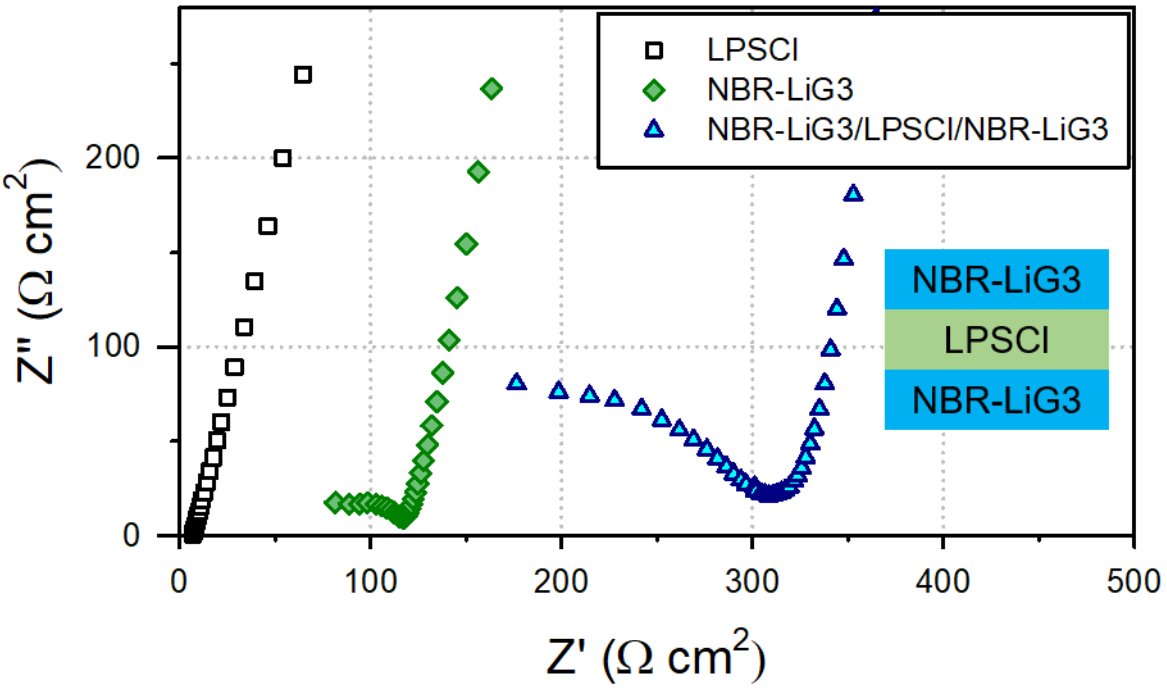

Figure 52. Nyquist plots for extracting interfacial resistance at LPSCl/NBR-LiG3. R_{int} (33.8 Ω cm ^{2}) was calculated by following equation; $R_{tot} = 2\cdot(R_{NBR\text{-}LiG3} + R_{int}) + R_{LPSCl}$. Reproduced with permission.[39] Copyright 2019, Wiley-VCH.

4.3.3 Sheet-type NCM electrodes fabricated by DBM-based wet-slurry protocol

To compare electrochemical performance varied by LiG3, the sheet-type electrodes were prepared *via* wet-slurry process using DBM and NBR (or NBR-LiG3). Detailed information for electrodes and test conditions are summarized in **Table 1** and **experimental section**, respectively. In the **Figure 53**, the sheet-type electrode employing NBR-LiG3 were free-standing and bendable in contrast to electrode fabricated without any polymeric scaffold, emphasizing the role of polymeric binders for developing large areal electrodes. In addition, the LiG3 didn't occur leakage problems even after pressed at 370 MPa.

The advantages of Li^+-conductive binder (NBR-LiG3) was assessed by comparing the electrochemical performance at 30 ºC. The first voltage profiles of NCM622/Li-In half-cells at 0.1C (0.26 mA cm^{-2}) are shown in **Figure 54**. The NCM622 employing only NBR exhibited a reversible capacity of 144 mA h g^{-1} that is only 80% of the ones using typical LEs (179 mA h g^{-1}, **Figure 55**). Surprisingly, the NCM622 employing NBR-LiG3 showed a higher discharge capacity of 174 mA h g^{-1}, which is almost close to conventional LIBs. Moreover, the initial coulombic efficiency increased from 78% (NBR) to 90% (NBR-LiG3), showing lower overpotential in the overall charge and discharge. The trend in rate capability as well as Nyquist plots (**Figure 56**) are also consistent with **Figure 55**. Also, NCM622 electrode with NBR-LiG3 showed the decent cycling behavior at elevated temperature (60 ºC, **Figure 57**) as well as the stable cycle retention (88% after 100^{th} cycle) at 30 ºC are notable. The ionic surface coverage on NCM622 electrodes, extracted from GITT results (**Figure 58**), for NBR and NBR-LiG3 are 27% and 42%, respectively. Moreover, Li^+ conductivities of NCM622 electrodes with NBR-LiG3 (0.2 mS cm^{-1}) is higher than the one with NBR (0.14 mS cm^{-1}), acquired by using electron-blocking Li-In/LPSCl/electrodes/LPSCl/Li-In symmetric cells (**Figure 59**). The NBR-LiG3 paved the interface of NCM622 particles and filled pores in electrodes, leading to facilitated Li^+ conduction pathways within the electrodes (**Figure 58, 59**) and increased electrode utilization (**Figure 54**). The porosities of NCM622 electrodes were 22% for NBR and 2.7% for NBR-LiG3, respectively, resulting from acting LiG3 as a plasticizer.

Figure 60 presents the ex-situ XRD patterns of sheet-type NCM electrodes with LiG3 and without LiG3 at different state-of-charge to estimate the degree of electrode utilization. The amount of Li in the NCM622 could be compared from the peak position of the (003) plane.[100-101] The (003) peaks shifted from 18.6º to lower angle (~18.2 º) as the NCM622 was charged to 4.3 V (vs. Li/Li^+) because the M-O slabs in the layer structured NCM622 suffered electrostatic repulsion along the c-axis at charged state. In opposite, (003) peaks were moved back to higher angle again after discharge to 3.0 V (vs. Li/Li^+). Importantly, the peak position after discharge for the NCM622 electrode without LiG3 appeared to be more negative than that for the one with LiG3, indicating that less Li^+ is intercalated back into NCM622 in the electrodes without LiG3 than with LiG3. This result evidences the incomplete utilization of active materials. This should be because of the slow kinetics associated with poor Li^+-ionic contacts and/or

pathways that could be solved by employing the Li^+-conductive binders, consistent with the complementary electrochemical analysis results (**Figure 54, 56, 58, 59**).

The sheet-type NCM711 electrodes with ultrahigh mass loading (45 or 30 mg_{NCM711} cm^{-2}) and higher fraction of active materials (80 or 83 wt%) were prepared to demonstrate strong advantage of ASLBs. Notably, conventional LIBs never realized such high mass loading because of wetting problems of LEs into porous electrodes. In **Figure 60**, cross-sectional FESEM images and their EDXS elemental maps exhibited compactly packed thick electrode (>200 μm) and homogenous distribution of components. The NCM711 electrodes with NBR-LiG3 (1.6 or 2.5 wt% LiG3) exhibited dramatically increased performance at 0.025C compared to that of 131 mA h g^{-1} of NCM711 with NBR. The highest areal capacity of 7.4 mA cm^{-2} was achieved for sheet-type NCM711 with NBR-LiG3 (2.5 wt% LiG3, 45 mg_{NCM711} cm^{-2}).

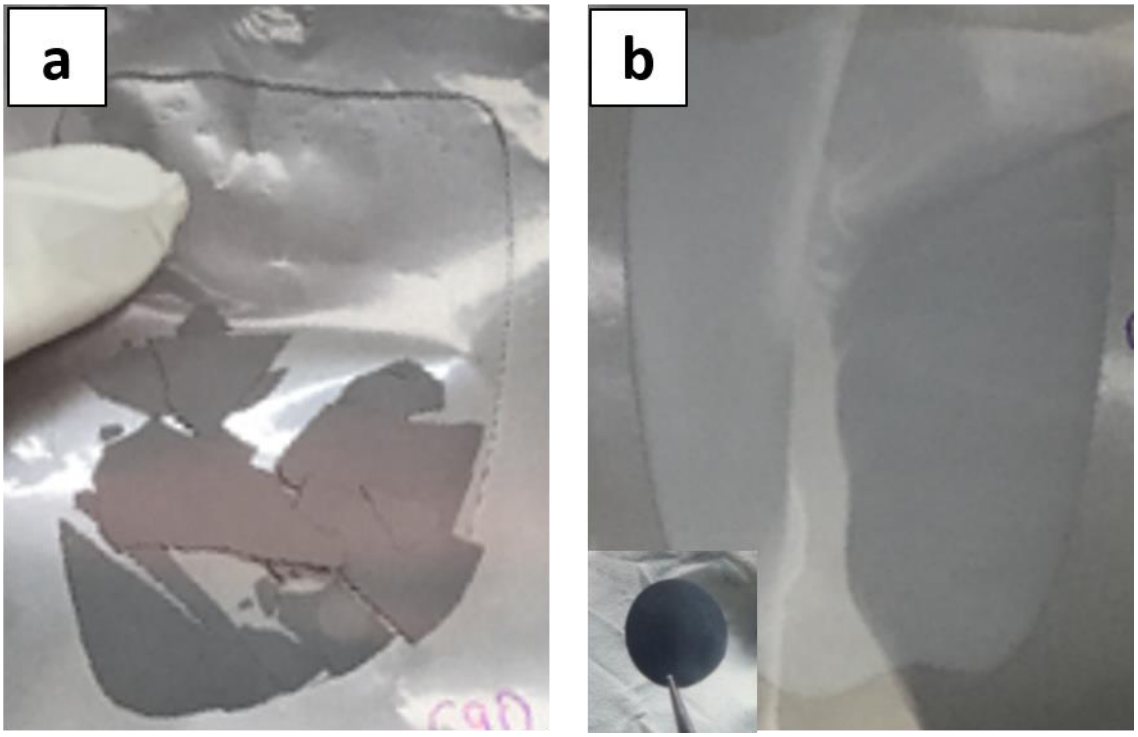

Figure 53. Photographs for sheet-type electrodes prepared by DBM-based wet-protocols (a) without NBR and (b) with NBR-LiG3. Reproduced with permission.[39] Copyright 2019, Wiley-VCH.

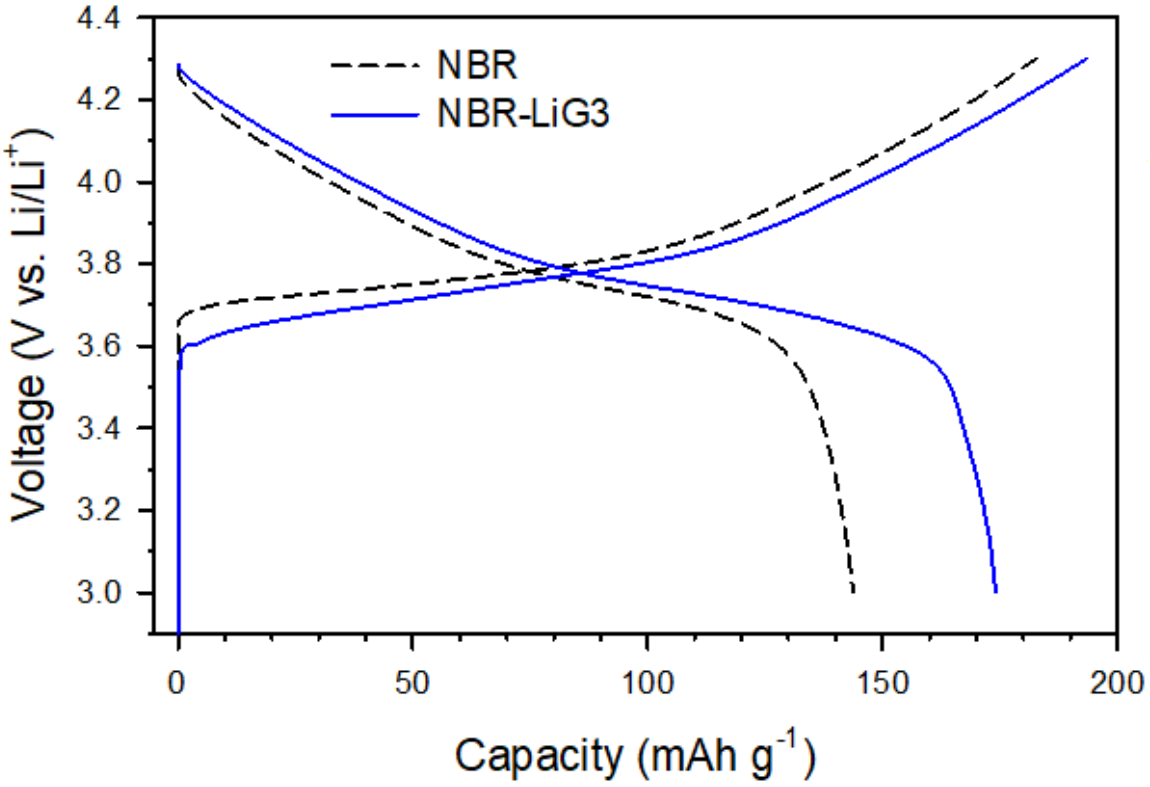

Figure 54. Electrochemical characterizations for the NCM622/Li-In half-cells at 30 °C, depending on sheet-type NCM622 electrodes fabricated by DBM-based slurry with NBR (black) and NBR-LiG3 (blue). The first-cycle voltage profiles are shown. Reproduced with permission.[39] Copyright 2019, Wiley-VCH.

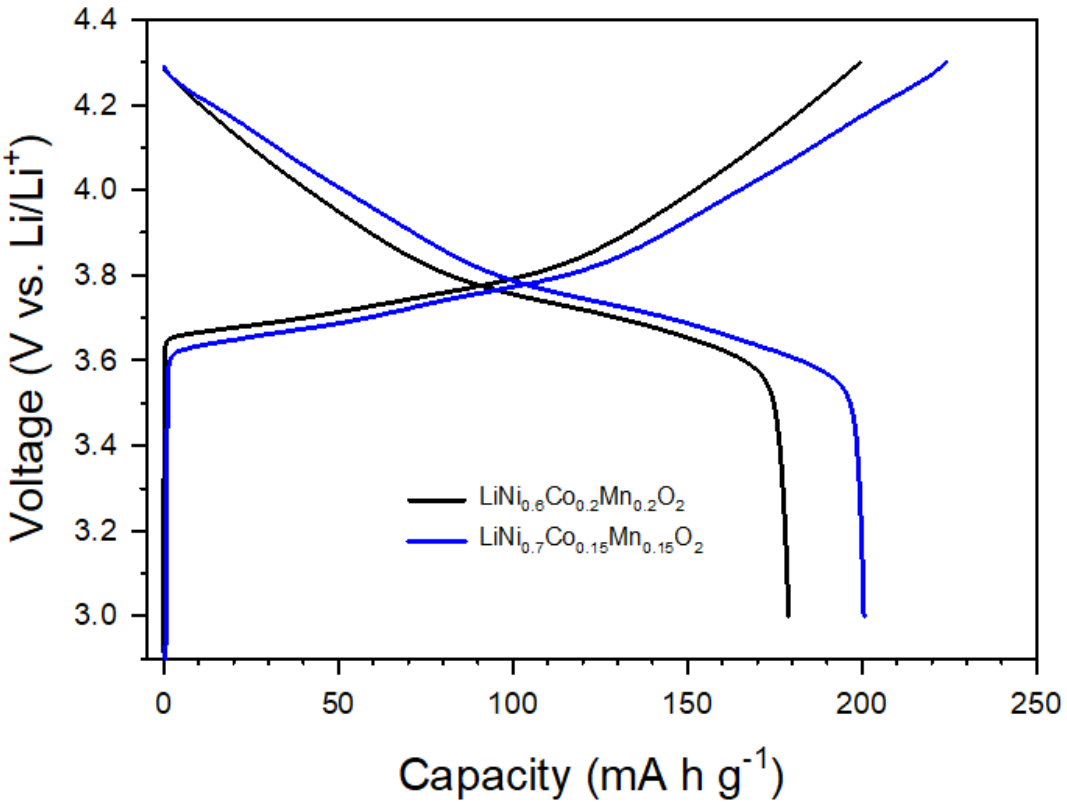

Figure 55. The first-cycle voltage profiles for NCM622 and NCM711. These profiles are obtained by using conventional LEs. Cycling tests using liquid electrolytes were performed using 2032-type coin cells. A 1 M solution of $LiPF_6$ dissolved in ethylene carbonate (EC), ethylmethyl carbonate (EMC), and dimethyl carbonate (DMC) (4:3:3 v/v, Panax Inc.) was used as the electrolyte. A porous polypropylene (PP)/polyethylene (PE)/PP tri-layer film (Celgard Inc.) was used as the separator. The compositions of electrodes for LIBs are followed; NCM : C : PVDF = 90 : 5 : 5 wt%. Reproduced with permission.[39] Copyright 2019, Wiley-VCH.

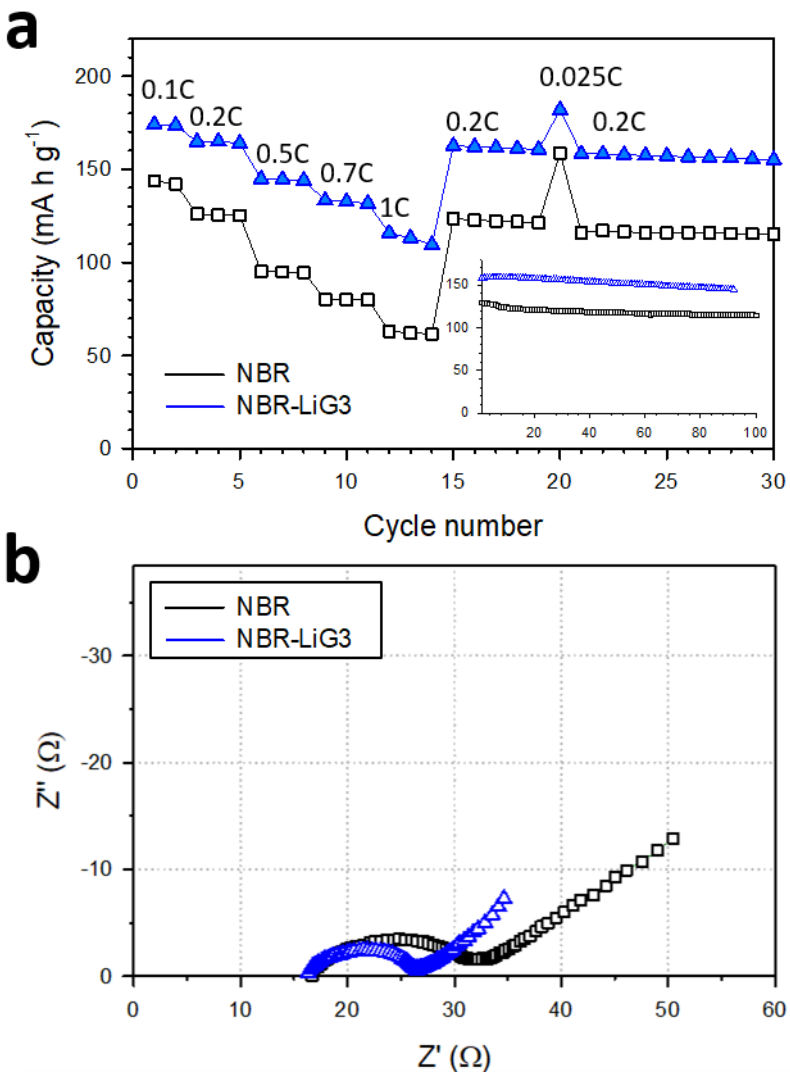

Figure 56. Comparative electrochemical characterization of NCM622/Li-In half-cell at 30 ºC, depending on sheet-type NCM622 electrodes fabricated by DBM-based slurry with NBR (black) and NBR-LiG3 (blue). (a) Rate capability, the cycle performances at 0.2C (0.52 mA cm^{-2}) are shown in the inset. (b) Nyquist plots obtained after charging at 4.3 V (vs. Li/Li^{+}). Reproduced with permission.[39] Copyright 2019, Wiley-VCH.

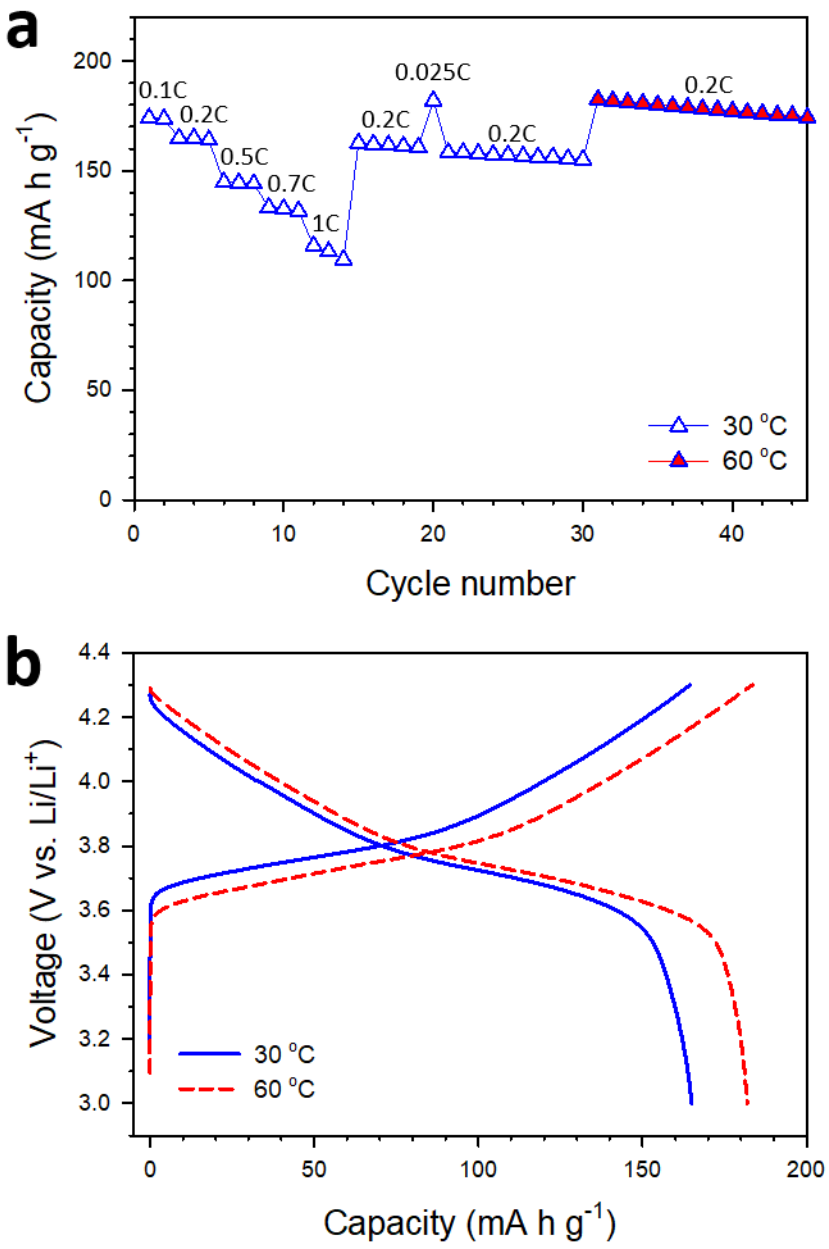

Figure 57. The subsequent cycling performance of NCM622 electrode with NBR-LiG3 for the data shown in **Figure 56a**. (a) The cycle data at 30°C and 60°C, (b) the voltage profiles at 30 °C (4th) and 60 °C (32th), tested at 0.2C both. Reproduced with permission.[39] Copyright 2019, Wiley-VCH.

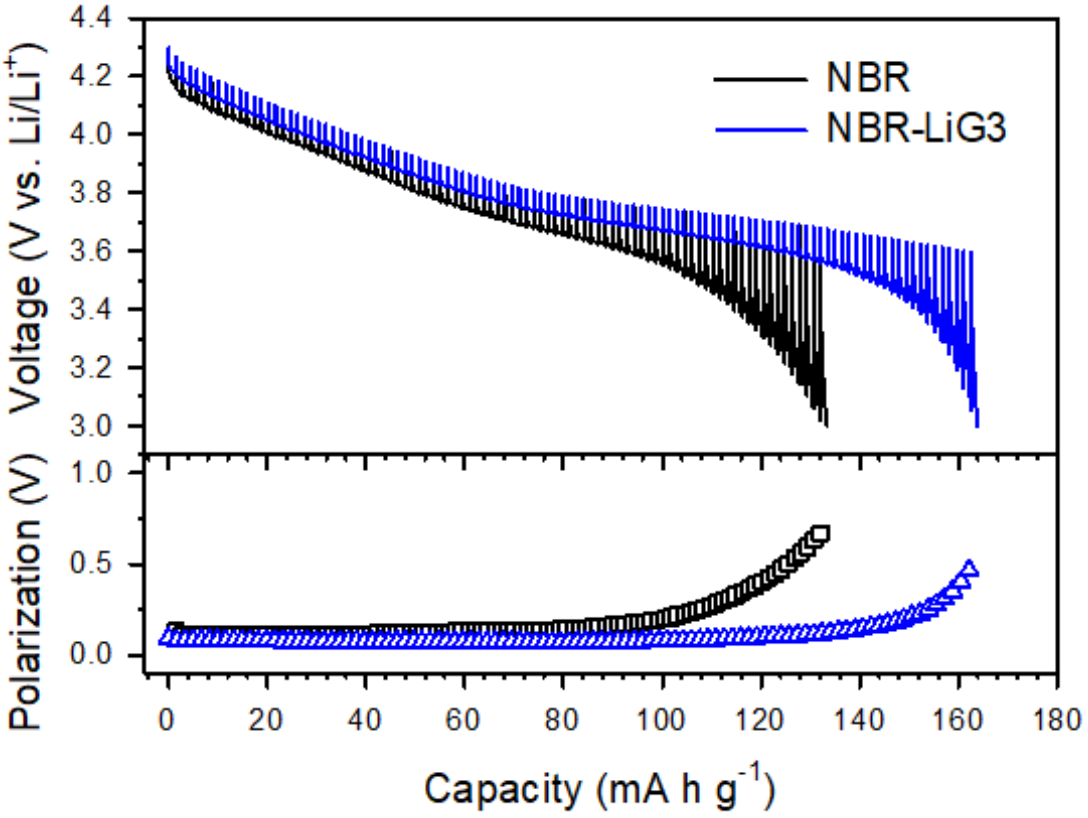

Figure 58. Transient voltage profiles and polarization plots acquired by GITT for NCM622/Li-In half-cell. NCM622 electrode with NBR (black) and NBR-LiG3 (blue). Reproduced with permission.[39] Copyright 2019, Wiley-VCH.

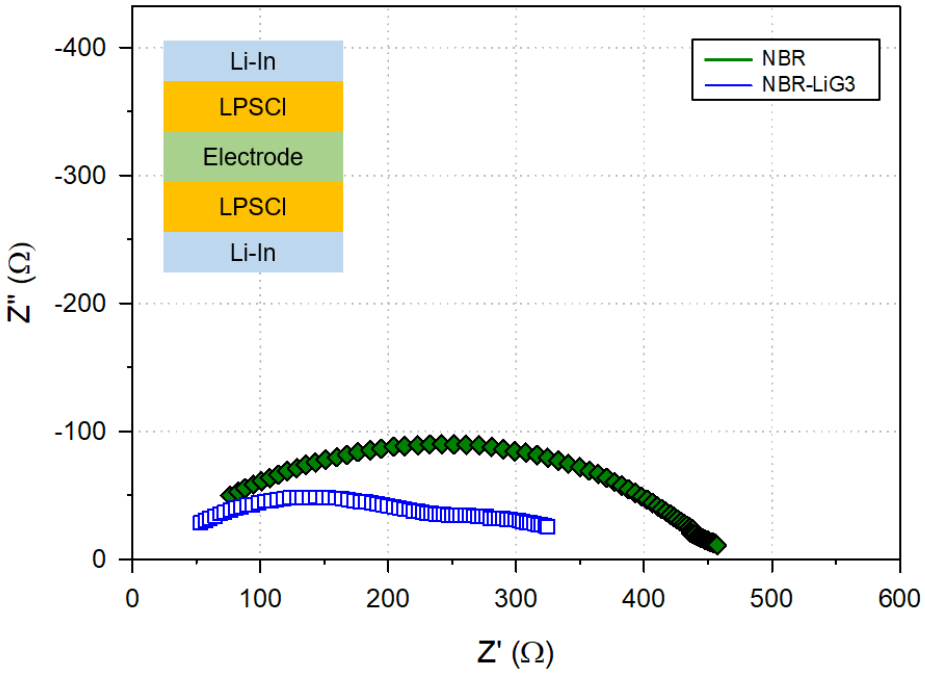

Figure 59. Nyquist plots for electron-blocking Li-In/LPSCl/electrodes/LPSCl/Li-In symmetric cells, depending on the presence of LiG3 in the electrodes. Schematic illustration for Li-In/LPSCl/electrode/LPSCl/Li-In cell is shown in the inset. Reproduced with permission.[39] Copyright 2019, Wiley-VCH.

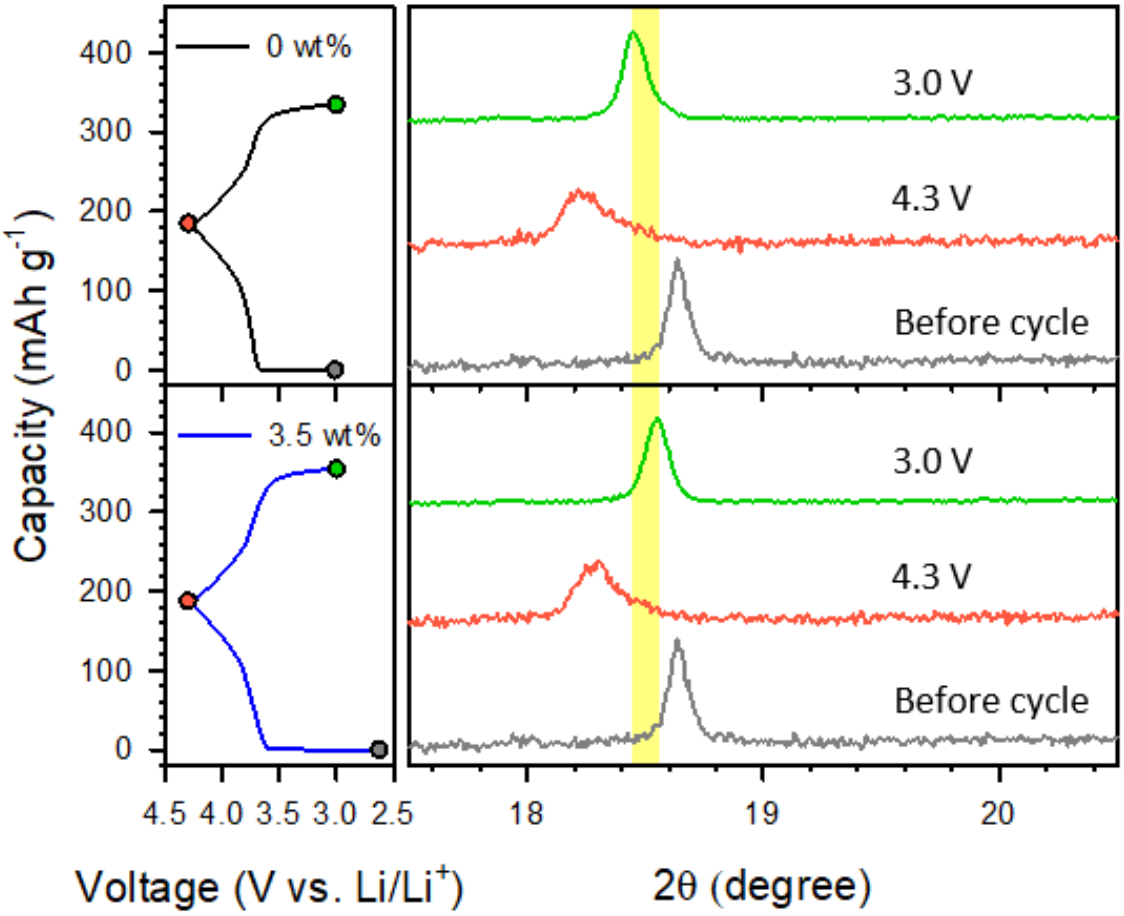

Figure 60. Ex-situ XRD patterns showing (003) peaks for NCM622 at different states of charge for the electrodes. The corresponding charge-discharge voltage profiles at 0.1C are shown in the left panel; NCM622 with NBR (black) and NBR-LiG3 (blue). Reproduced with permission.[39] Copyright 2019, Wiley-VCH.

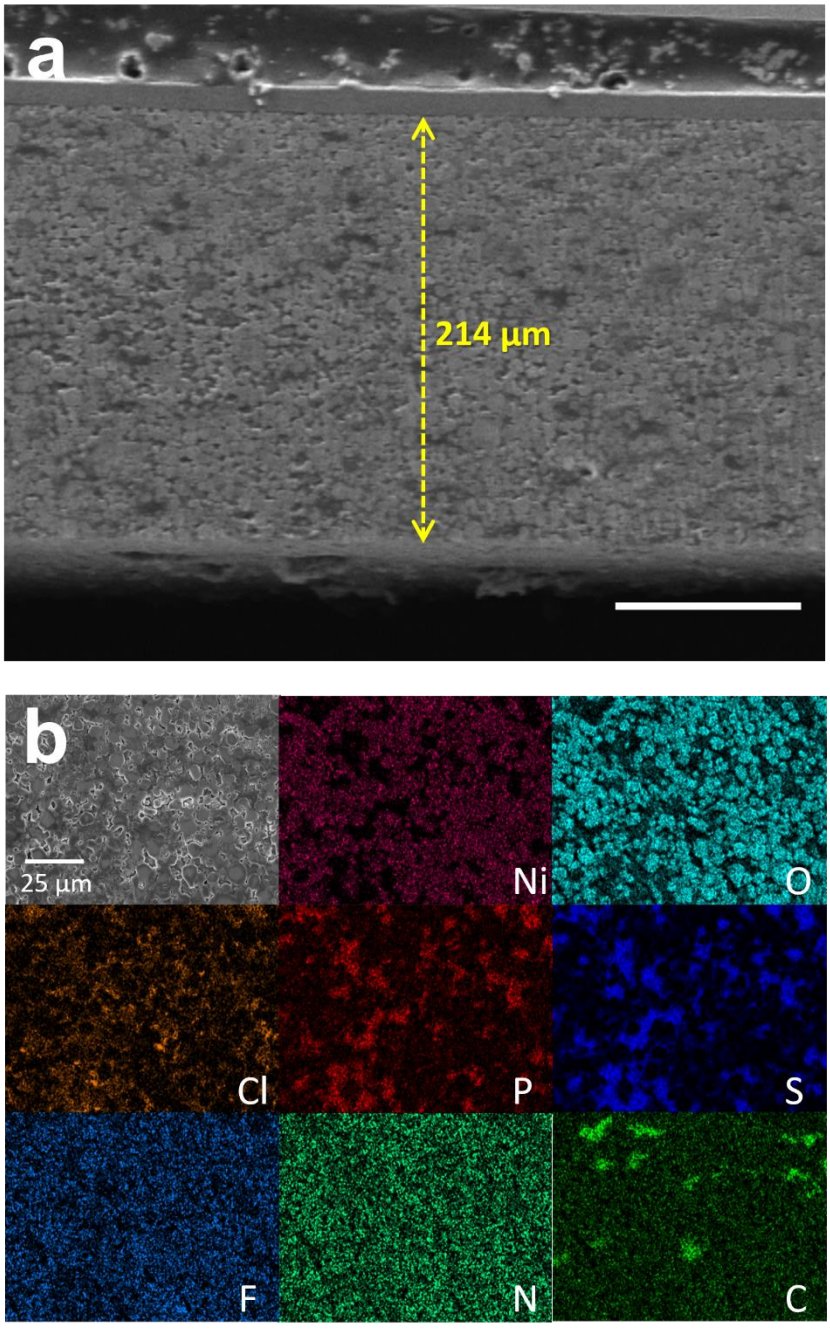

Figure 61. (a) Cross-sectional FESEM image and (b) corresponding EDXS elemental maps (b) for ultrathick NCM711 electrode employing NBR-LiG3. Reproduced with permission.[39] Copyright 2019, Wiley-VCH.

5. Conclusion

This research successfully investigated various hybrid protocols to handle issues and challenges for bulk-type ASLBs. To cope with poor chemical stability of sulfide SEs, especially, interplay between organic components and sulfide SEs were explored carefully by direct observations and complementary analyses.

First, SILs were suggested as an appropriate LEs to be inert to vulnerable sulfide SEs, by considering dissolution trends varied by concentration of glyme-based LEs. The strong complexation of G3 and Li^+ in the $[Li(G3)]^+$ suppressed nucleophilicity of G3, leading to excellent compatibility with sulfide SEs. Owing to non-solvent (or ionic-liquid-like) behaviors of SILs, quasi-sulfide-SEs involving LiG3 didn't suffer from thermal instability at elevated temperature (~130 ºC), confirmed by TGA. Moreover, the adoption of LiG3 into ASLBs enables to heal ionically dead zone such as inevitably formed pores or ionic-blocking obstacles, leading to remarkably enhanced performance in the carbon-coated LFP electrode.

Second, single-step wet-chemically fabricated sheet-type electrodes from the SE precursors were developed by using liquid-phase synthesis for sulfide SEs. Owing to moderately polar THF (or ACN), polymeric binder candidates for wet-slurry protocol were expanded. The excellent compatibility of NBR with sulfide SEs during wet-chemical route based on THF was confirmed by XRD measurement and Raman spectroscopy. Additionally, the electrochemical performance of sheet-type electrodes depending on the particle size was also assessed. Smaller SEs are desirable to improve ionic contacts and percolations within the electrodes. A rocking chair ASLBs employing wet-chemically fabricated electrodes were also estimated even in extreme conditions (100 ºC, 15C), showing a decent capacity of 110 mA h g^{-1}. Although these processes allowed to synthesize sulfide SEs and fabricate bendable sheet-type electrodes at the same time, highly reactive supernatant (Li_2S-P_2S_5 dissolved solution) corrupted cathode.

In last, wet-slurry protocols allowing sulfide SEs to accommodate gel polymer electrolytes as a Li^+-conductive binder were developed by using the intermediate-polar DBM. The DBM with negligible donor ability enabled to dilute LiG3 without disruption, which in turn influenced the chemical compatibility of the wet-slurry consisting of sulfide SEs and NBR. ^7Li NMR measurements and complementary electrochemical analyses revealed that single phase NBR-LiG3 boosted effective Li^+-conduction pathways within the sheet-type electrodes. Moreover, incomplete utilization of NCM electrodes underwent successful improvements by NBR-LiG3. For these reasons, the sheet-type NCM622 electrodes with NBR-LiG3 showed impressive first discharge capacity (174 mA h g^{-1}) and initial coulombic efficiency (90%), which is almost close to conventional LIBs.

Reference

1. Etacheri, V.; Marom, R.; Elazari, R.; Salitra, G.; Aurbach, D., Challenges in the development of advanced Li-ion batteries: a review. *Energy & Environ. Sci.* **2011,** *4* (9), 3243-3262.

2. Tarascon, J. M.; Armand, M., Issues and challenges facing rechargeable lithium batteries. *Nature* **2001,** *414* (6861), 359-367.

3. Goodenough, J. B.; Kim, Y., Challenges for Rechargeable Li Batteries. *Chem. Mater.* **2010,** *22* (3), 587-603.

4. Goodenough, J. B.; Park, K.-S., The Li-Ion Rechargeable Battery: A Perspective. *J. Am. Chem. Soc.* **2013,** *135* (4), 1167-1176.

5. Jung, Y. S.; Oh, D. Y.; Nam, Y. J.; Park, K. H., Issues and Challenges for Bulk-Type All-Solid-State Rechargeable Lithium Batteries using Sulfide Solid Electrolytes. *Israel Journal of Chemistry* **2015,** *55* (5), 472-485.

6. Nam, Y. J.; Cho, S.-J.; Oh, D. Y.; Lim, J.-M.; Kim, S. Y.; Song, J. H.; Lee, Y.-G.; Lee, S.-Y.; Jung, Y. S., Bendable and Thin Sulfide Solid Electrolyte Film: A New Electrolyte Opportunity for Free-Standing and Stackable High-Energy All-Solid-State Lithium-Ion Batteries. *Nano Lett.* **2015,** *15* (5), 3317-3323.

7. Park, K. H.; Bai, Q.; Kim, D. H.; Oh, D. Y.; Zhu, Y.; Mo, Y.; Jung, Y. S., Design Strategies, Practical Considerations, and New Solution Processes of Sulfide Solid Electrolytes for All-Solid-State Batteries. *Adv. Energy Mater.* **2018,** *8* (18), 1800035.

8. Chiku, M.; Tsujiwaki, W.; Higuchi, E.; Inoue, H., Microelectrode Studies on Kinetics of Charge Transfer at an Interface of Li Metal and Li_2S-P_2S_5 Solid Electrolytes. *Electrochemistry* **2012,** *80* (10), 740-742.

9. Kato, Y.; Hori, S.; Saito, T.; Suzuki, K.; Hirayama, M.; Mitsui, A.; Yonemura, M.; Iba, H.; Kanno, R., High-power all-solid-state batteries using sulfide superionic conductors. *Nat. Energy* **2016,** *1*, 16030.

10. Manthiram, A.; Yu, X.; Wang, S., Lithium battery chemistries enabled by solid-state e lectrolytes. *Nat. Rev. Mater.* **2017,** *2*, 16103.

11. Trevey, J.; Jang, J. S.; Jung, Y. S.; Stoldt, C. R.; Lee, S.-H., Glass–ceramic Li_2S–P_2S_5

electrolytes prepared by a single step ball billing process and their application for all-solid-state lithium–ion batteries. *Electrochem. Commun.* **2009,** *11* (9), 1830-1833.

12. Seino, Y.; Ota, T.; Takada, K.; Hayashi, A.; Tatsumisago, M., A sulphide lithium super ion conductor is superior to liquid ion conductors for use in rechargeable batteries. *Energy & Environ. Sci.* **2014,** *7* (2), 627-631.

13. Hanghofer, I.; Brinek, M.; Eisbacher, S. L.; Bitschnau, B.; Volck, M.; Hennige, V.; Hanzu, I.; Rettenwander, D.; Wilkening, H. M. R., Substitutional disorder: structure and ion dynamics of the argyrodites Li_6PS_5Cl, Li_6PS_5Br and Li_6PS_5I. *Physical Chemistry Chemical Physics* **2019,** *21* (16), 8489-8507.

14. Deiseroth, H.-J.; Kong, S.-T.; Eckert, H.; Vannahme, J.; Reiner, C.; Zaiß, T.; Schlosser, M., Li_6PS_5X: A Class of Crystalline Li-Rich Solids With an Unusually High Li^+ Mobility. *Angewandte Chemie* **2008,** *120* (4), 767-770.

15. Yu, C.; Ganapathy, S.; van Eck, E. R. H.; van Eijck, L.; Basak, S.; Liu, Y.; Zhang, L.; Zandbergen, Henny W.; Wagemaker, M., Revealing the relation between the structure, Li-ion conductivity and solid-state battery performance of the argyrodite Li_6PS_5Br solid electrolyte. *J. Mater. Chem. A* **2017,** *5* (40), 21178-21188.

16. Kamaya, N.; Homma, K.; Yamakawa, Y.; Hirayama, M.; Kanno, R.; Yonemura, M.; Kamiyama, T.; Kato, Y.; Hama, S.; Kawamoto, K.; Mitsui, A., A lithium superionic conductor. *Nat. Mater.* **2011,** *10*, 682.

17. Ito, S.; Fujiki, S.; Yamada, T.; Aihara, Y.; Park, Y.; Kim, T. Y.; Baek, S.-W.; Lee, J.-M.; Doo, S.; Machida, N., A rocking chair type all-solid-state lithium ion battery adopting Li_2O–ZrO_2 coated $LiNi_{0.8}Co_{0.15}Al_{0.05}O_2$ and a sulfide based electrolyte. *J. Power Sources* **2014,** *248*, 943-950.

18. Nam, Y. J.; Oh, D. Y.; Jung, S. H.; Jung, Y. S., Toward practical all-solid-state lithium-ion batteries with high energy density and safety: Comparative study for electrodes fabricated by dry- and slurry-mixing processes. *J. Power Sources* **2018,** *375*, 93-101.

19. Park, K. H.; Oh, D. Y.; Choi, Y. E.; Nam, Y. J.; Han, L.; Kim, J.-Y.; Xin, H.; Lin, F.; Oh, S. M.; Jung, Y. S., Solution-Processable Glass LiI-Li_4SnS_4 Superionic Conductors for All-Solid-State Li-Ion Batteries. *Adv. Mater.* **2016,** *28* (9), 1874-1883.

20. Sahu, G.; Rangasamy, E.; Li, J.; Chen, Y.; An, K.; Dudney, N.; Liang, C., A high-conduction

Ge substituted Li_3AsS_4 solid electrolyte with exceptional low activation energy. *J. Mater. Chem. A* **2014,** *2* (27), 10396-10403.

21. Banerjee, A.; Park, K. H.; Heo, J. W.; Nam, Y. J.; Moon, C. K.; Oh, S. M.; Hong, S.-T.; Jung, Y. S., Na_3SbS_4: A Solution Processable Sodium Superionic Conductor for All-Solid-State Sodium-Ion Batteries. *Angew. Chem. Int. Ed.* **2016,** *55* (33), 9634-9638.

22. Heo, J. W.; Banerjee, A.; Park, K. H.; Jung, Y. S.; Hong, S.-T., New Na-Ion Solid Electrolytes $Na_{4-x}Sn_{1-x}Sb_xS_4$ ($0.02 \leq x \leq 0.33$) for All-Solid-State Na-Ion Batteries. *Adv. Energy Mater.* **2018,** *8* (11), 1702716.

23. Sahu, G.; Lin, Z.; Li, J.; Liu, Z.; Dudney, N.; Liang, C., Air-stable, high-conduction solid electrolytes of arsenic-substituted Li_4SnS_4. *Energy & Environ. Sci.* **2014,** *7* (3), 1053-1058.

24. Liu, Z.; Fu, W.; Payzant, E. A.; Yu, X.; Wu, Z.; Dudney, N. J.; Kiggans, J.; Hong, K.; Rondinone, A. J.; Liang, C., Anomalous High Ionic Conductivity of Nanoporous β-Li_3PS_4. *J. Am. Chem. Soc.* **2013,** *135* (3), 975-978.

25. Wang, H.; Hood, Z. D.; Xia, Y.; Liang, C., Fabrication of ultrathin solid electrolyte membranes of β-Li_3PS_4 nanoflakes by evaporation-induced self-assembly for all-solid-state batteries. *J. Mater. Chem. A* **2016,** *4* (21), 8091-8096.

26. Wang, Y.; Lu, D.; Bowden, M.; El Khoury, P. Z.; Han, K. S.; Deng, Z. D.; Xiao, J.; Zhang, J.-G.; Liu, J., Mechanism of Formation of $Li_7P_3S_{11}$ Solid Electrolytes through Liquid Phase Synthesis. *Chem. Mater.* **2018,** *30* (3), 990-997.

27. Rangasamy, E.; Liu, Z.; Gobet, M.; Pilar, K.; Sahu, G.; Zhou, W.; Wu, H.; Greenbaum, S.; Liang, C., An Iodide-Based $Li_7P_2S_8I$ Superionic Conductor. *J. Am. Chem. Soc.* **2015,** *137* (4), 1384-1387.

28. Sedlmaier, S. J.; Indris, S.; Dietrich, C.; Yavuz, M.; Dräger, C.; von Seggern, F.; Sommer, H.; Janek, J., Li_4PS_4I: A Li^+ Superionic Conductor Synthesized by a Solvent-Based Soft Chemistry Approach. *Chem. Mater.* **2017,** *29* (4), 1830-1835.

29. Oh, D. Y.; Kim, D. H.; Jung, S. H.; Han, J.-G.; Choi, N.-S.; Jung, Y. S., Single-step wet-chemical fabrication of sheet-type electrodes from solid-electrolyte precursors for all-solid-state lithium-ion batteries. *J. Mater. Chem. A* **2017,** *5* (39), 20771-20779.

30. Hood, Z. D.; Wang, H.; Pandian, A. S.; Peng, R.; Gilroy, K. D.; Chi, M.; Liang, C.; Xia, Y.,

Fabrication of Sub-Micrometer-Thick Solid Electrolyte Membranes of β-Li_3PS_4 via Tiled Assembly of Nanoscale, Plate-Like Building Blocks. *Adv. Energy Mater.* **2018,** *8* (21), 1800014.

31. Yao, X.; Liu, D.; Wang, C.; Long, P.; Peng, G.; Hu, Y.-S.; Li, H.; Chen, L.; Xu, X., High-Energy All-Solid-State Lithium Batteries with Ultralong Cycle Life. *Nano Lett.* **2016,** *16* (11), 7148-7154.

32. Sakuda, A.; Hayashi, A.; Ohtomo, T.; Hama, S.; Tatsumisago, M., LiCoO2 Electrode Particles Coated with $Li_2S-P_2S_5$ Solid Electrolyte for All-Solid-State Batteries. *Electrochemical and Solid-State Letters* **2010,** *13* (6), A73-A75.

33. Choi, Y. E.; Park, K. H.; Kim, D. H.; Oh, D. Y.; Kwak, H. R.; Lee, Y.-G.; Jung, Y. S., Coatable Li_4SnS_4 Solid Electrolytes Prepared from Aqueous Solutions for All-Solid-State Lithium-Ion Batteries. *ChemSusChem* **2017,** *10* (12), 2605-2611.

34. Kim, D. H.; Oh, D. Y.; Park, K. H.; Choi, Y. E.; Nam, Y. J.; Lee, H. A.; Lee, S.-M.; Jung, Y. S., Infiltration of Solution-Processable Solid Electrolytes into Conventional Li-Ion-Battery Electrodes for All-Solid-State Li-Ion Batteries. *Nano Lett.* **2017,** *17* (5), 3013-3020.

35. Ziolkowska, D. A.; Arnold, W.; Druffel, T.; Sunkara, M.; Wang, H., Rapid and Economic Synthesis of a Li_7PS_6 Solid Electrolyte from a Liquid Approach. *ACS Appl. Mater. Interfaces* **2019,** *11* (6), 6015-6021.

36. Mercier, R.; Malugani, J.-P.; Fahys, B.; Robert, G., Superionic conduction in Li_2S - P_2S_5 - LiI - glasses. *Solid State Ionics* **1981,** *5*, 663-666.

37. Scott, I. D.; Jung, Y. S.; Cavanagh, A. S.; Yan, Y.; Dillon, A. C.; George, S. M.; Lee, S.-H., Ultrathin Coatings on Nano-$LiCoO_2$ for Li-Ion Vehicular Applications. *Nano Lett.* **2011,** *11* (2), 414-418.

38. Oh, D. Y.; Nam, Y. J.; Park, K. H.; Jung, S. H.; Cho, S.-J.; Kim, Y. K.; Lee, Y.-G.; Lee, S.-Y.; Jung, Y. S., Excellent Compatibility of Solvate Ionic Liquids with Sulfide Solid Electrolytes: Toward Favorable Ionic Contacts in Bulk-Type All-Solid-State Lithium-Ion Batteries. *Adv. Energy Mater.* **2015,** *5* (22), 1500865.

39. Oh, D. Y.; Nam, Y. J.; Park, K. H.; Jung, S. H.; Kim, K. T.; Ha, A. R.; Jung, Y. S., Slurry-Fabricable Li^+-Conductive Polymeric Binders for Practical All-Solid-State Lithium-Ion Batteries Enabled by Solvate Ionic Liquids. *Adv. Energy Mater.* **2019,** *9* (16), 1802927.

40. Yoshida, K.; Nakamura, M.; Kazue, Y.; Tachikawa, N.; Tsuzuki, S.; Seki, S.; Dokko, K.; Watanabe, M., Oxidative-Stability Enhancement and Charge Transport Mechanism in Glyme–Lithium Salt Equimolar Complexes. *J. Am. Chem. Soc.* **2011,** *133* (33), 13121-13129.

41. Wang, B.; Bates, J. B.; Hart, F. X.; Sales, B. C.; Zuhr, R. A.; Robertson, J. D., Characterization of Thin-Film Rechargeable Lithium Batteries with Lithium Cobalt Oxide Cathodes. *J. Electrochem. Soc.* **1996,** *143* (10), 3203-3213.

42. Bates, J. B.; Dudney, N. J.; Neudecker, B.; Ueda, A.; Evans, C. D., Thin-film lithium and lithium-ion batteries. *Solid State Ionics* **2000,** *135* (1), 33-45.

43. Sakuda, A.; Hayashi, A.; Tatsumisago, M., Sulfide Solid Electrolyte with Favorable Mechanical Property for All-Solid-State Lithium Battery. *Sci. Rep.* **2013,** *3*, 2261.

44. Mohtadi, R.; Orimo, S.-i., The renaissance of hydrides as energy materials. *Nat. Rev. Mater.* **2016,** *2*, 16091.

45. Kim, S.; Oguchi, H.; Toyama, N.; Sato, T.; Takagi, S.; Otomo, T.; Arunkumar, D.; Kuwata, N.; Kawamura, J.; Orimo, S.-i., A complex hydride lithium superionic conductor for high-energy-density all-solid-state lithium metal batteries. *Nat. Commun.* **2019,** *10* (1), 1081.

46. Long, L.; Wang, S.; Xiao, M.; Meng, Y., Polymer electrolytes for lithium polymer batteries. *J. Mater. Chem. A* **2016,** *4* (26), 10038-10069.

47. Dietrich, C.; Weber, D. A.; Sedlmaier, S. J.; Indris, S.; Culver, S. P.; Walter, D.; Janek, J.; Zeier, W. G., Lithium ion conductivity in Li_2S–P_2S_5 glasses – building units and local structure evolution during the crystallization of superionic conductors Li_3PS_4, $Li_7P_3S_{11}$ and $Li_4P_2S_7$. *J. Mater. Chem. A* **2017,** *5* (34), 18111-18119.

48. Hayashi, A.; Hama, S.; Morimoto, H.; Tatsumisago, M.; Minami, T., Preparation of Li_2S–P_2S_5 Amorphous Solid Electrolytes by Mechanical Milling. *J. Am. Ceram. Soc.* **2001,** *84* (2), 477-79.

49. Han, F.; Yue, J.; Zhu, X.; Wang, C., Suppressing Li Dendrite Formation in Li_2S-P_2S_5 Solid Electrolyte by LiI Incorporation. *Adv. Energy Mater.* **2018,** *8* (18), 1703644.

50. Yubuchi, S.; Uematsu, M.; Deguchi, M.; Hayashi, A.; Tatsumisago, M., Lithium-Ion-Conducting Argyrodite-Type Li_6PS_5X (X = Cl, Br, I) Solid Electrolytes Prepared by a Liquid-Phase Technique Using Ethanol as a Solvent. *ACS Applied Energy Materials* **2018,** *1* (8), 3622-

3629.

51. Yubuchi, S.; Uematsu, M.; Hotehama, C.; Sakuda, A.; Hayashi, A.; Tatsumisago, M., An argyrodite sulfide-based superionic conductor synthesized by a liquid-phase technique with tetrahydrofuran and ethanol. *J. Mater. Chem. A* **2019,** *7* (2), 558-566.

52. Muramatsu, H.; Hayashi, A.; Ohtomo, T.; Hama, S.; Tatsumisago, M., Structural change of Li_2S–P_2S_5 sulfide solid electrolytes in the atmosphere. *Solid State Ionics* **2011,** *182* (1), 116-119.

53. Koerver, R.; Walther, F.; Aygün, I.; Sann, J.; Dietrich, C.; Zeier, W. G.; Janek, J., Redox-active cathode interphases in solid-state batteries. *J. Mater. Chem. A* **2017,** *5* (43), 22750-22760.

54. Sakuda, A.; Hayashi, A.; Takigawa, Y.; Higashi, K.; Tatsumisago, M., Evaluation of elastic modulus of Li_2S-P_2S glassy solid electrolyte by ultrasonic sound velocity measurement and compression test. *J. Ceram. Soc. Jpn.* **2013,** *121* (1419), 946-949.

55. Kotobuki, M.; Munakata, H.; Kanamura, K.; Sato, Y.; Yoshida, T., Compatibility of $Li_7La_3Zr_2O_{12}$ Solid Electrolyte to All-Solid-State Battery Using Li Metal Anode. *J. Electrochem. Soc.* **2010,** *157* (10), A1076-A1079.

56. Kim, K. H.; Iriyama, Y.; Yamamoto, K.; Kumazaki, S.; Asaka, T.; Tanabe, K.; Fisher, C. A. J.; Hirayama, T.; Murugan, R.; Ogumi, Z., Characterization of the interface between $LiCoO_2$ and $Li_7La_3Zr_2O_{12}$ in an all-solid-state rechargeable lithium battery. *J. Power Sources* **2011,** *196* (2), 764-767.

57. Oh, D. Y.; Choi, Y. E.; Kim, D. H.; Lee, Y.-G.; Kim, B.-S.; Park, J.; Sohn, H.; Jung, Y. S., All-solid-state lithium-ion batteries with TiS_2 nanosheets and sulphide solid electrolytes. *J. Mater. Chem. A* **2016,** *4* (26), 10329-10335.

58. Zhu, Y.; He, X.; Mo, Y., Origin of Outstanding Stability in the Lithium Solid Electrolyte Materials: Insights from Thermodynamic Analyses Based on First-Principles Calculations. *ACS Appl. Mater. Interfaces* **2015,** *7* (42), 23685-23693.

59. Sakuda, A.; Hayashi, A.; Tatsumisago, M., Interfacial Observation between LiCoO2 Electrode and Li_2S−P_2S_5 Solid Electrolytes of All-Solid-State Lithium Secondary Batteries Using Transmission Electron Microscopy. *Chem. Mater.* **2010,** *22* (3), 949-956.

60. Jung, Y. S.; Lee, K. T.; Kim, J. H.; Kwon, J. Y.; Oh, S. M., Thermo-electrochemical Activation

of an In–Cu Intermetallic Electrode for the Anode in Lithium Secondary Batteries. *Adv. Funct. Mater.* **2008,** *18* (19), 3010-3017.

61. Nagao, M.; Hayashi, A.; Tatsumisago, M.; Kanetsuku, T.; Tsuda, T.; Kuwabata, S., In situ SEM study of a lithium deposition and dissolution mechanism in a bulk-type solid-state cell with a Li_2S–P_2S_5 solid electrolyte. *Physical Chemistry Chemical Physics* **2013,** *15* (42), 18600-18606.

62. Porz, L.; Swamy, T.; Sheldon, B. W.; Rettenwander, D.; Frömling, T.; Thaman, H. L.; Berendts, S.; Uecker, R.; Carter, W. C.; Chiang, Y.-M., Mechanism of Lithium Metal Penetration through Inorganic Solid Electrolytes. *Adv. Energy Mater.* **2017,** *7* (20), 1701003.

63. Zhang, W.; Schröder, D.; Arlt, T.; Manke, I.; Koerver, R.; Pinedo, R.; Weber, D. A.; Sann, J.; Zeier, W. G.; Janek, J., (Electro)chemical expansion during cycling: monitoring the pressure changes in operating solid-state lithium batteries. *J. Mater. Chem. A* **2017,** *5* (20), 9929-9936.

64. Koerver, R.; Aygün, I.; Leichtweiß, T.; Dietrich, C.; Zhang, W.; Binder, J. O.; Hartmann, P.; Zeier, W. G.; Janek, J., Capacity Fade in Solid-State Batteries: Interphase Formation and Chemomechanical Processes in Nickel-Rich Layered Oxide Cathodes and Lithium Thiophosphate Solid Electrolytes. *Chem. Mater.* **2017,** *29* (13), 5574-5582.

65. Shin, B. R.; Nam, Y. J.; Oh, D. Y.; Kim, D. H.; Kim, J. W.; Jung, Y. S., Comparative Study of TiS_2/Li-In All-Solid-State Lithium Batteries Using Glass-Ceramic Li3PS4 and Li10GeP2S12 Solid Electrolytes. *Electrochimica Acta* **2014,** *146*, 395-402.

66. Jung, S. H.; Oh, K.; Nam, Y. J.; Oh, D. Y.; Brüner, P.; Kang, K.; Jung, Y. S., Li_3BO_3–Li_2CO_3: Rationally Designed Buffering Phase for Sulfide All-Solid-State Li-Ion Batteries. *Chem. Mater.* **2018,** *30* (22), 8190-8200.

67. Auvergniot, J.; Cassel, A.; Ledeuil, J.-B.; Viallet, V.; Seznec, V.; Dedryvère, R. m., Interface stability of argyrodite Li_6PS_5Cl toward $LiCoO_2$, $LiNi_{1/3}Co_{1/3}Mn_{1/3}O_2$, and $LiMn_2O_4$ in bulk all-solid-state batteries. *Chem. Mater.* **2017,** *29* (9), 3883-3890.

68. Bron, P.; Roling, B.; Dehnen, S., Impedance characterization reveals mixed conducting interphases between sulfidic superionic conductors and lithium metal electrodes. *J. Power Sources* **2017,** *352*, 127-134.

69. Wenzel, S.; Randau, S.; Leichtweiß, T.; Weber, D. A.; Sann, J.; Zeier, W. G.; Janek, J. r., Direct observation of the interfacial instability of the fast ionic conductor $Li_{10}GeP_2S_{12}$ at the lithium metal anode. *Chem. Mater.* **2016,** *28* (7), 2400-2407.

70. Trevey, J. E.; Stoldt, C. R.; Lee, S.-H., High power nanocomposite TiS2 cathodes for all-solid-state lithium batteries. *J. Electrochem. Soc.* **2011,** *158* (12), A1282-A1289.

71. Yamamoto, M.; Terauchi, Y.; Sakuda, A.; Takahashi, M., Binder-free sheet-type all-solid-state batteries with enhanced rate capabilities and high energy densities. *Sci. Rep.* **2018,** *8* (1), 1212.

72. Lee, K.; Lee, J.; Choi, S.; Char, K.; Choi, J. W., Thiol–Ene Click Reaction for Fine Polarity Tuning of Polymeric Binders in Solution-Processed All-Solid-State Batteries. *ACS Energy Lett.* **2019,** *4* (1), 94-101.

73. Riphaus, N.; Strobl, P.; Stiaszny, B.; Zinkevich, T.; Yavuz, M.; Schnell, J.; Indris, S.; Gasteiger, H. A.; Sedlmaier, S. J., Slurry-Based Processing of Solid Electrolytes: A Comparative Binder Study. *J. Electrochem. Soc.* **2018,** *165* (16), A3993-A3999.

74. Cheng, X.-B.; Zhang, R.; Zhao, C.-Z.; Zhang, Q., Toward safe lithium metal anode in rechargeable batteries: a review. *Chem. Rev.* **2017,** *117* (15), 10403-10473.

75. Kim, H. W.; Manikandan, P.; Lim, Y. J.; Kim, J. H.; Nam, S.-c.; Kim, Y., Hybrid solid electrolyte with the combination of $Li_7La_3Zr_2O_{12}$ ceramic and ionic liquid for high voltage pseudo-solid-state Li-ion batteries. *J. Mater. Chem. A* **2016,** *4* (43), 17025-17032.

76. Park, J.-W.; Yamauchi, K.; Takashima, E.; Tachikawa, N.; Ueno, K.; Dokko, K.; Watanabe, M., Solvent effect of room temperature ionic liquids on electrochemical reactions in lithium–sulfur batteries. *J. Phys. Chem. C* **2013,** *117* (9), 4431-4440.

77. Dokko, K.; Tachikawa, N.; Yamauchi, K.; Tsuchiya, M.; Yamazaki, A.; Takashima, E.; Park, J.-W.; Ueno, K.; Seki, S.; Serizawa, N., Solvate ionic liquid electrolyte for Li–S batteries. *J. Electrochem. Soc.* **2013,** *160* (8), A1304-A1310.

78. Ueno, K.; Park, J.-W.; Yamazaki, A.; Mandai, T.; Tachikawa, N.; Dokko, K.; Watanabe, M., Anionic effects on solvate ionic liquid electrolytes in rechargeable lithium–sulfur batteries. *J. Phys. Chem. C* **2013,** *117* (40), 20509-20516.

79. Cuisinier, M.; Cabelguen, P. E.; Adams, B. D.; Garsuch, A.; Balasubramanian, M.; Nazar, L. F., Unique behaviour of nonsolvents for polysulphides in lithium–sulphur batteries. *Energy & Environ. Sci.* **2014,** *7* (8), 2697-2705.

80. Mandai, T.; Yoshida, K.; Ueno, K.; Dokko, K.; Watanabe, M., Criteria for solvate ionic liquids. *Physical Chemistry Chemical Physics* **2014,** *16* (19), 8761-8772.

81. Sun, Y.; Suzuki, K.; Hara, K.; Hori, S.; Yano, T.-a.; Hara, M.; Hirayama, M.; Kanno, R., Oxygen substitution effects in Li10GeP2S12 solid electrolyte. *J. Power Sources* **2016,** *324*, 798-803.

82. Kraft, M. A.; Ohno, S.; Zinkevich, T.; Koerver, R.; Culver, S. P.; Fuchs, T.; Senyshyn, A.; Indris, S.; Morgan, B. J.; Zeier, W. G., Inducing High Ionic Conductivity in the Lithium Superionic Argyrodites $Li_{6+x}P_{1-x}Ge_xS_5I$ for All-Solid-State Batteries. *J. Am. Chem. Soc.* **2018,** *140* (47), 16330-16339.

83. Furukawa, Y.; Ohta, H.; Sakamoto, A.; Tasumi, M., 1064-nanometer-excited Fourier transform Raman spectroscopy of conducting polymers. *Spectrochimica Acta Part A: Molecular Spectroscopy* **1991,** *47* (9), 1367-1373.

84. Rabek, J. F.; Shur, Y. J.; Rårnby, B., Studies of the photooxidation mechanism of polymers. III. Role of tetrahydrofuran in the photooxidative degradation of poly(vinyl chloride). *Journal of Polymer Science: Polymer Chemistry Edition* **1975,** *13* (6), 1285-1295.

85. Strauss, F.; Bartsch, T.; de Biasi, L.; Kim, A. Y.; Janek, J.; Hartmann, P.; Brezesinski, T., Impact of Cathode Material Particle Size on the Capacity of Bulk-Type All-Solid-State Batteries. *ACS Energy Lett.* **2018,** *3* (4), 992-996.

86. Choi, S.; Lee, S.; Park, J.; Nichols, W. T.; Shin, D., Facile synthesis of Li_2S-P_2S_5 glass-ceramics electrolyte with micron range particles for all-solid-state batteries via a low-temperature solution technique (LTST). *Appl. Surf. Sci.* **2018,** *444*, 10-14.

87. Kim, H.; Kim, M. G.; Jeong, H. Y.; Nam, H.; Cho, J., A new coating method for alleviating surface degradation of LiNi0. 6Co0. 2Mn0. 2O2 cathode material: nanoscale surface treatment of primary particles. *Nano Lett.* **2015,** *15* (3), 2111-2119.

88. Xu, K., Nonaqueous liquid electrolytes for lithium-based rechargeable batteries. *Chem. Rev.* **2004,** *104* (10), 4303-4418.

89. Chen, K.; Shinjo, S.; Sakuda, A.; Yamamoto, K.; Uchiyama, T.; Kuratani, K.; Takeuchi, T.; Orikasa, Y.; Hayashi, A.; Tatsumisago, M.; Kimura, Y.; Nakamura, T.; Amezawa, K.; Uchimoto, Y., Morphological Effect on Reaction Distribution Influenced by Binder Materials in Composite Electrodes for Sheet-type All-Solid-State Lithium-Ion Batteries with the Sulfide-based Solid Electrolyte. *J. Phys. Chem. C* **2019,** *123* (6), 3292-3298.

90. Osada, I.; de Vries, H.; Scrosati, B.; Passerini, S., Ionic-liquid-based polymer electrolytes for

battery applications. *Angew. Chem. Int. Ed.* **2016,** *55* (2), 500-513.

91. Cheng, X.; Pan, J.; Zhao, Y.; Liao, M.; Peng, H., Gel polymer electrolytes for electrochemical energy storage. *Adv. Energy Mater.* **2018,** *8* (7), 1702184.

92. Ueno, K.; Murai, J.; Moon, H.; Dokko, K.; Watanabe, M., A design approach to lithium-ion battery electrolyte based on diluted solvate ionic liquids. *J. Electrochem. Soc.* **2017,** *164* (1), A6088-A6094.

93. Ueno, K.; Murai, J.; Ikeda, K.; Tsuzuki, S.; Tsuchiya, M.; Tatara, R.; Mandai, T.; Umebayashi, Y .; Dokko, K.; Watanabe, M., Li^+ solvation and ionic transport in lithium solvate ionic liquids diluted by molecular solvents. *J. Phys. Chem. C* **2015,** *120* (29), 15792-15802.

94. Gao, J.; Lowe, M. A.; Kiya, Y.; Abruña, H. c. D., Effects of liquid electrolytes on the charge–discharge performance of rechargeable lithium/sulfur batteries: electrochemical and in-situ X-ray absorption spectroscopic studies. *J. Phys. Chem. C* **2011,** *115* (50), 25132-25137.

95. Tang, M.; Sarou-Kanian, V.; Melin, P.; Leriche, J.-B.; Ménétrier, M.; Tarascon, J.-M.; Deschamps, M.; Salager, E., Following lithiation fronts in paramagnetic electrodes with in situ magnetic resonance spectroscopic imaging. *Nat. Commun.* **2016,** *7*, 13284.

96. Wang, X.; Zhu, H.; Girard, G. M.; Yunis, R.; MacFarlane, D. R.; Mecerreyes, D.; Bhattacharyya, A. J.; Howlett, P. C.; Forsyth, M., Preparation and characterization of gel polymer electrolytes using poly (ionic liquids) and high lithium salt concentration ionic liquids. *J. Mater. Chem. A* **2017,** *5* (45), 23844-23852.

97. Zheng, J.; Tang, M.; Hu, Y. Y., Lithium ion pathway within $Li_7La_3Zr_2O_{12}$-polyethylene oxide composite electrolytes. *Angew. Chem. Int. Ed.* **2016,** *55* (40), 12538-12542.

98. Zheng, J.; Hu, Y.-Y., New Insights into the Compositional Dependence of Li-Ion Transport in Polymer–Ceramic Composite Electrolytes. *ACS Appl. Mater. Interfaces* **2018,** *10* (4), 4113-4120.

99. Zhang, D.; Haran, B.; Durairajan, A.; White, R. E.; Podrazhansky, Y.; Popov, B. N., Studies on capacity fade of lithium-ion batteries. *J. Power Sources* **2000,** *91* (2), 122-129.

100. Wang, Q.; Shen, C.-H.; Shen, S.-Y.; Xu, Y.-F.; Shi, C.-G.; Huang, L.; Li, J.-T.; Sun, S.-G., Origin of structural evolution in capacity degradation for overcharged NMC622 via operando coupled investigation. *ACS Appl. Mater. Interfaces* **2017,** *9* (29), 24731-24742.

101. Koerver, R.; Zhang, W.; de Biasi, L.; Schweidler, S.; Kondrakov, A. O.; Kolling, S.; Brezesinski, T.; Hartmann, P.; Zeier, W. G.; Janek, J., Chemo-mechanical expansion of lithium electrode materials–on the route to mechanically optimized all-solid-state batteries. *Energy & Environ. Sci.* **2018,** *11* (8), 2142-2158.

JOHN WILEY AND SONS LICENSE TERMS AND CONDITIONS

May 05, 2019

This Agreement between Mr. Dae Yang Oh ("You") and John Wiley and Sons ("John Wiley and Sons") consists of your license details and the terms and conditions provided by John Wiley and Sons and Copyright Clearance Center.

License Number	4582320929938
License date	May 05, 2019
Licensed Content Publisher	John Wiley and Sons
Licensed Content Publication	Advanced Energy Materials
Licensed Content Title	Design Strategies, Practical Considerations, and New Solution Processes of Sulfide Solid Electrolytes for All-Solid-State Batteries
Licensed Content Author	Kern Ho Park, Qiang Bai, Dong Hyeon Kim, et al
Licensed Content Date	Apr 23, 2018
Licensed Content Volume	8
Licensed Content Issue	18
Licensed Content Pages	24
Type of use	Dissertation/Thesis
Requestor type	Author of this Wiley article
Format	Print and electronic
Portion	Full article
Will you be translating?	No
Title of your thesis / dissertation	Hybrid Strategies for Sulfide Solid Electrolytes with Organic Materials: Toward Practical All-Solid-State Lithium-Ion Batteries
Expected completion date	Aug 2019
Expected size (number of pages)	150
Requestor Location	Mr. Dae Yang Oh 222 Wangsimni-ro, Seongdong-gu Seoul, 04763 Korea, Republic Of Attn: Mr. Dae Yang Oh
Publisher Tax ID	EU826007151
Total	0.00 USD
Terms and Conditions	

TERMS AND CONDITIONS

This copyrighted material is owned by or exclusively licensed to John Wiley & Sons, Inc. or one of its group companies (each a"Wiley Company") or handled on behalf of a society with which a Wiley Company has exclusive publishing rights in relation to a particular work (collectively "WILEY"). By clicking "accept" in connection with completing this licensing transaction, you agree that the following terms and conditions apply to this transaction (along with the billing and payment terms and conditions established by the Copyright Clearance

Center Inc., ("CCC's Billing and Payment terms and conditions"), at the time that you opened your RightsLink account (these are available at any time at http://myaccount.copyright.com).

Terms and Conditions

- The materials you have requested permission to reproduce or reuse (the "Wiley Materials") are protected by copyright.

- You are hereby granted a personal, non-exclusive, non-sub licensable (on a stand-alone basis), non-transferable, worldwide, limited license to reproduce the Wiley Materials for the purpose specified in the licensing process. This license, **and any CONTENT (PDF or image file) purchased as part of your order,** is for a one-time use only and limited to any maximum distribution number specified in the license. The first instance of republication or reuse granted by this license must be completed within two years of the date of the grant of this license (although copies prepared before the end date may be distributed thereafter). The Wiley Materials shall not be used in any other manner or for any other purpose, beyond what is granted in the license. Permission is granted subject to an appropriate acknowledgement given to the author, title of the material/book/journal and the publisher. You shall also duplicate the copyright notice that appears in the Wiley publication in your use of the Wiley Material. Permission is also granted on the understanding that nowhere in the text is a previously published source acknowledged for all or part of this Wiley Material. Any third party content is expressly excluded from this permission.

- With respect to the Wiley Materials, all rights are reserved. Except as expressly granted by the terms of the license, no part of the Wiley Materials may be copied, modified, adapted (except for minor reformatting required by the new Publication), translated, reproduced, transferred or distributed, in any form or by any means, and no derivative works may be made based on the Wiley Materials without the prior permission of the respective copyright owner.**For STM Signatory Publishers clearing permission under the terms of the STM Permissions Guidelines only, the terms of the license are extended to include subsequent editions and for editions in other languages, provided such editions are for the work as a whole in situ and does not involve the separate exploitation of the permitted figures or extracts,** You may not alter, remove or suppress in any manner any copyright, trademark or other notices displayed by the Wiley Materials. You may not license, rent, sell, loan, lease, pledge, offer as security, transfer or assign the Wiley Materials on a stand-alone basis, or any of the rights granted to you hereunder to any other person.

- The Wiley Materials and all of the intellectual property rights therein shall at all times remain the exclusive property of John Wiley & Sons Inc, the Wiley Companies, or their respective licensors, and your interest therein is only that of having possession of and the right to reproduce the Wiley

Materials pursuant to Section 2 herein during the continuance of this Agreement. You agree that you own no right, title or interest in or to the Wiley Materials or any of the intellectual property rights therein. You shall have no rights hereunder other than the license as provided for above in Section 2. No right, license or interest to any trademark, trade name, service mark or other branding ("Marks") of WILEY or its licensors is granted hereunder, and you agree that you shall not assert any such right, license or interest with respect thereto

- NEITHER WILEY NOR ITS LICENSORS MAKES ANY WARRANTY OR REPRESENTATION OF ANY KIND TO YOU OR ANY THIRD PARTY, EXPRESS, IMPLIED OR STATUTORY, WITH RESPECT TO THE MATERIALS OR THE ACCURACY OF ANY INFORMATION CONTAINED IN THE MATERIALS, INCLUDING, WITHOUT LIMITATION, ANY IMPLIED WARRANTY OF MERCHANTABILITY, ACCURACY, SATISFACTORY QUALITY, FITNESS FOR A PARTICULAR PURPOSE, USABILITY, INTEGRATION OR NON-INFRINGEMENT AND ALL SUCH WARRANTIES ARE HEREBY EXCLUDED BY WILEY AND ITS LICENSORS AND WAIVED BY YOU.

- WILEY shall have the right to terminate this Agreement immediately upon breach of this Agreement by you.

- You shall indemnify, defend and hold harmless WILEY, its Licensors and their respective directors, officers, agents and employees, from and against any actual or threatened claims, demands, causes of action or proceedings arising from any breach of this Agreement by you.

- IN NO EVENT SHALL WILEY OR ITS LICENSORS BE LIABLE TO YOU OR ANY OTHER PARTY OR ANY OTHER PERSON OR ENTITY FOR ANY SPECIAL, CONSEQUENTIAL, INCIDENTAL, INDIRECT, EXEMPLARY OR PUNITIVE DAMAGES, HOWEVER CAUSED, ARISING OUT OF OR IN CONNECTION WITH THE DOWNLOADING, PROVISIONING, VIEWING OR USE OF THE MATERIALS REGARDLESS OF THE FORM OF ACTION, WHETHER FOR BREACH OF CONTRACT, BREACH OF WARRANTY, TORT, NEGLIGENCE, INFRINGEMENT OR OTHERWISE (INCLUDING, WITHOUT LIMITATION, DAMAGES BASED ON LOSS OF PROFITS, DATA, FILES, USE, BUSINESS OPPORTUNITY OR CLAIMS OF THIRD PARTIES), AND WHETHER OR NOT THE PARTY HAS BEEN ADVISED OF THE POSSIBILITY OF SUCH DAMAGES. THIS LIMITATION SHALL APPLY NOTWITHSTANDING ANY FAILURE OF ESSENTIAL PURPOSE OF ANY LIMITED REMEDY PROVIDED HEREIN.

- Should any provision of this Agreement be held by a court of competent jurisdiction to be illegal, invalid, or unenforceable, that provision shall be deemed amended to achieve as nearly as possible the same economic effect as the original provision, and the legality, validity and enforceability of the remaining provisions of this Agreement shall not be affected or impaired thereby.

- The failure of either party to enforce any term or condition of this Agreement shall not constitute a waiver of either party's right to enforce each and every term and condition of this Agreement. No breach under this agreement shall be deemed waived or excused by either party unless such waiver or consent is in writing signed by the party granting such waiver or consent. The waiver by or consent of a party to a breach of any provision of this Agreement shall not operate or be construed as a waiver of or consent to any other or subsequent breach by such other party.

- This Agreement may not be assigned (including by operation of law or otherwise) by you without WILEY's prior written consent.

- Any fee required for this permission shall be non-refundable after thirty (30) days from receipt by the CCC.

- These terms and conditions together with CCC's Billing and Payment terms and conditions (which are incorporated herein) form the entire agreement between you and WILEY concerning this licensing transaction and (in the absence of fraud) supersedes all prior agreements and representations of the parties, oral or written. This Agreement may not be amended except in writing signed by both parties. This Agreement shall be binding upon and inure to the benefit of the parties' successors, legal representatives, and authorized assigns.

- In the event of any conflict between your obligations established by these terms and conditions and those established by CCC's Billing and Payment terms and conditions, these terms and conditions shall prevail.

- WILEY expressly reserves all rights not specifically granted in the combination of (i) the license details provided by you and accepted in the course of this licensing transaction, (ii) these terms and conditions and (iii) CCC's Billing and Payment terms and conditions.

- This Agreement will be void if the Type of Use, Format, Circulation, or Requestor Type was misrepresented during the licensing process.

- This Agreement shall be governed by and construed in accordance with the laws of the State of New York, USA, without regards to such state's conflict of law rules. Any legal action, suit or proceeding arising out of or relating to these Terms and Conditions or the breach thereof shall be instituted in a court of competent jurisdiction in New York County in the State of New York in the United States of America and each party hereby consents and submits to the personal jurisdiction of such court, waives any objection to venue in such court and consents to service of process by registered or certified mail, return receipt requested, at the last known address of such party.

WILEY OPEN ACCESS TERMS AND CONDITIONS

Wiley Publishes Open Access Articles in fully Open Access Journals and in Subscription journals offering Online Open. Although most of the fully Open Access journals publish open access articles under the terms of the Creative Commons Attribution (CC BY) License only, the subscription journals and a few of the Open Access Journals offer a choice of Creative Commons Licenses. The license type is clearly identified on the article.

The Creative Commons Attribution License

The Creative Commons Attribution License (CC-BY) allows users to copy, distribute and transmit an article, adapt the article and make commercial use of the article. The CC-BY license permits commercial and non-

Creative Commons Attribution Non-Commercial License

The Creative Commons Attribution Non-Commercial (CC-BY-NC)License permits use, distribution and reproduction in any medium, provided the original work is properly cited and is not used for commercial purposes.(see below)

Creative Commons Attribution-Non-Commercial-NoDerivs License

The Creative Commons Attribution Non-Commercial-NoDerivs License (CC-BY-NC-ND) permits use, distribution and reproduction in any medium, provided the original work is properly cited, is not used for commercial purposes and no modifications or adaptations are made. (see below)

Use by commercial "for-profit" organizations

Use of Wiley Open Access articles for commercial, promotional, or marketing purposes requires further explicit permission from Wiley and will be subject to a fee.

Further details can be found on Wiley Online Library
http://olabout.wiley.com/WileyCDA/Section/id-410895.html

Other Terms and Conditions:

v1.10 Last updated September 2015

Questions? customercare@copyright.com or +1-855-239-3415 (toll free in the US) or +1-978-646-2777.

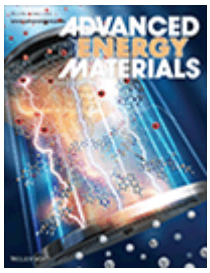

Title: Excellent Compatibility of Solvate Ionic Liquids with Sulfide Solid Electrolytes: Toward Favorable Ionic Contacts in Bulk-Type All-Solid-State Lithium-Ion Batteries

Author: Dae Yang Oh, Young Jin Nam, Kern Ho Park, et al

Publication: Advanced Energy Materials

Publisher: John Wiley and Sons

Date: Aug 3, 2015

Order Completed

Thank you for your order.

This Agreement between Mr. Dae Yang Oh ("You") and John Wiley and Sons ("John Wiley and Sons") consists of your license details and the terms and conditions provided by John Wiley and Sons and Copyright Clearance Center.

Your confirmation email will contain your order number for future reference.

printable details

License Number	4571810229543
License date	Apr 18, 2019
Licensed Content Publisher	John Wiley and Sons
Licensed Content Publication	Advanced Energy Materials
Licensed Content Title	Excellent Compatibility of Solvate Ionic Liquids with Sulfide Solid Electrolytes: Toward Favorable Ionic Contacts in Bulk-Type All-Solid-State Lithium-Ion Batteries
Licensed Content Author	Dae Yang Oh, Young Jin Nam, Kern Ho Park, et al
Licensed Content Date	Aug 3, 2015
Licensed Content Volume	5
Licensed Content Issue	22
Licensed Content Pages	7
Type of use	Dissertation/Thesis
Requestor type	Author of this Wiley article
Format	Electronic
Portion	Full article
Will you be translating?	No
Title of your thesis / dissertation	Hybrid Strategies for Sulfide Solid Electrolytes with Organic Materials: Toward Practical All-Solid-State Lithium-Ion Batteries
Expected completion date	Aug 2019
Expected size (number of pages)	150
Requestor Location	Mr. Dae Yang Oh 222 Wangsimni-ro, Seongdong-gu Seoul, 04763 Korea, Republic Of Attn: Mr. Dae Yang Oh
Publisher Tax ID	EU826007151

Total	0.00 USD

Would you like to purchase the full text of this article? If so, please continue on to the content ordering system located here: Purchase PDF

If you click on the buttons below or close this window, you will not be able to return to the content ordering system.

ORDER MORE CLOSE WINDOW

SPRINGER NATURE

Title: Sulfide Solid Electrolyte with Favorable Mechanical Property for All-Solid-State Lithium Battery

Author: Atsushi Sakuda, Akitoshi Hayashi, Masahiro Tatsumisago

Publication: Scientific Reports

Publisher: Springer Nature

Date: Jul 23, 2013

Creative Commons

The request you have made is considered to be non-commercial/educational. As the article you have requested has been distributed under a Creative Commons license (Attribution-Noncommercial), you may reuse this material for non-commercial/educational purposes without obtaining additional permission from Springer Nature, providing that the author and the original source of publication are fully acknowledged (please see the article itself for the license version number). You may reuse this material without obtaining permission from Springer Nature, providing that the author and the original source of publication are fully acknowledged, as per the terms of the license. For license terms, please see http://creativecommons.org/

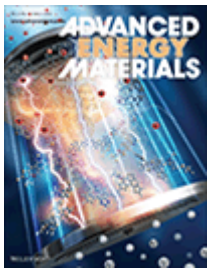

Title:	Slurry-Fabricable Li -Conductive Polymeric Binders for Practical All-Solid-State Lithium-Ion Batteries Enabled by Solvate Ionic Liquids
Author:	Dae Yang Oh, Young Jin Nam, Kern Ho Park, et al
Publication:	Advanced Energy Materials
Publisher:	John Wiley and Sons
Date:	Mar 5, 2019

Order Completed

Thank you for your order.

This Agreement between Mr. Dae Yang Oh ("You") and John Wiley and Sons ("John Wiley and Sons") consists of your license details and the terms and conditions provided by John Wiley and Sons and Copyright Clearance Center.

Your confirmation email will contain your order number for future reference.

printable details

License Number	4571810355106
License date	Apr 18, 2019
Licensed Content Publisher	John Wiley and Sons
Licensed Content Publication	Advanced Energy Materials
Licensed Content Title	Slurry-Fabricable Li -Conductive Polymeric Binders for Practical All-Solid-State Lithium-Ion Batteries Enabled by Solvate Ionic Liquids
Licensed Content Author	Dae Yang Oh, Young Jin Nam, Kern Ho Park, et al
Licensed Content Date	Mar 5, 2019
Licensed Content Volume	0
Licensed Content Issue	0
Licensed Content Pages	10
Type of use	Dissertation/Thesis
Requestor type	Author of this Wiley article
Format	Electronic
Portion	Full article
Will you be translating?	No
Title of your thesis / dissertation	Hybrid Strategies for Sulfide Solid Electrolytes with Organic Materials: Toward Practical All-Solid-State Lithium-Ion Batteries
Expected completion date	Aug 2019
Expected size (number of pages)	150
Requestor Location	Mr. Dae Yang Oh 222 Wangsimni-ro, Seongdong-gu Seoul, 04763 Korea, Republic Of Attn: Mr. Dae Yang Oh
Publisher Tax ID	EU826007151
Total	0.00 USD

Would you like to purchase the full text of this article? If so, please continue on to the content ordering system located here: Purchase PDF

If you click on the buttons below or close this window, you will not be able to return to the content ordering system.

ORDER MORE CLOSE WINDOW

(대학원생) 오대양 (에너지공학과)

보낸 사람: CONTRACTS-COPYRIGHT (shared) <Contracts-Copyright@rsc.org>
보낸 날짜: 2019년 4월 18일 목요일 오후 6:06
받는 사람: (대학원생) 오대양 (에너지공학과)
제목: RE: Permission Request Form: Dae Yang Oh

The Royal Society of Chemistry (RSC) hereby grants permission for the use of your paper(s) specified below in the printed and microfilm version of your thesis. You may also make available the PDF version of your paper(s) that the RSC sent to the corresponding author(s) of your paper(s) upon publication of the paper(s) in the following ways: in your thesis via any website that your university may have for the deposition of theses, via your university's Intranet or via your own personal website. We are however unable to grant you permission to include the PDF version of the paper(s) on its own in your institutional repository. The Royal Society of Chemistry is a signatory to the STM Guidelines on Permissions (available on request).

Please note that if the material specified below or any part of it appears with credit or acknowledgement to a third party then you must also secure permission from that third party before reproducing that material.

Please ensure that the thesis states the following:

Reproduced by permission of The Royal Society of Chemistry

and include a link to the paper on the Royal Society of Chemistry's website.

Please ensure that your co-authors are aware that you are including the paper in your thesis.

Best wishes,

Chloe Szebrat
Contracts and Copyright Executive
Royal Society of Chemistry
Thomas Graham House
Science Park, Milton Road
Cambridge, CB4 0WF, UK
Tel: +44 (0) 1223 438329
www.rsc.org

From: noreply@rsc.org <noreply@rsc.org>
Sent: 18 April 2019 09:01
To: CONTRACTS-COPYRIGHT (shared) <Contracts-Copyright@rsc.org>
Cc: ooddyy44@unist.ac.kr
Subject: Permission Request Form: Dae Yang Oh

Name : Dae Yang Oh
Address :

222 Wangsimni-ro, Seongdong-gu, Seoul 04763, Korea

Tel : +82 010 2053 1746
Fax :
Email : ooddyy44@unist.ac.kr

I am preparing the following work for publication:

Article/Chapter Title : Hybrid Strategies for Sulfide Solid Electrolytes with Organic Materials: Toward Practical All-Solid-State Lithium-Ion Batteries
Journal/Book Title : thesis for doctoral course
Editor/Author(s) : Dae Yang Oh
Publisher : UNIST

I would very much appreciate your permission to use the following material:

Journal/Book Title : Single-step wet-chemical fabrication of sheet-type electrodes from solid-electrolyte precursors for all-solid-state lithium-ion batteries
Editor/Author(s) : Dae Yang Oh, Dong Hyeon Kim, Sung Hoo Jung, Jung-Gu Han, Nam-Soon Choi and Yoon Seok Jung
Volume Number : 5
Year of Publication : 2017
Description of Material : Journal of Materials Chemistry
Page(s) : 20771-20779

Any Additional Comments :

I am the author "Single-step wet-chemical fabrication of sheet-type electrodes from solid-electrolyte precursors for all-solid-state lithium-ion batteries" published in "Journal of Materials Chemistry A". I need permission of that paper for my thesis.

SPRINGER NATURE LICENSE TERMS AND CONDITIONS

May 05, 2019

This Agreement between Mr. Dae Yang Oh ("You") and Springer Nature ("Springer Nature") consists of your license details and the terms and conditions provided by Springer Nature and Copyright Clearance Center.

License Number	4582330162825
License date	May 05, 2019
Licensed Content Publisher	Springer Nature
Licensed Content Publication	Nature Energy
Licensed Content Title	High-power all-solid-state batteries using sulfide superionic conductors
Licensed Content Author	Yuki Kato, Satoshi Hori, Toshiya Saito, Kota Suzuki, Masaaki Hirayama et al.
Licensed Content Date	Mar 21, 2016
Licensed Content Volume	1
Licensed Content Issue	4
Type of Use	Thesis/Dissertation
Requestor type	academic/university or research institute
Format	print and electronic
Portion	figures/tables/illustrations
Number of figures/tables/illustrations	1
High-res required	no
Will you be translating?	no
Circulation/distribution	<501
Author of this Springer Nature content	no
Title	Hybrid Strategies for Sulfide Solid Electrolytes with Organic Materials: Toward Practical All-Solid-State Lithium-Ion Batteries
Institution name	n/a
Expected presentation date	Aug 2019
Portions	supplementary information Figure S1
Requestor Location	Mr. Dae Yang Oh 222 Wangsimni-ro, Seongdong-gu Seoul, 04763 Korea, Republic Of Attn: Mr. Dae Yang Oh
Total	0.00 USD
Terms and Conditions	

Springer Nature Terms and Conditions for RightsLink Permissions

Springer Nature Customer Service Centre GmbH (the Licensor) hereby grants you a non-exclusive, world-wide licence to reproduce the material and for the

purpose and requirements specified in the attached copy of your order form, and for no other use, subject to the conditions below:

1. The Licensor warrants that it has, to the best of its knowledge, the rights to license reuse of this material. However, you should ensure that the material you are requesting is original to the Licensor and does not carry the copyright of another entity (as credited in the published version).

   If the credit line on any part of the material you have requested indicates that it was reprinted or adapted with permission from another source, then you should also seek permission from that source to reuse the material.

2. Where **print only** permission has been granted for a fee, separate permission must be obtained for any additional electronic re-use.

3. Permission granted **free of charge** for material in print is also usually granted for any electronic version of that work, provided that the material is incidental to your work as a whole and that the electronic version is essentially equivalent to, or substitutes for, the print version.

4. A licence for 'post on a website' is valid for 12 months from the licence date. This licence does not cover use of full text articles on websites.

5. Where **'reuse in a dissertation/thesis'** has been selected the following terms apply: Print rights of the final author's accepted manuscript (for clarity, NOT the published version) for up to 100 copies, electronic rights for use only on a personal website or institutional repository as defined by the Sherpa guideline (www.sherpa.ac.uk/romeo/).

6. Permission granted for books and journals is granted for the lifetime of the first edition and does not apply to second and subsequent editions (except where the first edition permission was granted free of charge or for signatories to the STM Permissions Guidelines http://www.stm-assoc.org/copyright-legal-affairs/permissions/permissions-guidelines/), and does not apply for editions in other languages unless additional translation rights have been granted separately in the licence.

7. Rights for additional components such as custom editions and derivatives require additional permission and may be subject to an additional fee. Please apply to Journalpermissions@springernature.com/bookpermissions@springernature.com for these rights.

8. The Licensor's permission must be acknowledged next to the licensed material in print. In electronic form, this acknowledgement must be visible at the same time as the figures/tables/illustrations or abstract, and must be hyperlinked to the journal/book's homepage. Our required acknowledgement format is in the Appendix below.

9. Use of the material for incidental promotional use, minor editing privileges (this does not include cropping, adapting, omitting material or any other changes that affect the meaning, intention or moral rights of the author) and copies for the disabled are permitted under this licence.

10. Minor adaptations of single figures (changes of format, colour and style) do not require the Licensor's approval. However, the adaptation should be credited as shown in Appendix below.

Appendix — Acknowledgements:

For Journal Content:
Reprinted by permission from [**the Licensor**]: [**Journal Publisher** (e.g. Nature/Springer/Palgrave)] [**JOURNAL NAME**] [**REFERENCE CITATION** (Article name, Author(s) Name), [**COPYRIGHT**] (year of publication)

For **Advance Online Publication papers:**
Reprinted by permission from [**the Licensor**]: [**Journal Publisher** (e.g.

Nature/Springer/Palgrave)] [**JOURNAL NAME**] [**REFERENCE CITATION** (Article name, Author(s) Name), [**COPYRIGHT**] (year of publication), advance online publication, day month year (doi: 10.1038/sj.[JOURNAL ACRONYM].)

For Adaptations/Translations:
Adapted/Translated by permission from [**the Licensor**]: [**Journal Publisher** (e.g. Nature/Springer/Palgrave)] [**JOURNAL NAME**] [**REFERENCE CITATION** (Article name, Author(s) Name), [**COPYRIGHT**] (year of publication)

Note: For any republication from the British Journal of Cancer, the following credit line style applies:

Reprinted/adapted/translated by permission from [**the Licensor**]: on behalf of Cancer Research UK: : [**Journal Publisher** (e.g. Nature/Springer/Palgrave)] [**JOURNAL NAME**] [**REFERENCE CITATION** (Article name, Author(s) Name), [**COPYRIGHT]** (year of publication)

For **Advance Online Publication** papers:
Reprinted by permission from The [**the Licensor**]: on behalf of Cancer Research UK: [**Journal Publisher** (e.g. Nature/Springer/Palgrave)] [**JOURNAL NAME**] [**REFERENCE CITATION** (Article name, Author(s) Name), [**COPYRIGHT**] (year of publication), advance online publication, day month year (doi: 10.1038/sj.[JOURNAL ACRONYM])

For Book content:
Reprinted/adapted by permission from [**the Licensor**]: [**Book Publisher** (e.g. Palgrave Macmillan, Springer etc) [**Book Title**] by [**Book author**(s)] [**COPYRIGHT**] (year of publication)

Other Conditions:

Version 1.1

SPRINGER NATURE LICENSE TERMS AND CONDITIONS

May 05, 2019

This Agreement between Mr. Dae Yang Oh ("You") and Springer Nature ("Springer Nature") consists of your license details and the terms and conditions provided by Springer Nature and Copyright Clearance Center.

License Number	4582340126905
License date	May 05, 2019
Licensed Content Publisher	Springer Nature
Licensed Content Publication	Nature Reviews Materials
Licensed Content Title	Lithium battery chemistries enabled by solid-state electrolytes
Licensed Content Author	Arumugam Manthiram, Xingwen Yu, Shaofei Wang
Licensed Content Date	Feb 14, 2017
Licensed Content Volume	2
Licensed Content Issue	4
Type of Use	Thesis/Dissertation
Requestor type	academic/university or research institute
Format	print and electronic
Portion	figures/tables/illustrations
Number of figures/tables/illustrations	1
High-res required	no
Will you be translating?	no
Circulation/distribution	<501
Author of this Springer Nature content	no
Title	Hybrid Strategies for Sulfide Solid Electrolytes with Organic Materials: Toward Practical All-Solid-State Lithium-Ion Batteries
Institution name	n/a
Expected presentation date	Aug 2019
Portions	Rader plots in Figures
Requestor Location	Mr. Dae Yang Oh 222 Wangsimni-ro, Seongdong-gu Seoul, 04763 Korea, Republic Of Attn: Mr. Dae Yang Oh
Total	0.00 USD

Terms and Conditions

Springer Nature Terms and Conditions for RightsLink Permissions

Springer Nature Customer Service Centre GmbH (the Licensor) hereby grants you a non-exclusive, world-wide licence to reproduce the material and for the purpose and requirements specified in the attached copy of your order form, and for no other use, subject to the conditions below:

1. The Licensor warrants that it has, to the best of its knowledge, the rights to license reuse of this material. However, you should ensure that the material you are requesting is original to the Licensor and does not carry the copyright of another entity (as credited in the published version).

   If the credit line on any part of the material you have requested indicates that it was reprinted or adapted with permission from another source, then you should also seek permission from that source to reuse the material.

2. Where **print only** permission has been granted for a fee, separate permission must be obtained for any additional electronic re-use.

3. Permission granted **free of charge** for material in print is also usually granted for any electronic version of that work, provided that the material is incidental to your work as a whole and that the electronic version is essentially equivalent to, or substitutes for, the print version.

4. A licence for 'post on a website' is valid for 12 months from the licence date. This licence does not cover use of full text articles on websites.

5. Where **'reuse in a dissertation/thesis'** has been selected the following terms apply: Print rights of the final author's accepted manuscript (for clarity, NOT the published version) for up to 100 copies, electronic rights for use only on a personal website or institutional repository as defined by the Sherpa guideline (www.sherpa.ac.uk/romeo/).

6. Permission granted for books and journals is granted for the lifetime of the first edition and does not apply to second and subsequent editions (except where the first edition permission was granted free of charge or for signatories to the STM Permissions Guidelines http://www.stm-assoc.org/copyright-legal-affairs/permissions/permissions-guidelines/), and does not apply for editions in other languages unless additional translation rights have been granted separately in the licence.

7. Rights for additional components such as custom editions and derivatives require additional permission and may be subject to an additional fee. Please apply to Journalpermissions@springernature.com/bookpermissions@springernature.com for these rights.

8. The Licensor's permission must be acknowledged next to the licensed material in print. In electronic form, this acknowledgement must be visible at the same time as the figures/tables/illustrations or abstract, and must be hyperlinked to the journal/book's homepage. Our required acknowledgement format is in the Appendix below.

9. Use of the material for incidental promotional use, minor editing privileges (this does not include cropping, adapting, omitting material or any other changes that affect the meaning, intention or moral rights of the author) and copies for the disabled are permitted under this licence.

10. Minor adaptations of single figures (changes of format, colour and style) do not require the Licensor's approval. However, the adaptation should be credited as shown in Appendix below.

Appendix — Acknowledgements:

For Journal Content:
Reprinted by permission from [**the Licensor**]: [**Journal Publisher** (e.g. Nature/Springer/Palgrave)] [**JOURNAL NAME**] [**REFERENCE CITATION** (Article name, Author(s) Name), [**COPYRIGHT**] (year of publication)

For **Advance Online Publication papers:**
Reprinted by permission from [**the Licensor**]: [**Journal Publisher** (e.g. Nature/Springer/Palgrave)] [**JOURNAL NAME**] [**REFERENCE CITATION** (Article name, Author(s) Name), [**COPYRIGHT**] (year of publication),

advance online publication, day month year (doi: 10.1038/sj.[JOURNAL ACRONYM].)

For Adaptations/Translations:
Adapted/Translated by permission from [**the Licensor**]: [**Journal Publisher** (e.g. Nature/Springer/Palgrave)] [**JOURNAL NAME**] [**REFERENCE CITATION** (Article name, Author(s) Name), [**COPYRIGHT**] (year of publication)

Note: For any republication from the British Journal of Cancer, the following credit line style applies:

Reprinted/adapted/translated by permission from [**the Licensor**]: on behalf of Cancer Research UK: : [**Journal Publisher** (e.g. Nature/Springer/Palgrave)] [**JOURNAL NAME**] [**REFERENCE CITATION** (Article name, Author(s) Name), [**COPYRIGHT]** (year of publication)

For **Advance Online Publication** papers:
Reprinted by permission from The [**the Licensor**]: on behalf of Cancer Research UK: [**Journal Publisher** (e.g. Nature/Springer/Palgrave)] [**JOURNAL NAME**] [**REFERENCE CITATION** (Article name, Author(s) Name), [**COPYRIGHT**] (year of publication), advance online publication, day month year (doi: 10.1038/sj.[JOURNAL ACRONYM])

For Book content:
Reprinted/adapted by permission from [**the Licensor**]: [**Book Publisher** (e.g. Palgrave Macmillan, Springer etc) [**Book Title**] by [**Book author**(s)] [**COPYRIGHT**] (year of publication)

Other Conditions:

Version 1.1

Title: Comparative Study of TiS2/Li-In All-Solid-State Lithium Batteries Using Glass-Ceramic Li3PS4 and Li10GeP2S12 Solid Electrolytes

Author: Bum Ryong Shin,Young Jin Nam,Dae Yang Oh,Dong Hyeon Kim,Jin Wook Kim,Yoon Seok Jung

Publication: Electrochimica Acta

Publisher: Elsevier

Date: 10 November 2014

JOHN WILEY AND SONS LICENSE TERMS AND CONDITIONS

Ma

This Agreement between Mr. Dae Yang Oh ("You") and John Wiley and S ("John Wiley and Sons") consists of your license details and the terms ar conditions provided by John Wiley and Sons and Copyright Clearance C

License Number	4580260743946
License date	May 01, 2019
Licensed Content Publisher	John Wiley and Sons
Licensed Content Publication	Israel Journal of Chemistry
Licensed Content Title	Issues and Challenges for Bulk-Type All-Solid-State Rechai Lithium Batteries using Sulfide Solid Electrolytes
Licensed Content Author	Yoon Seok Jung, Dae Yang Oh, Young Jin Nam, et al
Licensed Content Date	Jan 23, 2015
Licensed Content Volume	55
Licensed Content Issue	5
Licensed Content Pages	14
Type of use	Dissertation/Thesis
Requestor type	Author of this Wiley article
Format	Electronic
Portion	Full article

Print This Page